

Role of Endothelial Nanog in Homeostasis of Adult Tissue Microenvironment

BY

JUGAJYOTI BARUAH

B.Sc., Bangalore University, India, 2009

M.Sc., Vellore Institute of Technology, India, 2011

THESIS

Submitted in partial fulfillment of the requirements
for the degree of Doctor of Philosophy in Cellular and Molecular Pharmacology
in the Graduate College of the
University of Illinois at Chicago, 2018
Chicago, Illinois

Defense Committee:

Kishore K. Wary, Ph.D., Advisor

Viswanathan Natarajan, Ph.D., Chair

Youyang Zhao, Ph.D., Northwestern University

Irena Levitan, Ph.D.

Owen Tamplin, Ph.D.

Richard D. Minshall, Ph.D.

For my family, friends and most importantly the pillar of my strength, my husband, Tatsat. Without their love and support, I would not have been able to translate my dream into a reality.

ACKNOWLEDGMENTS

I could not have made this far without the adequate guidance and generous help provided by several key people in Dr. Wary's laboratory and in the Department of Pharmacology.

First, Dr. Kishore Wary, for accepting me as a graduate research assistant in his laboratory to pursue a PhD degree in Cellular and Molecular Pharmacology with a focus in Regenerative Biology. In Dr. Wary's laboratory, soon I found independence to pursue my own idea, and design and carry out experiments independently. Thus, he allowed me to develop my analytical- and problem-solving skills. The training process was intense, but fun. He made sure my data was reproducible and presentable. He made sure I practiced my presentations for at least 3 times, and presented my research data with confidence and clarity, addressed questions and concerns adequately and positively. Along the way throughout my training period, I received several awards and accolades. Importantly, I have learned writing and revising manuscripts, presenting data, and writing fellowship grants, and "life skills" that I believe, will be key to my next career move and beyond. So, I thank you Dr. Wary.

Second, I thank my committee members, Dr. Irena Levitan, Dr. Owen Tamplin, Dr. Richard Minshall, Dr. Youyang Zhao and Dr. Viswanathan Natarajan for their inputs. Their critiques and feedbacks at each presentation were key to my growth as a PhD research trainee and to developing a strong hypothesis driven research. They generously spent hours to write letters of recommendation in support of my fellowship and post-doctoral applications.

Third, I thank Dr. Asrar B. Malik, Dr. Jaehyung 'Gus' Cho, Dr. Yulia Komarova and Dr. Randal Skidgel (former DGS), for providing me with valuable feedback on my research during the Friday student forum and work-in-progress seminars, and in our annual departmental retreats. I

also enjoyed the meeting with invited guest seminar speakers on Wednesdays. These interactions have been intellectually rewarding for me.

Fourth, I would like to thank Dr. Ishita Chatterjee and Dr. Erin Kohler-Lurie for their guidance and training during my early years in the program. I also thank my friends Jaba, Mark, Dheeraj, Tina, Ryan, Suhkrita, Victoria and Isabella. They have been an excellent support system and provided me with technical help, perceptive comments that kept me on track as well as other life commitments.

Fifth, I would like to acknowledge and thank the Imaging, Histology, and Flow Cytometry core facilities. They have always helped me to troubleshoot any issues that occurred during my experimental design or data acquisition. A big shout out to the staff members of the Pharmacology Department, who have helped me with the numerous administrative issues during my training period. I also acknowledge the numerous mice whose contribution turned my research a success.

Sixth, I acknowledge the research funding from the National Institute of Health (NIH), American Heart Association, and the CCTS-PECTS program at the UIC.

Seventh, I am forever indebted to my parents, my three sisters whose support and best wishes push me constantly.

Finally, and the most importantly, words are not enough to thank my loving and supporting husband, Tatsat. He is a source of inspiration, a shoulder to lean on during my high and low times, and have helped me focus on what has been a highly enriching and rewarding process.

TABLE OF CONTENTS

<u>CHAPTER</u>	<u>PAGE</u>
I. INTRODUCTION.....	1
A. Background.....	1
B. Rationale.....	5
C. Hypothesis.....	6
D. Significance.....	6
II. LITERATURE REVIEW.....	10
A. Homeostasis at the Level of Endothelial Cells.....	10
B. Wnt Signaling Pathway.....	14
C. Transcription Factor NANOG.....	18
D. Telomerase Reverse Transcriptase.....	22
E. Cardiac Hypertrophy.....	27
III. MATERIALS AND METHODS.....	32
A. Antibodies and Reagents.....	32
B. Western Blot Analysis.....	33
C. RNA Extraction and q-RT-PCR.....	34
D. Chromatin Immunoprecipitation (ChIP) Assay, PCR and qPCR.....	37
E. <i>siRNA</i> and <i>shRNA</i> mediated Gene Knockdown.....	39
F. BrdU Incorporation Assay.....	39

<u>CHAPTER</u>	<u>PAGE</u>
G. Immunofluorescent Staining, Immunohistochemistry on Cryo- and Paraffin- Sections	40
H. Telomerase Repeat Amplification Protocol (TRAP) Assay	44
I. Luciferase Reporter Assay	45
J. Formation of Branching Point Structures and Tube Formation Assay	46
K. Terminal deoxynucleotidyl transferase dUTP nick end labeling (TUNEL) Staining.....	47
L. Animal Breeding, DNA extraction, Genotyping and Isolation of ECs.....	48
M. Inducible Deletion using the Genetically Engineered Modified Mice (GEMM) System	51
N. Echocardiography	52
O. JC-1 Staining of Mitochondria.....	53
P. Statistics	53
IV. RESULTS.....	54
A. Nanog Expression in Adult Tissues and Vascular Endothelium	54
B. Wnt3a Induced hTERT Expression and Telomerase Activity (TA) in Vascular ECs.....	57
C. Wnt3a Induced NANOG Binds to <i>hTERT</i> Promoter and Mediates its Transcription	61
D. Loss and Gain-of-NANOG Expression in ECs Alters hTERT Expression.....	65
E. Generation of Timed Inducible Single <i>Nanog</i> Allele Deletion Mice	68
F. Deletion of Endothelial Single <i>Nanog</i> Allele Reduces mTERT Expression <i>in vivo</i>	70
G. <i>Nanog</i> Haplo-insufficiency in ECs Results in Apoptosis of Vascular and non-Vascular Cells of the Heart.....	74

<u>CHAPTER</u>	<u>PAGE</u>
H. <i>Nanog</i> Haplo-insufficiency in ECs Results in Vascular and Perivascular Fibrosis.....	77
I. Loss of single EC- <i>Nanog</i> allele Mice Hearts Displays Cardiac Hypertrophy like Phenotype	79
J. NANOG>hTERT Axis is Necessary for Preventing Apoptosis and Angiogenesis	84
K. NANOG Depletion in ECs Results in a Hyperpolarization of the Mitochondria.....	87
V. DISCUSSION	91
VI. FUTURE DIRECTIONS.....	98
VII. APPENDICES.....	102
A. Sequence Alignment of -3.6kb of human and mouse <i>TERT</i> promoter DNA.	102
B. Dot Matrix Plot of human and mouse <i>TERT</i> promoter.....	108
C. Copy of Approved Vertebrate Animal Protocol	109
VIII. CITED LITERATURE	111
IX. VITA	122

LIST OF TABLES

<u>TABLE</u>	<u>PAGE</u>
Table I: Primer Sequences for qRT-PCR.....	36
Table II. Primer Sequences for Genotyping	51
Table III: Cardiac Physiological Parameters in Control and EC <i>Nanog</i> ^{-/+} Mice	90

LIST OF FIGURES

<u>FIGURE</u>	<u>PAGE</u>
Figure 1: NANOG connects Wnt signaling to hTERT activity in ECs	4
Figure 2: Disruption of EC Homeostasis in the context of cardiovascular pathologies	11
Figure 3: Mitochondria in EC apoptosis	13
Figure 4: Wnt/ β -catenin signaling pathway	16
Figure 5: Transcription factor NANOG	19
Figure 6: Linear structure of hTERT and regulatory elements in hTERT promoter	24
Figure 7: Schematic of events associated with cardiac hypertrophy	30
Figure 8: Expression of NANOG in adult human tissues	55
Figure 9: Expression of Nanog in adult mouse tissues	55
Figure 10: Microscopic analyses of Nanog ⁺ cells in human and mouse heart tissues	56
Figure 11: Wnt3a induced expression of NANOG and hTERT mRNA in arterial and venous ECs	58
Figure 12: hTERT expression and telomerase activity in ECs	60
Figure 13: Scheme of human and mouse <i>TERT</i> promoters indicating NANOG binding sites	63
Figure 14: NANOG binds to the <i>hTERT</i> promoter region and regulates its transcription	64
Figure 15: NANOG knockdown decreases hTERT expression in ECs	66
Figure 16: NANOG mediates expression of hTERT in ECs	67
Figure 17: Generation of the <i>Rosa^{mT/mG}::Nanog^{fl/+}::Cdh5^{CreERT2}</i> mice	69
Figure 18: <i>Cdh5^{CreERT2}</i> mediated timed-inducible deletion of single <i>Nanog</i> allele in adult mouse hearts	73

<u>FIGURE</u>	<u>PAGE</u>
Figure 19: Characterization of Apoptotic (TUNEL ⁺) cells in vWF+ vessels in mice myocardium.	75
Figure 20: NANOG knockdown induces apoptosis in ECs.....	76
Figure 21: Visualizing fibrotic lesion in EC-single Nanog allele deleted mouse hearts	78
Figure 22: Echocardiographic evaluation of EC-specific single <i>Nanog</i> allele deletion in the mouse hearts.....	81
Figure 23. Phenotypic analyses of cardiomyocytes and the cardiac vasculature	82
Figure 24: Cardiac hypertrophy as a result of EC- <i>Nanog</i> haploinsufficiency.....	83
Figure 25: hTERT expression is required for NANOG mediated angiogenic activities of ECs ..	86
Figure 26: Assessing mitochondrial polarization state in response to NANOG depletion in ECs	88
Figure 27: Summary Model	89
Figure 28. Dot Matrix of sequence similarity between the human and mouse TERT promoter DNA.....	108

LIST OF ABBREVIATIONS

AGM	Aorta-Gonad-Mesonephros
AMI	Acute Myocardial Infarction
ANOVA	Analysis of Variance
ANP	Atrial Natriuretic Peptide
AP-1	Activator Protein-1
APC	Adenomatous polyposis coli
BCIP	5-Bromo-4-chloro-3-indolyl phosphate/nitroblue tetrazolium (BCIP/NBT)
BMP	Bone Morphogenetic Protein
BNP	Brain Natriuretic Peptide
BrdU	5-bromo-2'-deoxyuridine
BSA	Bovine Serum Albumin
BW	Body Weight
CD31	Cluster of Differentiation 31
Cdh5 ^{CreERT2}	Cadherin 5-Cre Estrogen Receptor Type 2
cDNA	Complimentary Deoxyribonucleic acid
CH	Cardiac Hypertrophy
CHAPS	3-((3-cholamidopropyl) dimethylammonio)-1-propanesulfonate
CHF	Congestive Heart Failure
ChIP	Chromatin Immunoprecipitation
CKI α	Casein Kinase I alpha
CO	Cardiac Output
Co-IP	Co-Immunoprecipitation
CVD	Cardiovascular Disease
DAAM1	Disheveled Associated Activator of Morphogenesis 1
DAPI	4',6-diamidino-2-phnylindole
DMEM	Dulbecco's Modified Eagle Medium
DNA	Deoxyribonucleic Acid
Dsh/Dvl-1	Dishevelled or Disheveled-1

LIST OF ABBREVIATIONS (continued)

EC	Endothelial Cell
EDTA	Ethylenediaminetetraacetic acid
EF	Ejection Fraction
EG	Embryonic Germ
ELISA	Enzyme-linked Immunosorbent Assay
EMSA	Electrophoretic Mobility Shift Assay
EndMT	Endothelial-Mesenchymal Transition
EpiSCs	Epiblast Stem Cells
ESC	Embryonic Stem Cell
ET-1	Endothelin-1
FGF	Fibroblast Growth Factor
Fl	flanked by loxP (aka Floxed)
FLK1	Fetal Liver Kinase-1
FS	Fractional Shortening
Fzd	Frizzled
GAPDH	Glyceraldehyde-3-phosphate dehydrogenase
GEMM	Genetically Engineered Mouse Model
GF	Growth Factor
GFP	Green Fluorescent Protein
GL-H	Gaussia Luciferase-High Sensitivity
GLuc	Gaussia Luciferase
GSK-3 β	Glycogen Synthase Kinase-3 β
H&E	Hematoxylin & Eosin
HA	Hemagglutinin
HBSS	Hanks Balanced Salt Solution
HEPES	4-(2-hydroxyethyl)-1-piperazineethanesulfonic acid
HIF	Hypoxia Inducible Factor
HPAEC	Human Pulmonary Artery Endothelial Cell
HRP	Horseradish Peroxidase

LIST OF ABBREVIATIONS (continued)

HSaVEC	Human Saphenous Vein Endothelial Cell
HUVEC	Human Umbilical Vein Endothelial Cell
ICM	Inner Cell Mass
iPSCs	Induced Pluripotent Stem Cells
KLF	Krüppel Like Factor
KOMP	Knockout Mouse Project
LIF/STAT	Leukemia Inhibitory Factor/Signal Transducers and Activators of Transcription
LRP	Lipoprotein Receptor-related Protein
LV	Left Ventricle
LVDd	Left Ventricular Diameter at diastole
LVVd	Left Ventricular Volume at diastole
MAPK	Mitogen Activated Protein Kinase
MEM	Minimum Essential Medium
Mesp1	Mesoderm Posterior 1 Homolog
mG	Membrane-targeted EGFP
MI	Myocardial Infarction
mRNA	Messenger Ribonucleic Acid
mT	Membrane-Targeted Tomato protein
MTA	Material Transfer Agreement
Myh7	Myosin Heavy Chain isoform-7
NBE	NANOG Binding Element
NC	Nitrocellulose
NFAT	Nuclear Factor of Activated-T cells
NIH	National Institute of Health
NO	Nitric Oxide
NP	Natriuretic Peptides
OCT	Optimal Cutting Temperature
OCT4	Octamer-4
PAD	Peripheral Arterial Disease

LIST OF ABBREVIATIONS (continued)

PAX	Paired box
PBS	Phosphate Buffered Saline
PBST	PBS containing 0.1% Triton-X 100
PCP	Planar Cell Polarity
PDGF	Platelet Derived Growth Factor
PEST	Proline, Glutamic, Serine Threonine
PFA	Paraformaldehyde
PGC-1	Peroxisome proliferator Gamma Co-receptor-1
PGC	Primordial Germ Cell
PI	Propidium Iodide
PI3K	Phosphoinositol-3-Kinase
PIC	Phosphatase Inhibitor Cocktail
PTM	Post Translational Modification
QC	Quality Control
qPCR	Quantitative PCR
qRT-PCR	Quantitative Real-Time Polymerase Chain Reaction
RIPA	Radioimmunoprecipitation Assay
RNP	Ribonucleoprotein
ROSA	Reverse Orientation Splice Acceptor
RV	Right Ventricle
RVH	Right Ventricular Hypertrophy
SDS	Sodium Dodecyl Sulphate
SEAP	Secreted Alkaline Phosphatase
SFRP1	Secreted Frizzled-Related Protein 1
shRNA	Short hairpin RNA
siRNA	Small interfering RNA
SOX	<u>S</u> ry-related HMG <u>box</u>
SV	Stroke Volume
TA	Telomerase Activity

LIST OF ABBREVIATIONS (continued)

TAM	Tamoxifen
TBS	Tris Buffered Saline
TBST	Tris Buffered Saline with 0.1% Tween-20
TCF/LEF	T-Cell Factor/Lymphoid Enhancer Factor
TdT	Terminal deoxynucleotidyl Transferase
TE	Tris-EDTA
TEN	Telomerase Essential N-terminal domain
TER	Telomerase RNA
TERC	Telomerase RNA Component
TERT	Telomerase Reverse Transcriptase
TF	Transcription Factor
TGF β	Transforming Growth Factor-beta
TnT	Troponin T
TRAP	Telomerase Repeat Amplification Protocol
TRBD	Telomerase RNA Binding Domain
TS	Template Specific
TSS	Transcription Start Site
TUNEL	Terminal Deoxynucleotidyl transferase dUTP nick end labeling
UC	University of California
VE-cadherin	Vascular Endothelial-cadherin
VEGF	Vascular Endothelial Growth Factor
VEGFR2	Vascular Endothelial Growth Factor Receptor-2
vWF	von Willebrand Factor
WB	Western Blotting
WGA	Wheat Germ Agglutinin
Wnt	Wingless Int-1
α SMA	Alpha Smooth Muscle Actin
β -MHC	Beta-Myosin Heavy Chain

SUMMARY OF THE DOCTORATE THESIS

The vascular endothelium represents an important physiological and functional entity in the mammalian heart (Aird 2007; Rocha and Adams 2009; Pircher et al. 2016). A variety of genetic and non-genetic components play a crucial role in maintaining the homoeostatic balance in the cardiac microvasculature (Dejana, Hirschi, and Simons 2017; Hogan et al. 2017). Vascular endothelial cell (EC) homeostasis is an important biological process which includes multiple events such as survival, proliferation, regulation of vascular tone, response to inflammation or re-vascularization of injured tissues following injury (Rubanyi 1993; Aird 2008; Favero et al. 2014; Gimbrone and Garcia-Cardena 2016). In this context, the Wnt/ β -catenin signaling pathway plays an important role in the regulation of cardiovascular physiology (Bergmann 2010; Marinou et al. 2012). Importantly, the intracellular signaling components of the canonical Wnt signaling pathway are present in the adult myocardial ECs (Aisagbonhi et al. 2011). Accordingly, Wnt/ β -catenin signaling induced expression of Nanog in myocardial ECs (Baruah et al. 2017). Together, these reports indicate that the canonical Wnt/ β -catenin pathway in adult myocardial ECs plays an important role in maintaining coronary vasculature *via* the Nanog transcriptional network.

NANOG is detectable in primary ECs including HUVECs and lung microvascular ECs, however, its expression is increased in a Wnt3a ligand dependent manner (Kohler et al. 2011; Kohler et al. 2014; Baruah et al. 2017). The role of NANOG in regulating angiogenic activities of ECs, such as proliferation and the ability to form capillary-like networks *in vitro* and *in vivo* have been previously established by us (Kohler et al. 2014; Baruah et al. 2017). NANOG mediates this activity by transcriptionally upregulating *vascular endothelial growth factor receptor 2 (VEGFR2)* mRNA, which encodes a cell surface receptor tyrosine kinase, a key

component of proliferative and survival activities of ECs. In addition, the increased expression of NANOG led to activation of NANOG target genes in ECs (Kohler et al. 2014). Interestingly, the global *Nanog* gene knockout is incompatible with life, as the embryos die as early as E4.5 days and conditional deletion of *Nanog* induced apoptosis in mouse migrating primordial germ cells (PGC) (Yamaguchi et al. 2009; Chen, Du, and Lu 2012). The studies performed herein confirmed Nanog expression in the cardiac microvasculature. Upon activation of the canonical Wnt signaling pathway in ECs, we observed a quantitative increase in the expression of NANOG. This event in-turn increased the expression of human telomerase reverse transcriptase (hTERT) at the mRNA and protein levels in ECs in a quantitative manner. Furthermore, utilizing high-resolution confocal imaging and telomerase repeat amplification protocol (TRAP) assay, we detected and quantified increased expression of hTERT and induction of telomerase activity (TA) in ECs.

hTERT is a recently described target of the canonical Wnt signaling pathway (Hoffmeyer et al. 2012; Y. Zhang et al. 2012). hTERT is an important component of ECs and reduced expression have been suggested to compromise endothelial function (Falchetti et al. 2008; Zurek et al. 2016). hTERT is also important in promoting and maintaining cell survival in multiple cell types including ECs (Chang et al. 2005; Falchetti et al. 2008). Although, several signaling pathways could mediate the expression of hTERT in several cell types (Ramlee et al. 2016), however, its regulation in ECs is less understood. To activate canonical Wnt signaling in ECs, I carried-out a chromatin immunoprecipitation (ChIP) assay in these cells after Wnt3a stimulation; I found that Wnt3a induced NANOG protein binding to the upstream DNA promoter regions of the *hTERT* gene. Next, I conducted transfection experiments and promoter activity assays using promoter-luciferase reporter (wild-type and deletion mutants) constructs of *hTERT* that harbored

putative NANOG binding elements (NBE). Interestingly, the increased expression of NANOG in response to Wnt3a stimuli led to direct binding of NANOG to the *hTERT* promoter region, and an increased transcription. This increase in expression of NANOG and hTERT maintained the survival phenotype of ECs.

We further validated NANOG mediated transcriptional regulation of hTERT in ECs by conducting loss and gain-of-function studies. With the use of *shRNA* mediated *NANOG*-knockdown studies, we detected a decrease in hTERT expression at the gene and protein levels. Interestingly, overexpressing *NANOG* in cultured ECs led to increased expression of hTERT protein along with additional NANOG target genes such as *CYCLIN-D1* and *VEGFR2*.

In order to determine the functional relevance of the NANOG>hTERT signaling axis *in vivo*, we utilized the genetically engineered mouse model (GEMM) system. The global deletion of *Nanog* is embryonic lethal, its function in adult tissues has not been addressed and the loss of single *Nanog* allele (haploinsufficiency) has not been examined (Yamaguchi et al. 2009; Chen et al. 2012). Therefore, using our GEMM system allowed us to inducibly delete a single allele of *Nanog* in a time-dependent manner in adult. Upon tamoxifen (TAM) administration, the *Cdh5^{CreERT2}* mediated Cre recombinase activity deleted a single allele of *Nanog* effectively in the adult vascular ECs in their native microenvironment. The use of the *Rosa^{mT/mG}* reporter background allowed us to monitor the fidelity of TAM-mediated Cre expression and deletion of single *Nanog* allele in adult ECs. In Control and EC *Nanog^{-/+}* mouse hearts, the CD31⁺ cardiac ECs showed a reduced expression of *Tert* and *Vegfr2* at the mRNA and protein levels.

Given that *Nanog* and *Tert* are critical regulators of cell survival, we analyzed the phenotype resulting from deletion of single *Nanog* allele in adult mouse hearts. Phenotypic evaluation of mouse hearts at days 7, 14, 21 and 30 post-TAM administration using

immunohistochemistry indicated increased apoptotic death of vascular ECs and non-vascular cells. While it was interesting to observe apoptotic death in the non-vascular cellular compartments, I did not address the mechanism as to how the loss of single *Nanog* allele in the vascular EC compartment led to death of adjacent cells of the heart tissue. These results were confirmed *in vitro* when we observed that *shRNA* mediated depletion of *NANOG* in ECs resulted in an increased Annexin-V⁺ and Propidium iodide (PI)⁺ apoptotic cells.

Unwanted apoptotic cell death *in vivo* can lead to a deleterious effect on the surrounding tissue microenvironment (Kockx and Knaapen 2000; van Empel and De Windt 2004; Winn and Harlan 2005). Deletion of single *Nanog* allele in adult mice resulted in altered vascular structures. Morphometric analysis of myocardial tissue sections after Masson's trichrome staining revealed increased collagen deposits in and around the vascular structures.

In concert with immunohistological and morphometric analyses, we conducted an echocardiographic (ECG) evaluation of Control and EC *Nanog*^{-/+} mouse hearts at day 30 post-TAM administration. Unwanted apoptotic cell death and fibrosis are some of the key events associated with the progression of cardiac hypertrophy (CH) (Krijnen et al. 2002; van Empel et al. 2005; Segura, Frazier, and Buja 2014). EC *Nanog*^{-/+} mouse hearts displayed an increase in parameters which indicated CH concomitant with a decline in cardiac function. Upon examining freshly excised hearts, EC *Nanog*^{-/+} mouse hearts were enlarged in size compared to the control group. Hematoxylin and Eosin (H and E) staining and wheat germ agglutinin (WGA) staining of thin myocardial sections revealed increased cardiomyocyte area, a key hallmark of hypertrophic hearts. Importantly, the expression of *Anp*, *Bnp*, *Myh7* and *Et-1*, genes that are associated with CH were increased. *NANOG* depletion, thereafter a rescue experiment indicated the role of

NANOG in the regulation of *hTERT* transcription in ECs, which restored the survival phenotype of these cells.

Together, the results presented in this thesis establish a novel mechanism by which the basal expression of EC-Nanog plays an essential role in maintaining EC homeostasis in adult cardiac vasculature.

I. INTRODUCTION

A. Background

Nanog is a member of the homeobox family of DNA binding transcription factors and is essential in maintaining self-renewal and pluripotency of Embryonic Stem Cells (ESCs) (Chambers et al. 2003; Chambers et al. 2007; Silva et al. 2009). Nanog is detected early on during development, specifically in ESCs, embryonic germ (EG) cells, aorta-gonad mesonephros, and numerous tumor cell lines (Wang et al. 2008; Komatsu and Fujimori 2015; Jeter et al. 2015). Nanog plays a crucial role in the preimplantation stage of development and safeguards pluripotency (Wang et al. 2008; Silva et al. 2009; Komatsu and Fujimori 2015). In conjunction with the Yamanaka factors (OCT-4, SOX2, KLF4, and c-MYC), NANOG can mediate the efficient conversion of somatic cells into induced pluripotent stem cells (iPSCs) (Boyer et al. 2005; Takahashi and Yamanaka 2006; Chambers et al. 2007). Upon implantation, the pluripotency factors, including Nanog, is silenced in most tissues. Therefore, Nanog was thought to be a ‘stem cell exclusive’ factor, with no role in non-ESCs and adult tissues. Interestingly, NANOG is frequently found to be overexpressed in human cell carcinomas (Jeter et al. 2015). A systemic analysis of *Nanog* expression in non-transformed cells and adults tissues, has contradicted this existing idea (Busch et al. 2008; Luo et al. 2014; Piazzolla et al. 2014; Li et al. 2017; Baruah et al. 2017). Immunohistological analysis confirm Nanog expression in sprouting ECs and we have previously shown that Wnt3a induces expression of NANOG in ECs and stimulated cell proliferation and angiogenesis during neovascularization events (Busch et al. 2008; Kohler et al. 2011; Baruah et al. 2017). In a clinically relevant model of acute myocardial infarction (AMI), there was a strong upregulation of Nanog in ischemic hearts, which indicated the relevance of this protein in adult tissues repair (Baruah et al. 2017). Therefore, although *Nanog* was initially identified as the ‘master gene’ of ESC pluripotency and its

expression thought to be repressed in adult tissues, I observed that low levels of Nanog are detectable in the adult endothelium comprising the cardiac microvasculature where it plays a role in maintaining tissue homeostasis.

ECs that comprise the adult vascular tree are quiescent and have extremely low or no regenerative potential (Anversa et al. 2007; Kajstura et al. 2010; Frati et al. 2011; De Bock, Georgiadou, and Carmeliet 2013). These quiescent ECs are known to play an important role in regulating the homeostatic function of the endothelium by maintaining integrity, responding to inflammation, or proliferating in response to tissue injury in order to reestablish the blood flow (Rubanyi 1993; Deanfield, Halcox, and Rabelink 2007; Khazaei, Moien-Afshari, and Laher 2008; Sandoo et al. 2010). In this context, Wnt-signaling is known to activate quiescent or post-mitotic cells in the adult tissues in a temporal and spatial manner (Korn et al. 2014; Loh, van Amerongen, and Nusse 2016). The canonical Wnt signaling pathway is activated when a Wnt ligand binds to its receptor, Frizzled (Fzd), resulting in the inhibition of the Glycogen Synthase Kinase-3 β , thus stabilizing β -catenin polypeptide species. This leads to nuclear translocation of β -catenin where it activates Wnt target genes (Cadigan 2008; Ramakrishnan and Cadigan 2017). Another important factor responsible for maintaining endothelial integrity and function is Tert (Edo and Andres 2005; Higashi, Kihara, and Noma 2012). Downregulation of Tert in ECs as a consequence of aging leads to loss of homeostatic endothelial function. In this study, we utilized a GEMM system, combined with *in vitro* gain and loss-of-function studies to understand the role of Nanog expression in the adult microvasculature. The GEMM *Rosa^{mT/mG}::Nanog^{fl/+}::Cdh5^{CreERT2}* allowed us to inducibly delete a single *Nanog* allele specifically in the adult vascular endothelium and determine its role in tissue homeostasis.

In the current study, I addressed the role of Nanog expression in the coronary vasculature in the adult mouse. I analyzed the importance of Nanog and its downstream effector Tert in

maintaining the homeostatic role of ECs in the cardiac microenvironment. I propose that Wnt3a-induced NANOG binds to the *hTERT* promoter region and regulates hTERT expression in ECs, and that Tert maintains the EC homeostasis in cardiac vasculature by promoting the survival phenotype of these cells (**Figure 1**).

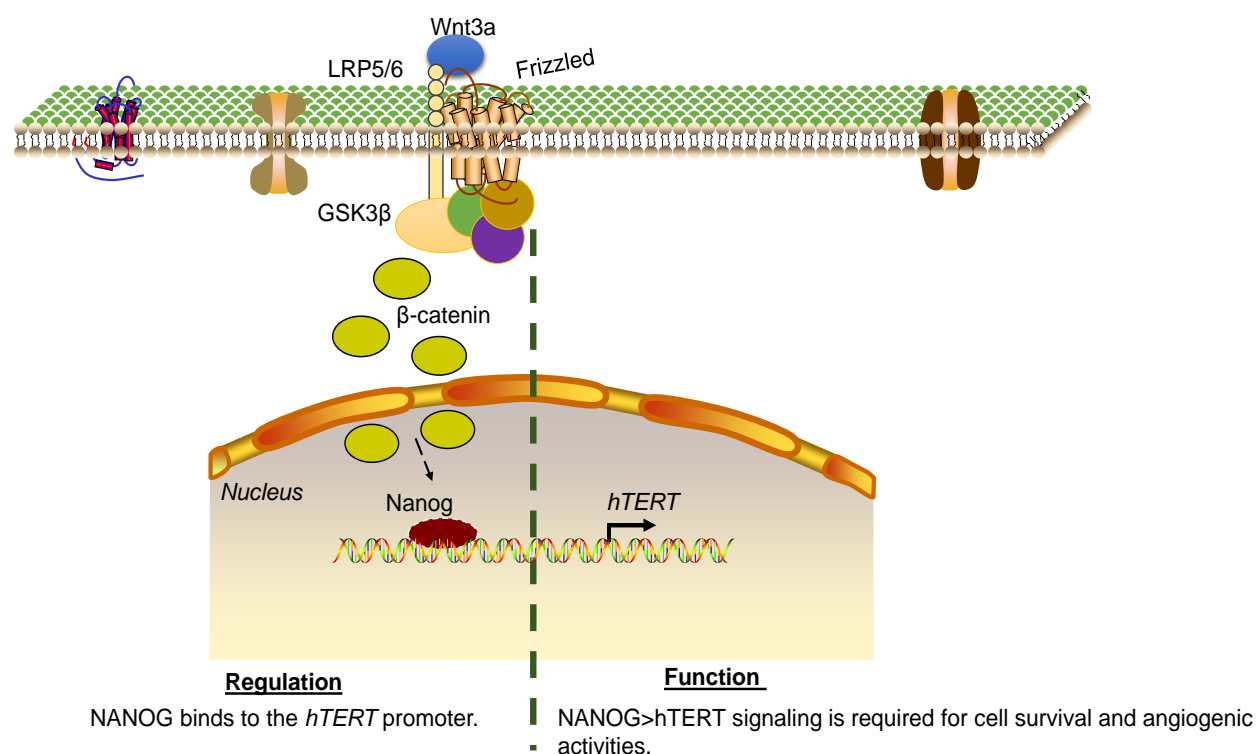


Figure 1: NANOG connects Wnt signaling to hTERT activity in ECs. Stimulation with Wnt3a leads to stabilization of β-catenin in the cytosol. Activities of Wnt/β-catenin drive expression of NANOG in ECs. Thereafter, NANOG binds to the *hTERT* promoter and induces expression of hTERT and telomerase enzymatic activity in ECs. Accordingly, NANOG>hTERT signaling axis is important in maintaining a survival phenotype of ECs and in the regulation of angiogenic activities of these cells.

B. Rationale

Neovascularization, primarily driven by the ECs, is an essential biological process required for the survival of tissues that normally occurs during embryonic development and wound healing. In the adult, excessive or insufficient neovascularization is associated with many cardiovascular diseases (CVD) including heart failure and peripheral arterial disease (PAD). Revascularization or re-establishment of blood supply to the ischemic tissue, is a clinically relevant goal. However, mechanisms underlying neovascularization of ischemic and/or injured tissues in the adult remain incompletely understood. The transcription factor (TF) Nanog is highly expressed in the embryonic stem cells (ESC) and to a lesser extent in adult stem cells. We have observed low levels of Nanog expression in adult ECs, however, the functional significance of expression of Nanog is incompletely understood.

Genetic haploinsufficiency results when a single copy of a gene is inadequate to maintain the normal function of the gene. This is a major cause of “autosomal dominant disease”. Importantly, several genetically predisposed heart conditions are inherited in an “autosomal dominant manner”. ‘Autosomal’ means that both sexes are equally affected, whereas, ‘dominant’ means that although there are two copies of each gene, a mutation in just one copy is sufficient to cause disease. Here, I created a mouse model to address the concept of haploinsufficiency by deleting one copy of the *Nanog* gene in an EC-specific manner that resulted in cardiac hypertrophy.

C. Hypothesis

Here, I address *the central hypothesis* that

- a. Quantitative changes in the level of expression of Nanog and Tert in ECs critically regulate EC-homeostasis and neovascularization potential in the adult.*
- b. We also address the hypothesis that NANOG and hTERT signaling module might be key to understanding the cardiac hypertrophy (CH) phenotype, secondary to decreased level of Nanog expression in adult ECs.*

D. Significance

In the United States alone, 1 out of 3 individuals die from a cardiovascular disease (CVD) and heart disease is currently the number one cause of death (Benjamin et al. 2018). Among them, acute ischemic injury and cardiomyocyte hypertrophy (CH) represents the most common manifestations of acute and chronic insults to the heart (Tardiff 2006; Carabello 2014; Anderson and Morrow 2017). CH can be physiological as seen in trained athletes or during normal growth, or it can be pathological if it arises as secondary event associated with myocardial infarction (MI), hypertension, valvular heart disease, or cardiomyopathy (Frey and Olson 2003; Hill 2015). During later stages of the disease, pathological hypertrophy can result in systolic and diastolic dysfunction of the heart and interstitial fibrosis leading to deleterious consequences including congestive heart failure, arrhythmia, and sudden death (Treibel et al. 2017).

The hypertrophic growth of cardiomyocytes is primarily due to mechanical stress and neurohumoral stimuli, which in turn leads to activation of a cascade of cellular responses like gene transcription, protein synthesis, alteration in sarcomere assembly, and/or changes in ion channel properties (Frey and Olson 2003; Selvetella et al. 2004; Tardiff 2006; Shimizu and

Minamino 2016). The cellular composition of the heart is diverse, consisting of ECs, cardiac fibroblasts, inflammatory cells, and other non-myocytes (Pinto et al. 2016; Zhou and Pu 2016). It is now clear that multiple signaling events that mediate the direct or indirect communication between the cardiomyocytes and non-myocytes trigger events associated with CH (Kamo, Akazawa, and Komuro 2015; Lim et al. 2015). Interestingly, ECs which form the endothelium comprise approximately 60% of the non-myocyte cell population in the heart (Pinto et al. 2016; Zhou and Pu 2016). In the basal state, or uninjured heart, the endothelium serves as a barrier between circulating blood and the walls of the vessels or cardiac chambers, as well as act as a dynamic sensor to fine-tune myocardial structure and function, thereby maintaining homeostasis in the heart (Rubanyi 1993; Deanfield et al. 2007; Khazaei et al. 2008; Sandoo et al. 2010). But, in the event of an injury to the heart, myocardium releases various angiogenic growth factors to stimulate angiogenic growth which in turn accommodate an increase in myocardial mass and performance (Deanfield et al. 2007; Red-Horse et al. 2007; Favero et al. 2014). In addition to this, various factors that are secreted by the endothelium such as Nitric Oxide (NO) and endothelin-1 (ET-1) are known to be critical factors in mediating angiogenesis-induced myocardial hypertrophy (Kempf and Wollert 2004; Bohm and Pernow 2007; Farah, Michel, and Balligand 2018).

In this context, the Wnt signaling pathway is known to play an important role both during embryonic development and remodeling of the adult heart (Brade, Manner, and Kuhl 2006; Mazzotta et al. 2016). During cardiac development, Wnt/ β -catenin signaling is stage-specific, and *Mesp1/2⁺* progenitor cells from the mesoderm give rise to nascent cardiac structures. During later stages of cardiac differentiation, Wnt/ β -catenin signaling is repressed in the cardiac mesoderm (David et al. 2008). Such altered expression ensures amplification of cardio myogenic

precursors of the first and second heart field, which ultimately give rise to the left and right ventricle of the heart (Kwon, Cordes, and Srivastava 2008). Most importantly, in an adult heart, canonical Wnt signaling activity is confined to the larger vessels and coronary vasculature (Aisagbonhi et al. 2011). However, the significance of Wnt signaling in adult coronary vessels remains incompletely understood.

The Wnt/ β -signaling pathway activates a cascade of genes that play distinct roles in cell proliferation, migration, and survival (Cohen, Tian, and Morrissey 2008; Franco, Liebner, and Gerhardt 2009; Mazzotta et al. 2016). ECs are known to express all components of the canonical Wnt signaling pathway, and therefore express a variety of Wnt target genes which are essential in different EC functions (Goodwin, Sullivan, and D'Amore 2006; Korn et al. 2014). Our laboratory has shown Wnt3a stimulation of cultured ECs or the allosteric inhibition of GSK-3 β induced expression of Nanog in ECs *in vitro* and *in vivo* (Kohler et al. 2011; Kohler et al. 2014; Baruah et al. 2017). Recently, we have shown that coronary ECs which participate in neovascularization events express Nanog during the reparative phases of myocardial tissues after episode of acute myocardial infarction (AMI) (Baruah et al. 2017). This indicated a potential role of the Nanog transcriptional network in the mechanism of the adaptive response. As *Nanog* is a Wnt target gene in adult vascular ECs, here I examined the potential protective role of *Nanog* in the adult ECs in cardiac vascular beds.

In this study, we addressed the mechanism of Wnt3a induced NANOG transcription in ECs and determined the functional significance of low level expression of Nanog in these cells. We further explored the phenotypic effects of inducible loss of a single *Nanog* allele in mouse myocardial ECs and delineated the potential downstream effectors of NANOG transcriptional networks in ECs. With the use of genetic EC-lineage tracing methodology, I determined the

effect of loss of Nanog expression in myocardial vasculature and elucidated the role of quantitative changes in Nanog expression in cardiac ECs in relation to EC-homeostasis. The results of my research further our understanding of the potential role of Nanog transcriptional networks in adult ECs.

II. LITERATURE REVIEW

A. Homeostasis at the Level of Endothelial Cells

Homeostasis at the level of a tissue is a self-regulating process which maintains stability and optimal conditions for survival by responding to both internal and external stimuli (Biteau, Hochmuth, and Jasper 2011; Brown et al. 2017). In the cardiovascular system, homeostasis is maintained by a complex interplay of genetic and epigenetic events, and disruption of this equilibrium can lead to complications such as myocardial infarction, stroke, hypertrophy, and atherosclerosis (**Figure 2**). The vasculature which is comprised of ECs, smooth muscle cells, and fibroblasts form an integrated system to maintain tissue homeostasis (Aird 2007; Rocha and Adams 2009; Ramasamy, Kusumbe, and Adams 2015; Awgulewitsch, Trinh, and Hatzopoulos 2017). ECs that line the vessels respond to physiological alterations within the vessel wall and the target organs via multiple factors which affects its structure and function (Aird 2008; Favero et al. 2014; Pircher et al. 2016). Thus, ECs are not only called the vascular gatekeepers but can contribute to the pathogenesis of cardiovascular disease (Deng, Huo, and Luo 2014).

Endothelial homeostasis role broadly encompass miscellaneous functions such as regulation of vasomotor tone, promotion and prevention of vascular growth, acute responses to adapt to blood flow according to tissue demands, and sustained responses such as re-vascularization during an injury (Michiels 2003; Kazmi, Boyce, and Lwaleed 2015). The EC functions that support repair of damaged endothelium are re-vascularization, sprouting of ECs, and survival, during stress (Tang and Conti 2004; Dauwe et al. 2016). In this context, a fundamental event that regulates endothelial homeostatic functions is apoptosis (Kockx and Knaapen 2000).

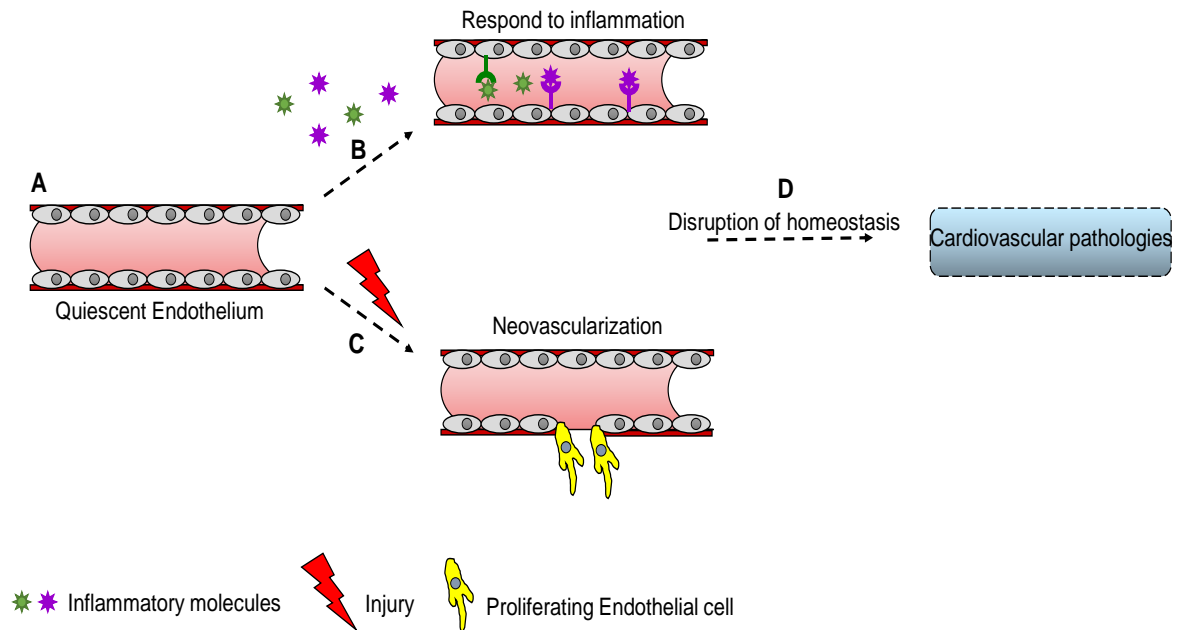


Figure 2: Disruption of EC Homeostasis in the context of cardiovascular pathologies. A) A quiescent or intact endothelium regulates flow of blood to tissue. B) In the presence of inflammatory molecules, ECs upregulate various receptors in order to maintain a homeostatic environment. C) During a physiological or pathological injury, resident ECs respond to different paracrine or autocrine factors, resulting in EC proliferation to mediate neovascularization. D) An imbalance or disruption of the homeostatic state of the endothelium can lead to aberrant physiological responses associated with cardiovascular pathologies.

In vivo ECs get exposed to stimuli that may either promote or prevent apoptosis. Any event that disrupts the balance between pro and anti-apoptotic stimuli can contribute to the pathogenesis of numerous cardiovascular diseases (CVDs) (Kockx and Knaapen 2000; Dimmeler and Zeiher 2000; Chavakis and Dimmeler 2002; Gimbrone and Garcia-Cardena 2016). Apoptosis of ECs *in vivo* can trigger vascular leakage, the release of chemokines or inflammatory molecules, along with active recruitment of inflammatory cells and fibroblasts in the adjacent tissue (Rock and Kono 2008; Sprague and Khalil 2009). An apoptotic EC can become proadhesive towards platelets and leukocytes or can promote coagulation *in situ*, before detachment (Winn and Harlan 2005). EC apoptosis, which disrupts the homeostasis of ECs, has

been reported in human patients with Congestive Heart Failure (CHF) and in animal models of hypertension (Winn and Harlan 2005). In addition, apoptosis has also been implicated in hypertension, atherosclerosis, and vascular proliferative diseases (van Empel et al. 2005; Winn and Harlan 2005).

At the molecular level, apoptosis or programmed cell death is initiated in the mitochondria, which is the metabolic powerhouse of the cell (Kluge, Fetterman, and Vita 2013). **(Figure 3)** represents a schematic of mitochondria as a central mediator of apoptosis in ECs. *In vivo*, several physiological stimuli such as hypoxia and ischemic injury to tissues can lead to mitochondrial stress and thus leads to activation of the apoptotic cascade in ECs (Davidson and Duchon 2007). In addition to physiological stimuli, alterations in the molecular machinery that ensures cell survival can lead to ectopic death in ECs. In this context, we have found that NANOG acts upstream of *VEGFR2*, also known as the *Fetal Liver Kinase-1 (FLK1)* signaling pathway (Kohler et al. 2011). VEGFR2 binds to the Vascular Endothelial Growth Factor (VEGF) class of ligands and ensures EC survival. Interestingly, *Nanog* knockdown in ESCs induced growth arrest and apoptosis (Chen et al. 2012), and conditional depletion of Nanog in migrating mouse primordial germ cells (PGCs) induced apoptotic cell death (Yamaguchi et al. 2009). These data suggest that *in vivo*, Nanog expression in other cell types is important in preventing apoptosis and it is possible that low levels of Nanog expression in adult ECs also prevents apoptotic cell death and thereby maintains the homeostatic environment of the vasculature. In this study, we utilized the Genetically Engineered Mouse Model (GEMM) system complemented with *in vitro* loss and gain-of NANOG function studies to characterize the phenotype resulting from *Nanog* deletion in the vascular endothelium, and precisely address whether Nanog loss in vascular ECs of adult tissue leads to apoptotic cell death.

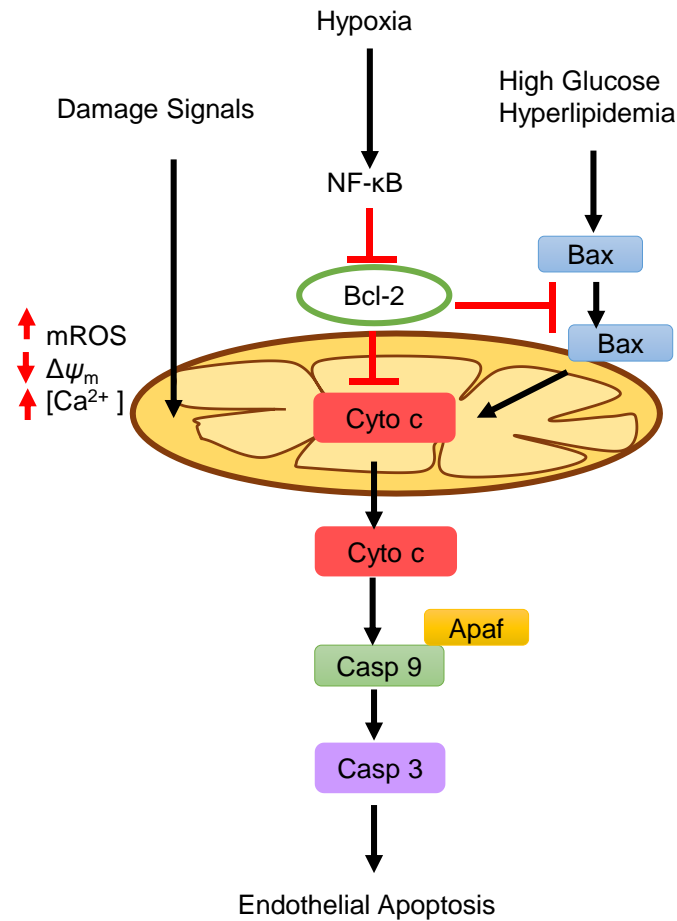


Figure 3: Mitochondria in EC apoptosis. Multiple factors such as hypoxia, metabolic stress (High glucose, Hyperlipidemia), or damage signals, alters signaling events upstream of the mitochondria. These events lead to the release of cytochrome-c (cyto C) into the cytosol from the mitochondria. Cyto c activates caspase-9 (casp-9), which is the initiator caspase. This leads to the activation of apoptotic cascade in a cell, resulting in cell death. *Adapted from Tang et al, Frontiers in Physiology 2014.*

B. Wnt Signaling Pathway

The Wingless (Wnt) signaling pathway is a well-established and developmentally regulated pathway. It regulates various biological processes involved in embryonic development as well as the physiology of adult tissues and organs in a spatiotemporal manner (Komiya and Habas 2008; MacDonald, Tamai, and He 2009; Clevers, Loh, and Nusse 2014). Structurally, Wnts are comprised of a primary sequence that has 21 cysteine residues which are spaced in a specific manner. As extracellular signaling molecules, Wnts can mediate diverse effects ranging from cell proliferation, apoptosis, migration, polarization, stem cell maintenance and differentiation, and tissue homeostasis (Clevers et al. 2014). Wnt signaling is highly complex and characterized by the presence of 19 Wnt ligands that bind to 10 different members of the seven transmembrane-spanning family of G-protein coupled Frizzled (Fzd) receptors (Cadigan 2008; Reis and Liebner 2013). Therefore, depending on the type of interaction between Wnt and Fzd, combined with the presence of co-receptors, the downstream effects of Wnt signaling can vary.

The Wnt signaling pathway is described by three divergent pathways; canonical Wnt/ β -catenin signaling, non-canonical Wnt- Ca^{2+} , and the planar cell polarity (PCP) pathway (MacDonald et al. 2009). The non-canonical pathways are known to be initiated by Wnt4, Wnt5a and Wnt11 ligands (Cadigan 2008; MacDonald et al. 2009). In case of the Ca^{2+} pathway, binding of Wnt ligand to its receptor leads to activation of the protein Dishevelled (Dsh or Dvl) followed by phospholipase C activation which increases calcium influx in cells. This leads to the activity of Ca^{2+} -sensitive enzymes and the activation of nuclear factor of activated-T cells (NFAT), a transcription factor that is known to regulate VEGF induced angiogenesis during normal vessel patterning (MacDonald et al. 2009; Franco et al. 2009; Samarzija et al. 2009). The PCP pathway proceeds by activation of small GTPases Rac1, Cdc42 and RhoA/B leading to cell polarization

and cytoskeletal rearrangement. In ECs, the downstream effect of the PCP pathway activates Dishevelled associated activator of morphogenesis 1 (DAAM1), a factor that inhibits proliferation and migration (Franco et al. 2009; Samarzija et al. 2009). Although canonical Wnt signaling is relatively novel in ECs, it is well understood in comparison to the non-canonical pathways.

The Wnt/ β -catenin pathway is activated when a ligand such as Wnt3a binds to the Fzd receptor and its co-receptor, low-density lipoprotein receptor-related protein 6 (LRP6) or co-receptor LRP5 (MacDonald et al. 2009). This leads to the recruitment of the Axin protein complex to the receptor proximity. The Axin degradation complex consists of Axin, Adenomatous polyposis coli (APC), Casein kinase 1 α (CK1 α), and Glycogen Synthase Kinase-3 β . Recruitment of the Axin complex to the membrane proximity inactivates the degradation complex, thereby leading to stabilization of β -catenin in the cytosol. Consequently, β -catenin translocates to the nucleus where it replaces Groucho, thus converting TCF/LEF from the repressive state to a transcriptionally active state leading to active transcription of Wnt target genes (**Figure 4**). In the absence of a Wnt ligand, the cytoplasmic β -catenin is constantly degraded by the Axin complex. Sequential phosphorylation by CK1 α and GSK-3 β targets β -catenin for recognition by β -Trcp, a component of the ubiquitin-mediated proteasome degradation pathway (MacDonald et al. 2009).

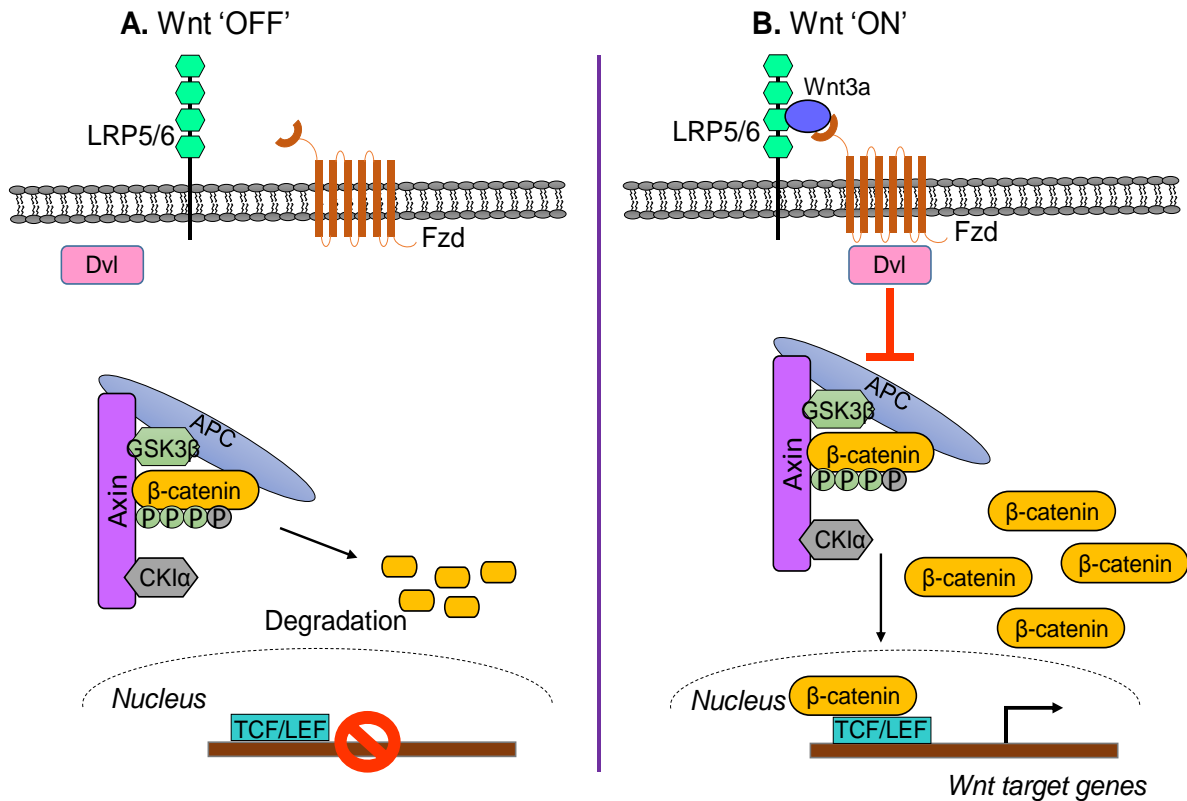


Figure 4: Wnt/β-catenin signaling pathway. A) In the absence of natural ligand (Wnt3a), β-catenin is held in complex with Axin and Adenomatous polyposis coli (APC) protein. Constitutive phosphorylation by GSK-3β and CK1α results in the degradation of β-catenin by the ubiquitin mediated proteasome degradation pathway. B) In the presence of a ligand (such as Wnt3a), binding of Wnt to its cognate receptor Frizzled (Fzd) and co-receptors LRP5/6 leads to recruitment of scaffolding protein Dishevelled (Dvl) to receptor. This leads to inhibition of the Axin-APC complex, leading to stabilization of β-catenin in the cytosol. Cytosolic β-catenin then translocates to the nucleus where it forms complex with the TCF/LEF family of transcription factors leading to active transcription of Wnt target genes. Adapted and modified from V. Stylianidis *et al.* 2017.

Transcriptional targets of the Wnt pathway include multiple genes involved in cell proliferation, survival, migration, and tissue homeostasis such as *Nanog*, *c-myc*, *Cyclin-D1* and *Tert* (Hoffmeyer et al. 2012; Kohler et al. 2014; Ramakrishnan and Cadigan 2017). The transcription factor NANOG plays a role in EC proliferation and angiogenic activities. Cyclin-D1 is a critical regulator of cell cycle progression and initiates the transition of G1 to S phase of the cell cycle (X. Zhang et al. 2009). Interestingly, hTERT is also essential for cell proliferation, survival, and for immortalization of multiple cell types including ECs and is upregulated by the canonical Wnt/ β catenin pathway (Chang et al. 2005; Hoffmeyer et al. 2012). Exogenous expression of hTERT in ECs prolongs doubling time without a significant change in EC phenotype and also regulates angiogenic activities of ECs (Yang et al. 1999). Importantly, a decline in hTERT expression in somatic cells and mutations in the *hTERT* loci predisposes individuals to CVD (Edo and Andres 2005; Higashi et al. 2012; Zurek et al. 2016). Because the Wnt signaling pathway is an important pathway in regulating cardiovascular physiology, and because it is evident that larger vessels of the adult heart have Wnt activity, it is important to understand the effect of ablating *Nanog*, a downstream target of Wnt, on the physiology of the adult heart. In this study, we used the ligand Wnt3a to activate the canonical Wnt/ β -catenin pathway in cultured ECs and to thereby induce the expression of NANOG. *In vitro* studies complemented the *in vivo* observations and helped to delineate the NANOG transcriptional axis in ECs.

C. Transcription Factor NANOG

Nanog derives its name from the mythological Celtic land of the ever young, Tir nan Og (Chambers et al. 2003; Yates and Chambers 2005). Nanog is referred as the ‘Gateway’ to the pluripotent ground state and plays a central role in regulating the cell fate of the inner cell mass (ICM), maintaining pluripotency and promoting self-renewal of ESCs ((Yates and Chambers 2005; Chambers et al. 2007; Silva et al. 2009). As a TF, Nanog is a key regulator of embryonic development and cellular reprogramming.

The murine and human *Nanog* gene is located on chromosome 12. Both genes encode for a protein containing 305 amino acids (aa) (Chambers et al. 2003; Mitsui et al. 2003; Hart et al. 2004; Yates and Chambers 2005). Interestingly, the homeodomain region consisting of 60 amino acids share 87% homology between murine and human Nanog (Hart et al. 2004). This indicates that while there is evolutionary conservation between proteins from both species, they might also be functionally conserved. Human NANOG consists of three distinct regions (**Figure 5**): N terminal region (aa 1-95) rich in serine and threonine aa, the central or homeobox domain containing the DNA binding motif (aa 96-155), and the C-terminal region (aa 156-305). The C-terminal domain has strong transactivation activity and consists of a tryptophan repeat (WR) region that is involved in dimerization. The WR motif is flanked by CD1 and CD2 domains. In addition, the N terminus contains transcriptional activity and this motif is regulated via phosphorylation of serine, threonine and proline residues as well as other post-translational modifications that control its phosphorylation. Nuclear localization signals (NLS) are located in both N and CD domains. The NLS serve as the key regulatory mechanism for transport of Nanog into the nucleus of a cell, where it regulates transcriptional activity of Nanog target genes.

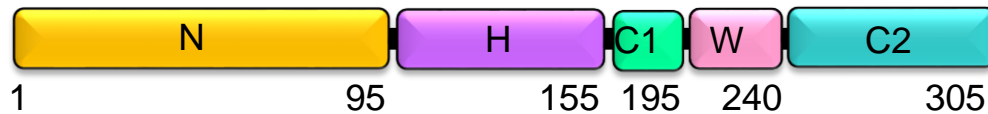


Figure 5: Transcription factor NANOG. The linear structure of NANOG shows the presence of N terminal domain spanning from amino acids 1 to 95 and is followed by DNA binding homeodomain H consisting of amino acids 95 to 155. C terminal domain extends from amino acids 156 to 305 and has a short span of tryptophan (W) repeats that start at amino acid 196 and ending at amino acid residue 240.

Nanog is expressed in pluripotent cells of pre-implantation and post-implantation embryos, and the ES and embryonic germ (EG) cells (Mitsui et al. 2003; Hart et al. 2004). *In vivo*, *Nanog* mRNA is detected in the compacted morula, with expression localized to the interior cells and future inner cell mass (ICM) (Chambers et al. 2003). During the blastocyst stage, expression is confined to the ICM and is absent in the trophectoderm (Chambers et al. 2003). In the late blastocyst, *Nanog* mRNA is further limited to the epiblast and is absent in the primitive endoderm (Hart et al. 2004; Komatsu and Fujimori 2015). Once it reaches the implantation stage, *Nanog* mRNA is significantly downregulated. Independent analysis by *Chambers et al.* and *Yamaguchi et al.*, showed that *Nanog* is detectable in the germ cells of E7.5. The abundance of Nanog expression through the developmental stages of PGC primes the role of Nanog as a

molecular marker of proliferating and migrating PGCs. Thus, *Nanog*-null embryos are lethal due to the failure of PGC migration.

Nanog is a developmentally regulated protein. Therefore, its expression is controlled via multiple regulatory mechanisms. At the molecular level, Nanog expression is influenced by both transcription and translation machinery (Rodda et al. 2005; Pan and Thomson 2007; Moretto-Zita et al. 2010). While the expression of Nanog in ES cells is reasonably well understood, its regulation in non-ES cells is an emerging area. Heterogeneity of Nanog expression in individual cells dictates the propensity to either self-renew or undergo differentiation (Torres-Padilla and Chambers 2014). During blastocyst formation, *Nanog* expression varies between embryos and blastomeres (Hart et al. 2004; Komatsu and Fujimori 2015). Nanog expression is upregulated in the ICM and repressed in the endoderm lineage. Interestingly, Nanog auto-repression controls the switching of *Nanog* transcription. Oct3/4 and Sox2 motifs at the proximal promoter also modulate *Nanog* expression (Rodda et al. 2005).

In addition to transcriptional regulation, Nanog protein stability is maintained by post-translational modifications (PTM) (Moretto-Zita et al. 2010; Xie et al. 2014). Nanog undergoes phosphorylation at four putative sites- Ser-52, Ser-5, Ser-71, and Thr-287, leading to increased stability and activity. Lys-48 and Lys-63 located in the Nanog PEST motif (aa 47-72) undergo ubiquitination leading to subsequent degradation. At the cellular level, signaling pathways that govern reprogramming act as a switch for Nanog expression. This includes the LIF/STAT, BMP, PI3K, FGF-2, Wnt, TGF β and MAPK pathways (Rodda et al. 2005; Kohler et al. 2011; Komatsu and Fujimori 2015).

Interestingly, there is some evidence of Nanog expression in the cardiovascular system (Guo et al. 2015). The initial link between Nanog and the cardiovascular system came from

studies conducted in experimental models of MI, where exogenous addition of adult stem cells expressing Nanog and other stem cell factors, promoted efficient recovery of the heart (Orlic et al. 2001). While the precise mechanism is unclear, it was evident that these exogenous cells and a small population of native cells are involved in the recovery process, and these cells frequently expressed Nanog. There is also direct evidence for a role of endogenous Nanog expression in myocardial and vascular tissue development and repair (Luo et al. 2014; Baruah et al. 2017). The work of *Lou et al.* confirmed that Nanog expression is up-regulated in rat myocardial tissues subjected to MI. We have shown that CD31⁺ vascular ECs in the heart express Nanog, and that this is crucial in the neovascularization process after injury (Baruah et al. 2017). In addition, systematic analysis revealed that Nanog is expressed in the myocardial tissues during development, plateauing at E18 and gradually declining by P30 (Guo et al. 2015). Thus, it is possible that Nanog plays a role in both development and onset of disease in mammalian cardiovascular system.

D. Telomerase Reverse Transcriptase

Telomeres are the specialized nucleoprotein structures which are found at the ends of the eukaryotic chromosome. They serve as a protective cap and ensure genomic stability by preventing end-to-end fusion, degradation, and aberrant recombination (Greider and Blackburn 1985). In mammals, TTAGGG is tandemly repeated to form long stretches of Telomeric DNA. Due to the inability of DNA polymerase I to synthesize DNA at the terminal ends, telomeres shorten with each cell division (Blackburn 1991). When the Telomeric DNA lengths are critically shorter, cells undergo cell cycle arrest and eventually cell death occurs. Therefore, the length of Telomeric DNA acts like a molecular clock which regulates the lifespan of proliferating cells. The length of this Telomeric DNA is maintained by the activity of TERT, the enzyme responsible for adding DNA to the ends of the chromosome. Interestingly, telomerase activity (TA) in humans is repressed after birth in most somatic cells or is extremely low, in stark contrast to TA in germ cell, stem and progenitor cell compartments, and cancer cells (Blackburn, Epel, and Lin 2015).

Telomerase is a specialized reverse transcriptase ribonucleoprotein (RNP) consisting of two main components, TERT protein and a non-coding RNA component (TER, telomerase RNA). TER consists of a short template sequence which is transcribed during telomere replication (Blackburn and Collins 2011). TERT and TER minimal complex are sufficient for enzymatic activity *in vitro*. TA counteracts the loss of Telomeric DNA length. The human TERT or hTERT gene is located on chromosome 5p15.33. It is a relatively high molecular weight RNP composed of 1132 amino acids (Blackburn and Collins 2011). The structure of TERT protein consists of three major domains; the telomerase essential N-terminal (TEN) domain, the TERT RNA binding domain (TRBD), and the reverse transcriptase domain which contains the

enzymatic activity (**Figure 6A**) (Ramlee et al. 2016). The TEN domain provides an anchor site that binds Telomeric DNA upstream of the primer-template interaction. It is a highly conserved domain among vertebrates. In addition, hTERT consist of a DAT motif which has been implicated in telomerase recruitment. Crystallographic studies revealed that TRBD secures the RNA template (TER) with motifs that hold the RNA template onto the protein, forming a stable RNP complex while allowing the template to pass through the active site. The reverse transcriptase domain is comprised of motifs 1, 2 and A-E, which represent the finger and palm of a hand, and a C-terminal extension, which represents the thumb subdomain and is also a less conserved protein region (Ramlee et al. 2016).

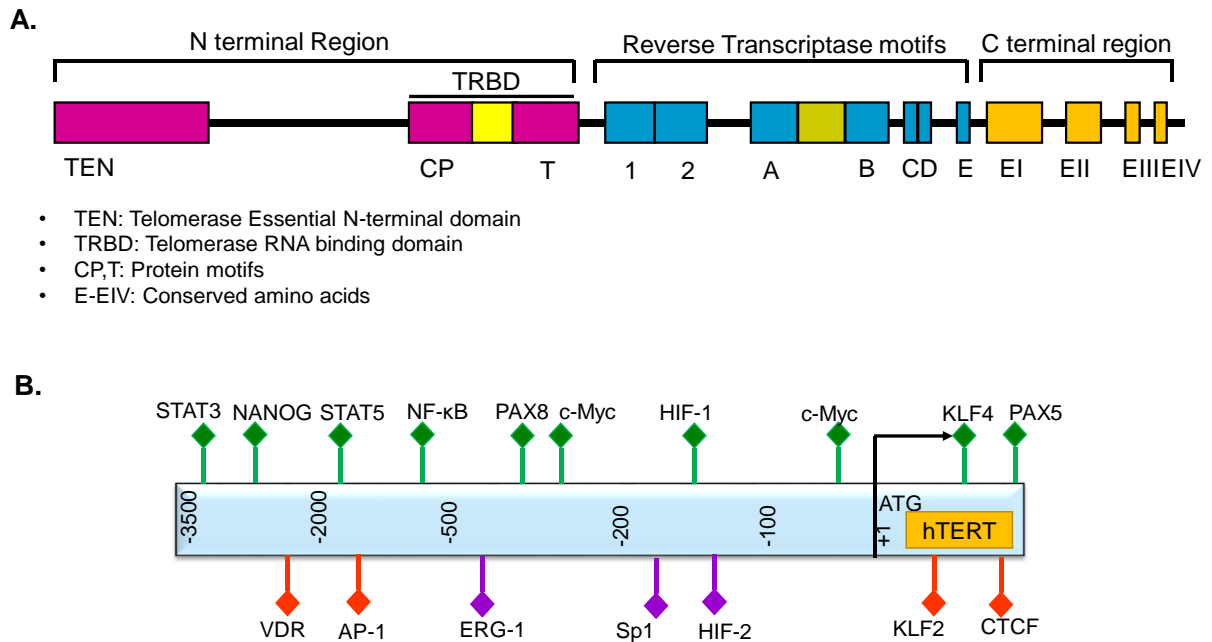


Figure 6: Linear structure of hTERT and regulatory elements in hTERT promoter. A) Linear structure of hTERT shows the presence of the N terminal domain that consists of Telomerase Essential N-terminal domain that is necessary for transcriptional activity of the protein. The telomerase RNA binding domain (TRBD) contains site for interacting with the RNA component TERC. TRBD contains protein motifs CP and T. The reverse transcriptase motif is comprised of subdomains A- E. This motif catalyzes DNA dependent RNA polymerase activity. The C terminal domain has EI-EIV, which is evolutionary conserved across multiple species. B) *hTERT* promoter region up to 3.5kb shows presence of different regulator elements as indicated in the figure. Red indicates repression, green indicates activation, and purple indicates regulatory region. Images are not to scale. Adapted and modified from Ramlee *et al.* 2016

During normal growth and development, TA is regulated to meet the proliferative needs of specific cellular functions, but TA is absent or low in most differentiated somatic cells such as ECs (Yang *et al.* 1999; Chang *et al.* 2005). Loss of TA or inhibition of TA leads to telomere shortening and apoptotic cell death (Falchetti *et al.* 2008). In human cells, expression of

telomerase is transcriptionally regulated. Deletion mapping studies indicate that -330bp upstream from the hTERT transcription start site (TSS) is optimal for inducing its transcription (Ramlee et al. 2016). Multiple signaling pathways that upregulate specific transcription factors such as c-Myc, Nanog, HIF, PAX, AP-1, KLF4 can induce hTERT expression in different cell types (**Figure 6B**). Interestingly, hTERT is also a direct target of the canonical Wnt/ β -catenin signaling pathway (Hoffmeyer et al. 2012; Y. Zhang et al. 2012). Because the hTERT promoter has no TATA or CAAT boxes but is highly enriched in GC nucleotides, it is proposed that the GC-rich nucleotide sequences form a larger CpG island near the TSS which may be methylated and thus repressing hTERT expression in post-natal life.

TA is detected in proliferating ECs in culture and is also activated transiently *de novo* during wound healing and injury (Yang et al. 1999; Chang et al. 2005; Richardson et al. 2012). Ectopic expression of hTERT in ECs enables cells to bypass replicative senescence without affecting their differentiated phenotype (Chang et al. 2005). With advancing age, the integrity of EC function is compromised, which in turn contributes to phenotypic and hemodynamic changes in the vasculature commonly observed in CVD states (Edo and Andres 2005; Wong et al. 2009; Zurek et al. 2016). Although the Telomeric length of mice is much greater than human, studies conducted in the *TERC*^{-/-} mouse revealed a potential phenotypic defect in the cardiovascular system in the later generations (Wong et al. 2009). This included but was not limited to defects in angiogenic potential, cardiomyocyte hypertrophy, impaired cardiac function etc. Interestingly, Telomerase overexpression in an animal model of acute MI provided a cardio protective benefit in the mouse hearts (Bar et al. 2014). Data from the *TERT*^{-/-} mouse is sparse and Sahin E et al. have reported a compromise in the mitochondrial metabolic function of *TERT*^{-/-} adult murine hearts (Sahin and Depinho 2010). Therefore, phenotypic observations obtained from TERC null

mouse revealed an important role of telomerase in regulating and maintaining cardiovascular phenotype and function. Interestingly, the mammalian heart has low but functionally significant levels of telomerase expression (Richardson et al. 2012). To delineate the cellular contribution of TA in neonatal, adult and cryoinjured hearts, *Richardson et al.*, utilized the *mTERT-GFP* mouse and found that a heterogeneous population of cells, including ECs and cardiomyocytes, expressed telomerase which can be upregulated in response to injury. They were able to localize CD31⁺ GFP⁺ cells in two distinct regions of the heart which included the endothelial layer of the lumen of coronary vessels and within the myocardium of the ventricular walls. This raises an exciting possibility that TERT expression in the vascular component can play a role in maintaining vascular integrity and thereby homeostasis of the cardiac microvasculature. Importantly, genetic ablation of TERT in mouse resulted in mitochondrial dysfunction in post-mitotic organs such as the heart (Wong et al. 2009; Sahin and Depinho 2010). This effect was mediated by dysregulation of an important gene involved in mitochondrial metabolism (PGC-1, α , and β isoforms) (Sahin and Depinho 2010). However, signaling events or upstream regulators that maintain telomerase expression in the cardiac vasculature is less understood. With our current study, we hope to establish a previously unknown mechanism for regulating TERT expression in the adult ECs of the cardiac microvasculature. Understanding TERT regulatory pathway can highlight potential therapeutic interventions in age-associated cardiovascular disease.

E. Cardiac Hypertrophy

Cardiac hypertrophy (CH) is a physiological response to changes in pressure or volume, mutations of the sarcomere or other related proteins, or loss of contractile mass due to injury which can sometimes become maladaptive (Frey and Olson 2003; Selvetella et al. 2004; Shimizu and Minamino 2016). A hypertrophic growth occurs secondarily to various forms of heart disease such as ischemic heart disease, hypertension, heart failure, or valvular disease. While concentric hypertrophic growth resulting from pressure-overload is a compensatory mechanism, ventricular hypertrophy seen during an injury can lead to a risk of heart failure or arrhythmia (Selvetella et al. 2004; Shimizu and Minamino 2016). Hypertrophic growth of the heart can occur in three distinct stages; 1) developing hypertrophy, where pressure load exceeds the output, 2) compensatory hypertrophy, where the ratio of workload to mass is regulated and basal cardiac output is maintained, and 3) overt heart failure, when in spite of the activation of hypertrophic response, ventricles dilate and a gradual decline of cardiac output follows thereafter (Selvetella et al. 2004; Tardiff 2006; Shimizu and Minamino 2016). This culminates in functional disturbances of cellular calcium homeostasis, ion channel functions and morphological changes such as increased rate of apoptosis and fibrosis, along with dilated chambers of the heart (van Empel et al. 2005; Tardiff 2006; Hill 2015).

At the cellular level, CH is characterized by an increase in cardiomyocyte cell size, increased protein synthesis, and tightened organization of the sarcomere bundles (Frey and Olson 2003). Two different hypertrophy phenotypes are evident which include concentric hypertrophy due to pressure overload and is characterized by lateral growth of the cardiomyocytes and the parallel addition of sarcomeres. In eccentric hypertrophy, which results from volume overload post-injury, sarcomeres are added in series and cardiomyocytes grow longitudinally (Frey and

Olson 2003; Carabello 2014; Shimizu and Minamino 2016). These events lead to thickening of the interventricular wall and/or septum (Frey and Olson 2003). Even though the heart is a post-mitotic organ with limited ability to regenerate or re-enter the cell cycle, intracellular pathways that regulate cell proliferation in other cell types of the cardiac microenvironment can stimulate hypertrophic growth of cardiomyocytes (Molkentin and Dorn 2001; T. Oka et al. 2014). The idea that CH can be directly or indirectly influenced by the non-myocyte cell population is gaining importance. In this context, cardiac ECs, which comprise a significant percentage of the cellular composition in adult heart are beginning to be investigated with regards to induction of CH.

Cardiac ECs secrete a variety of vasoactive substances such as NO, endothelin -1 (ET-1), prostaglandins, and a variety of growth factors such as VEGF, fibroblast growth factor (FGF), platelet-derived growth factor (PDGF) (Kamo et al. 2015; Lim et al. 2015). It is well established that angiogenesis controls the growth and size of adult organs including the heart (Walsh and Shiojima 2007; T. Oka et al. 2014). In response to hypertrophic stimuli, the myocardium secretes angiogenic GFs which can sufficiently induce vascular growth, thereby increasing myocardial mass and performance (Walsh and Shiojima 2007; T. Oka et al. 2014). Experimental evidence indicated that endothelium-derived NO is a critical factor that can mediate angiogenesis induced CH (Kempf and Wollert 2004). ET-1 is a potent vasoconstrictor and an important autocrine and paracrine regulator of CH. ET-1 is synthesized from ECs and non-ECs including cardiomyocytes and cardiac fibroblasts (Bohm and Pernow 2007). It is thought that the endothelium-derived secreted factors may act in a paracrine manner on the cardiomyocyte population. *In vitro* studies showed that ET-1 stimulation of neonatal rat cardiomyocytes induced a hypertrophic response accompanied by an increase in cell size, protein synthesis, and re-expression of the fetal genetic signatures such as *Atrial Natriuretic peptide (ANP)*, *brain natriuretic peptide (BNP)*, and *beta-*

Myosin heavy chain also known as *myosin heavy chain isoform 7 (Myh7)* (Carreno et al. 2006; Kerkela, Ulvila, and Magga 2015).

The natriuretic peptides (NPs) belong to a family of small molecule peptide hormones and play a major role in cardiovascular homeostasis (Carreno et al. 2006; Kerkela et al. 2015) (**Figure 7**). In response to pathological hypertrophic stimuli, there is an upregulation of the ANP and BNP genes. These proteins are abundant in embryonic cardiomyocytes and repressed in adults, but are re-expressed during CH. Multiple regulatory elements have been identified that converge on and lead to activation of fetal genes via the activities of alpha adrenergic agents or ET-1 (Perez-Rivero et al. 2006; Bohm and Pernow 2007). ANP is produced in the ventricular myocytes, with the highest expression seen during late fetal and early neonatal stages, and is diminished in adult hearts after the first few weeks of birth. However, it is re-expressed along with other putative fetal genes during CH. BNP was initially isolated in porcine brain, with later studies confirming its expression largely in the heart tissues for most species. In contrast to ANP, BNP is highly synthesized in the cardiac atria and dramatically increased in CH. Expression of both of these genes is used as reliable prognostic markers in clinical CH (Carreno et al. 2006; Kerkela et al. 2015). In addition to the NPs, a shift in the myosin heavy chain isoform from alpha to the beta can result from CH (Mouton et al. 2016). The beta form of myosin heavy chain (β MHC or Myh7) is predominantly present in the normal adult hearts, and increased expression is indicative of a diseased phenotype of CH (Greber-Platzer et al. 2001; Kraft et al. 2016). Alterations in the Myh7 gene expression affects the contractile properties of the heart, leading to left ventricular dysfunction and dilation of the chambers (Kraft et al. 2016).

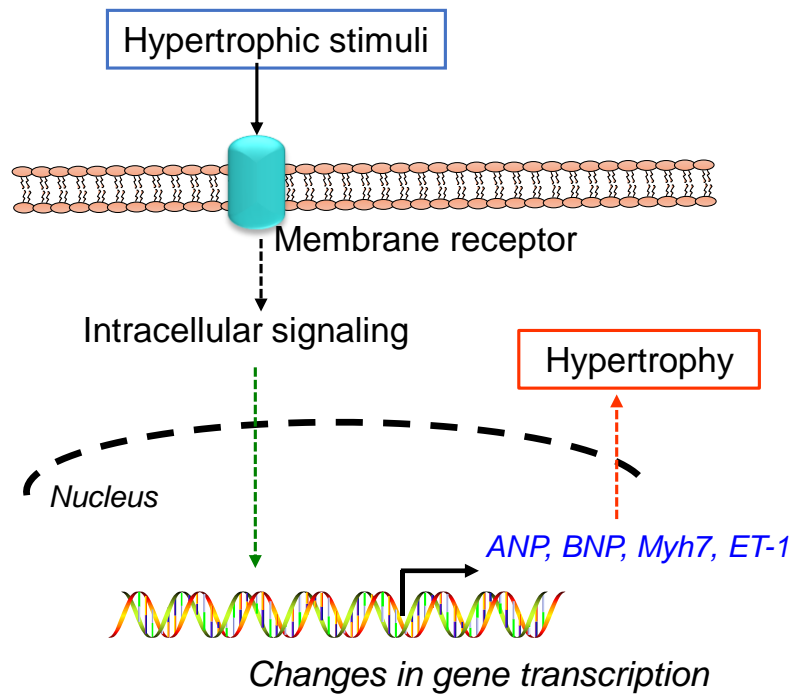


Figure 7: Schematic of events associated with cardiac hypertrophy. In the presence of a hypertrophic stimuli, signaling events are transduced from the receptor level to the nucleus of the responding cell. This in turn mediates gene transcription events, leading to synthesis of the natriuretic peptides and genes associated with cardiac hypertrophy. *ANP: Atrial Natriuretic Peptide, BNP: Brain Natriuretic Peptide, Myh7: β -Myosin Heavy Chain isoform 7, ET-1: Endothelin-1.* Adapted and Modified from Carreno et al. 2006.

The canonical Wnt/ β -catenin signaling pathway is important both in cardiac development as well as vascular development, and EC specification (Brade et al. 2006; Franco et al. 2009). Interestingly, Wnt signaling activity is detected in the vascular endothelium of adult hearts but is suppressed in other cell populations and gets reactivated upon injury or physiological stimuli (Brade et al. 2006; Aisagbonhi et al. 2011; Stylianidis, Hermans, and Blankestijn 2017). Alterations in the Wnt/ β -catenin signaling can occur at various levels, which

in turn can lead to a hypertrophic response in cardiomyocytes. Wnt modulators, the soluble Frizzled Receptor Proteins (sFRP) have been shown to prevent a hypertrophic response (van de Schans, Smits, and Blankesteyn 2008). However, most of the studies were conducted in animal models with cardiac-specific ablation or overexpression of the gene of interest. There are no known studies that address the role of endothelial Wnt/ β -catenin signaling in the induction of a hypertrophic phenotype of the mammalian heart. Through our studies, we hope to complement the understanding of the role of the endothelial compartment in the progression of a hypertrophic phenotype.

III. MATERIALS AND METHODS

A. Antibodies and Reagents

Recombinant human Wnt3a (5036-WN) was purchased from R&D Systems (Minneapolis, MN). Growth Factor Reduced Matrigel (#356237) was purchased from BD Biosciences (San Jose, CA) (Baruah et al. 2017). Tamoxifen (T5648), Corn oil (C8267), dimethyl sulphoxide (DMSO, 472301), Dispase-I (4818), Bovine Serum Albumin (BSA) (05470), were purchased from Sigma-Aldrich Chemical Company (St. Louis, MO). A stock solution of Tamoxifen was prepared in corn oil at a concentration of 2mg/ml, sterile filtered using a 0.22-micron filter and stored at 4°C for one week or -20°C for long-term storage. Rabbit anti-Nanog (A300-397A) was purchased from Bethyl Laboratories (Montgomery, TX). Rabbit-anti-Nanog (Nb 100-58842) was purchased from Novus Biologicals (Littleton, CO). Mouse-anti β -catenin (E5), Mouse anti-NANOG (J-29), mouse-anti VE-cadherin (Sc-9989), mouse anti-Glyceraldehyde 3 phosphate dehydrogenase (GAPDH) (4G5), rabbit-anti-Telomerase Reverse Transcriptase (TERT, Sc-7212), goat anti-TERT (Sc-7215), Polybrene (Sc-134220) were purchased from Santa Cruz Biotechnology (Dallas, TX). Rabbit anti-TERT (MABE14) and rabbit anti-vWF (AB7356) were purchased from Millipore (Billerica, MA). Rabbit anti-Vascular Endothelial Growth Factor Receptor-2(VEGFR2)/FLK1 (C-1158), rabbit anti-GAPDH (mAb#14C10), rabbit anti-Cyclin D1 (mAb#2978) were purchased from Cell Signaling (Danvers, MA). Rabbit-anti-HA (AP1012a) was purchased from Abgent (San Diego, CA). Anti-mouse Troponin T Cardiac Isoform Antibody (cTnT, MA512960) from ThermoFisher (Waltham, MA). Secondary antibodies goat anti-mouse HRP, donkey anti-rabbit HRP were purchased from BioRad (Hercules, CA). Donkey anti-rabbit Alexa Fluor-594, donkey anti-mouse 488, chicken anti-rabbit 647, donkey-anti-goat 647, Lipofectamine™ 2000, Opti-MEM I

Reduced Serum Medium, Dulbecco's Modified Eagle Medium (DMEM), *NANOG* *siRNA* (modified 25-mer duplexes), Negative Universal Control *siRNA* (scrambled sequences) and sheep anti-rat Dynabeads (#11035) were purchased from Invitrogen (Carlsbad, CA). Collagenase Type IV (#17104019, Gibco™), 1x insulin transferrin selenium (41400-045, Gibco™) were purchased from ThermoFisher Scientific (Waltham, MA). Human umbilical vein endothelial cells (HUVECs) and EndoGRO-VEGF Complete Media Kit were purchased from Millipore (Billerica, MA). Human pulmonary arterial endothelial cells (HPAECs) and human lung microvascular endothelial cells (HLMECs), cultured in EndoGRO-VEGF Complete Media, were purchased from Lonza (Allendale, NJ). Human saphenous vein endothelial cells (HSAVECs) and Endothelial Cell Growth Medium were purchased from PromoCell (Heidelberg, Germany). All ECs were cultured up to 5-6 passages. HuSH 29mer *shRNA* in p-RFP-C-RS constructs against *NANOG* were purchased from Origene (Rockville, MD) (Baruah et al. 2017). *hTERT*-cDNA (#G204) lentiviral particles were purchased from ABM (Richmond, BC, Canada). *HA*-tagged human *NANOG* cDNA (Lot: 102036S-2/T98134) was subcloned into pLCNX2 and purchased from Genscript (Piscataway, NJ).

B. Western Blot Analysis

Total cell lysates from cultured cells were prepared by washing the adherent cells two times with 1x phosphate buffered saline (PBS), followed by adding radioimmunoprecipitation assay (RIPA) buffer [50mM HEPES, 150mM NaCl, 2mM EDTA, pH 8, 1% Triton X-100, 0.1 % SDS, 2.66 g Sodium pyrophosphate, 4.2 g Sodium fluoride, 0.28 g Sodium orthovanadate] containing 1x protease inhibitor (PI) cocktail (P8564, Sigma). Cells were scraped in RIPA buffer and collected into Eppendorf tubes. After a brief incubation of 5 minutes on ice, tubes were centrifuged at 14,000 rpm for 20 minutes in a cooling centrifuge at 4°C. The supernatant

containing the total cellular protein was used to estimate protein concentration for downstream analysis or stored at -80°C until future use. Protein concentration was determined using Pierce 660nm Protein Assay reagent (#22660) purchased from ThermoFisher Scientific (Waltham, MA). Lysates were mixed with 2x reducing sample buffer (pH 6.8) and boiled for 5 minutes. Samples were resolved using sodium dodecyl sulfate (SDS)-polyacrylamide gel (PAGE) in 1x Tris/SDS/Glycine buffer. The separated proteins were then transferred onto a nitrocellulose (NC) membrane (Bio-rad, Hercules, CA) using 1x Transfer buffer (Tris -8g, Glycine- 48g and Methanol-600ml in 3 liters of water). Protein transfer was confirmed by Ponceau S stain (0.2% [w/v] Ponceau S in 3% [v/v] acetic acid). Thereafter, Ponceau stain was washed with two rinses of 1x TBS for 5 minutes each. The NC membrane was then blocked with 5% carnation milk in 1x tris buffered saline (TBS) or 5% BSA for phospho-specific antibodies only, in 1x TBS for a minimum of one hour at room temperature or overnight at 4°C . The membrane was then washed three times with 1x TBS and incubated with a primary antibody prepared in 1x TBS containing 3% BSA and 0.02% Sodium azide for overnight at 4°C . The membrane was washed three times for 10 minutes each with 1x TBST (1x TBS containing 0.1% Tween-20), followed by incubation with secondary HRP conjugate antibody prepared in 1x TBST for 1 hour at room temperature. This was followed by three washes with 1x TBST for 15 minutes each. Chemiluminescent signal was developed on Blue Biofilm (Denville, South Plainfield, NJ) by using SuperSignal West Pico and SuperSignal West Femto substrate kit by ThermoFisher Scientific (Waltham, MA).

C. RNA Extraction and q-RT-PCR

Total mRNA from cultured cells or tissues was extracted using TRIzol reagent (#15596026, InvitrogenTM). In brief, cultured cells or tissues were washed two times with 1x PBS and suspended in the TRIzol reagent. Cells were lysed by vigorously pipetting several times

whereas tissues were homogenized using a manual eppietube pestle and incubated for 5 minutes at room temperature with gentle shaking. To this, 0.2 ml of chloroform per 1ml of TRIzol reagent was added and incubated for 3 minutes at room temperature. The samples were centrifuged at 12,000 rpm for 15 minutes at 4°C. The upper aqueous phase which contained RNA was then transferred into a new Eppendorf tube. RNA was precipitated by adding 0.5 ml of isopropanol to the aqueous phase and incubated for 10 minutes at room temperature. This was followed by a quick spin at 12,000 rpm for 10 minutes at 4°C. RNA formed a gel-like pellet and settled at the bottom of the Eppendorf tube. The supernatant was discarded and RNA pellet was resuspended in 1 ml of 75% ethanol, then centrifuged at 7500 rpm for 5 minutes at 4°C. Thereafter, the pellet was air dried and resuspended in RNase free water, followed by incubation in a heat block set at 55°C for 15 minutes. RNA was quantified using standard spectrophotometer by measuring absorbance at 260 nm. 1µg of RNA was used in quantitative real-time PCR analysis (q-RT-PCR). q-RT-PCR assay was performed using one-step qRT-PCR (#4389986) kit from Applied Biosystems as per manufacturer's instruction. Primers used are listed in **(Table I)** and were custom designed by IDT (Coralville, IO). Data obtained from the q-RT-PCR run with ViiA program was analyzed using ExpressionSuite software (freeware download available at ThermoFisher Scientific website).

Table I: Primer Sequences for qRT-PCR

	Name	Species	Sequence (5'-3')	Accession#
1	<i>NANOG</i>	human	(F) 5'-TTAGTAGAGACGGGGTTTCACTG-3' (R) 5'-GTGGATCACAAGGTCAGGAGAT-3'	NM_024865.3
2	<i>CYCLIN-D1</i>	human	(F) 5'-CCAACAACCTCCTGTCCTACTACC-3' (R) 5'-GGTCACACTTGATCACTCTGGA-3'	BC000076.2
3	<i>VE-CADHERIN</i>	human	(F) 5'-CTCTGTCTACTCCTTATCCCTTGG-3' (R) 5'-AGTTCCTGAGATGTGACAACAG-3'	X79981.1
4	<i>VEGFR2</i>	human	(F) 5'-GTGTGGTGTCAAAGTTTCAGGAAG-3' (R) 5'-GGTTTACTGGAGTAGAGGCCAAAT-3'	NM_002253.2
5	<i>TERT</i>	human	(F) 5'-TGACACCTCACCTCACCCAC-3' (R) 5'-CACTGTCTTCGGCAAGTT-3'	NM_001193376.1
6	<i>18S rRNA</i>	consensus	(F) 5'-GGAGGTTCTGAAGACGATCAGA-3' (R) 5'-GCATCGTTTATGGTCGGAAC-3'	NR_003286.2
7	<i>Nanog</i>	mouse	(F) 5'-ATGTTTAAGGTCGGGCTGTAGA-3' (R) 5'-GAGTGACAGGACATTCGAACAA-3'	NC_000072.6
8	<i>Anp</i>	mouse	(F) 5'-TCTTCCTCGTCTTGGCCTTT-3' (R) 5'-AGAGGGCAGATCTATCGGAG-3'	NM_008725.3
9	<i>Bnp</i>	mouse	(F) 5'-CCAGTCTCCAGAGCAATTCAAG-3' (R)-5'-GGAATTTTGAGGTCTCTGCTGG-3'	NM_008726.5
10	<i>Myh7</i>	mouse	(F) 5'-CAACACCAACCTGTCCAAGTTC-3' (R) 5'-GGTTCTTCCTGTCTTCCTCTGT-3'	XM_017315841.1
13	<i>Endothelin-1</i>	mouse	(F) 5'-CCAAAGTACCATGCAGAAAAGC-3' (R) 5'-CAGCTTTCAACTTTGCAACACG-3'	NM_010104.4
14	<i>Vegfr2</i>	mouse	(F) 5'-TAGCTCATGCCAGTACCTGAGA-3' (R) 5'-AAGGAAGTAGAATCCCCTCGAG-3'	XM_006496487.3
13	<i>Tert</i>	mouse	(F) 5'-CAGACTTTGGAGGTGTTCTGT-3' (R) 5'-CAAGACCGACAGGAGCTTGTTTC-3'	XR_001780771.1

D. Chromatin Immunoprecipitation (ChIP) Assay, PCR and qPCR

To determine NANOG binding to *hTERT* promoter regions, ECs were cultured in EndoGRO-VEGF Complete media. Cells were either unstimulated (Control group) and stimulated with Wnt3a (50 ng/ml for 18 hours). ChIP assay was performed using the EZ-Magna ChIP kit (Millipore, Billerica, MA) (Kohler et al. 2014). To reversibly link the protein/DNA interaction, cells were incubated with 1% formaldehyde in complete media for 10 minutes at room temperature. The reaction was stopped by adding 10x Glycine. Plates were then washed twice with 1x PBS/protease inhibitor II cocktail mixture and cells were collected into Eppendorf tubes. Samples were centrifuged at 800g for 5 minutes at 4°C. To the cell pellet, 500µl of Lysis Buffer and 2.5µl protease inhibitor cocktail was added. Samples were incubated for 15 minutes on ice with a brief vortex every 5 minutes. The cell suspension was centrifuged at 800 g for 5 minutes at 4°C. The supernatant was discarded and the pellet resuspended in 500µl of Nuclear Lysis Buffer containing 2.5µl of Protease Inhibitor II cocktail. Chromatin was sonicated using Covaris S2 (Woburn, MA) to generate 1500 bp fragments with the following specifications (Intensity-4, Duty Cycle-2%, Cycles per Burst-200, Treatment Time (seconds)-15) at 7°C. Sonicated chromatin material was centrifuged at 10,000 g for 10 minutes at 4°C, to remove the cellular debris. 50µl of the supernatant was aliquoted into new tubes and 450µl of ChIP dilution buffer containing PI cocktail II was added to each tube. 5µl of the supernatants were saved as ‘Input’. Anti-NANOG, isotype control anti-rabbit IgG antibodies 2µg each and 20µl of fully suspended protein A magnetic beads were added to each tube and incubated in a nutator overnight at 4°C. The following day, beads were pelleted using a magnetic separator and supernatant was completely removed. The protein A bead-antibody/DNA complex was serially washed once with Low Salt Immune Complex Wash Buffer, High Salt Immune Complex Wash

Buffer, LiCl Immune Complex Wash Buffer, and TE Buffer with magnetic clearance between each wash to remove unbound, non-specific chromatin (Kohler et al. 2014). The beads were incubated with 100µl of warm ChIP elution buffer containing 1µl Proteinase K at 62°C for 2 hours with gentle shaking, followed by a 10-minute incubation at 95°C. Once the samples had cooled down to room temperature, beads were separated using the magnet and supernatant removed to new Eppendorf tube. To the 100µl of the supernatant, 500µl of Bind Reagent A was added and transferred to a Spin Filter attached to a Collection Tube. Spin Filters were centrifuged at 10,000 g for 30 seconds. The liquid was discarded from the collection tube and above step was repeated once with Wash Buffer B. The above step was repeated one more time and the remaining liquid and the spin tube was discarded. 50µl of Elute Reagent C was added to the Spin Filter and a new collection tube was placed. Spin Filters were centrifuged at 10,000 g for 30 seconds and eluate contained the purified DNA. The spin filter was discarded and DNA used for qPCR and PCR analysis.

5µl of purified DNA was used to run qPCR using Fast SYBR master mix (#4385612, Applied Biosystems) with forwarding primer 5'-AAGTCCATCCCTCCTACTCTACTG-3' and reverse primer 5'-TTTCTCTTTGCAGGTTCTCAGG-3' directed to amplify hTERT promoter. C_T (Cycle Threshold) values obtained from the run was used to determine the percent Input of NANOG binding to hTERT promoter in Control and treated groups. Similarly, 5µl of DNA was used to amplify hTERT promoter fragments using a 2X master mix from ThermoFisher Scientific (K0171) and amplicons were separated using a 1.5% Agarose gel. Images were captured using Fotodyne (Hartland, WI).

E. *siRNA* and *shRNA* mediated Gene Knockdown

For *siRNA* transfection, ECs were plated at 60% confluency and complete EndoGRO media was removed and washed with 1x PBS. In a 6 well plate, per well: 1.7 ml of Opti-MEM I reduced serum media was added prior to adding RNAi-Lipofectamine mix. In one tube, 12pmol RNAi duplex was added to 150µl of Opti-MEM I reduced serum medium and mixed gently. In the second tube, 60µl of Lipofectamine RNAimax was added to 150µl of Opti-MEM I medium. The components of both the tubes were mixed together and incubated for 20 minutes at room temperature. The ~300µl Opti-MEM I media containing RNAi-Lipofectamine mix was added to the plates and plates were gently swirled and placed in the CO₂ incubator at 37°C for 6 hours. After 6 hours, reduced serum media was aspirated and replenished with EC complete media and incubated for an additional 42 hours.

shRNA transfection into ECs was carried out using 10cm confluent plates. On the day of transfection, complete EC media was removed and plates were washed with basal medium free of serum and growth factors. 8µg/ml Polybrene containing basal media was added to the plates and incubated in a CO₂ incubator at 37°C for 4 hours. After 4 hours, 50% v/v of viral soup containing *NANOG shRNA* or *HA-NANOG* or *hTERT* cDNA was added to the plates with a final concentration of Polybrene at 4µg/ml and incubated overnight (Baruah et al. 2017). Next day, viral soup and Polybrene containing media were aspirated and complete EC media was added and incubated in a CO₂ incubator at 37°C for additional 36 hours.

F. BrdU Incorporation Assay

To assess cell proliferation, we measured the extent of 5-Bromo-2'-deoxyuridine (BrdU) incorporation in cultured ECs in response to different experimental conditions, using BrdU Labeling and Detection Kit II (Roche, Indianapolis, IN). In a 24 well plate, ECs were cultured on

0.2% gelatin-coated coverslips to 90% confluency. Cells were supplemented with complete media containing 1:1000 dilution of BrdU labeling media and incubated in a CO₂ incubator at 37°C for overnight. Next day, media was aspirated and wells were rinsed with 1x PBS two times. 200µl of fixative (50mM glycine solution in 100% ethanol with pH 2) was added to each well and the plate was incubated at -20°C for 20 minutes. After three washes with 1x BrdU wash buffer, cells were incubated with 1:50 dilution of anti-BrdU antibody made in incubation buffer. The coverslips were placed in a humidified chamber at 37°C for 30 minutes. After three washes with 1x BrdU wash buffer, cells were incubated with 1:50 dilution of anti-mouse Ig-Alkaline Phosphate(AP) made in 1x PBS for 30 minutes in a humidified 37°C incubator. Thereafter, coverslips were washed three times with 1x BrdU wash buffer. For colorimetric detection of BrdU-positive nuclei, cells were incubated with 200µl/well of substrate buffer (100mM Tris HCl, 100mM NaCl, 40mM MgCl₂ pH 9.5) containing X-phosphate and BCIP. An incubation period of 15 minutes at room temperature led to colored substrate reaction. Thereafter, coverslips were stained with Hematoxylin for 2 minutes followed by 3 washes with water and then cytoplasmic staining was done by Eosin, followed by three washes with water. Coverslips were mounted on Prolong anti-fade mounting media and edges were sealed with clear nail paint. Images were captured at either 10x or 20x magnification using Axiovert 40C microscope (Carl Zeiss AG). The percentage of BrdU incorporation was determined by using ImageJ from NIH (Bethesda, MD).

G. Immunofluorescent Staining, Immunohistochemistry on Cryo- and Paraffin-Sections

Immunostaining of cultured ECs was done by growing monolayer ECs on glass coverslips in a 24 well plate. After stimulation with Wnt3a (50ng/ml) for 6 hours, ECs were fixed with pre-warmed 2% Paraformaldehyde (PFA) containing culture media in the 37°C

incubator for 5 minutes. Thereafter, PFA containing media was aspirated and cells were washed with 1x Hanks balanced salt solution (HBSS) two times. 4% PFA in 1x PBS was added to the well and incubated on ice for 10 minutes. Excess PFA was aspirated and cells were washed with 1x HBSS three times for 5 minutes each. Cells were permeabilized using freshly prepared 0.5% Triton X-100 in 1x PBS for 15 minutes at room temperature. After three washes of 1x HBSS for 5 minute each, cells were blocked with 0.5% (Bovine serum albumin) BSA prepared in 1x HBSS and incubated in a humidified chamber at room temperature for 30 minutes. Thereafter, a primary antibody with 1:200 dilution prepared in 0.5% BSA blocker was added to the coverslips and incubated at 4°C for 1 hour. After three 5-minute washes with 1x HBSS, a secondary antibody prepared in 1:200 or 1: 1000 dilution in 0.5% BSA was added to coverslips for 30 minutes at room temperature and away from light. Coverslips were washed in 3 changes of 1x HBSS for 5 minutes each and mounted on prolong anti-fade DAPI containing mounting media. The edges of coverslip were sealed with nail paint, and slides were stored at 4°C, away from light until imaging.

Freshly excised hearts from anesthetized mice were washed with chilled 1x PBS two times to remove excess blood and cut into three regions. The top region was snap frozen in liquid nitrogen for RNA or protein analysis. The mid region was fixed in 10% zinc-formalin solution for 72 hours before paraffin embedding. The lower region was Cryo-preserved in a mold containing Optimal cutting temperature (OCT) compound (#23-730-571, Tissue-Tek, ThermoFisher), which was allowed to solidify gradually on a 100% ethanol-dry ice bath. Thereafter, 5 μ m thickness serial sections were prepared from either the cryopreserved or paraffin-embedded fractions using services from the UIC histology core. Human heart slides (HP-802) was purchased from Zyagen (San Deigo, CA). To visualize endogenous expression of

fluorescent red and green proteins, slides containing cryosections were equilibrated to room temperature for 5 minutes and a drop of 1x PBS was placed on the tissue section to prevent it from drying. Images were captured at 10x or 20x magnification with the Olympus BX51.

To conduct immunostaining on cryosections, slides were equilibrated to room temperature in a coupling jar containing 1x PBS for 5 minutes. Slides were fixed with 1% PFA for 7 minutes at room temperature. Slides were washed with 1x PBS three times for 5 minutes each. Peroxidase activity of the tissue sections was inhibited by incubating slides with freshly prepared 3% hydrogen peroxide (H_2O_2) in 1x PBS at room temperature for 20 minutes of gentle rocking. Slides were washed for 5 minutes each with three changes of 1x PBS. Tissue sections were first permeabilized using freshly prepared 0.5% Triton X-100 in 1x PBS for 15 minutes at room temperature followed by three washes with 1x PBS for 5 minutes each. Then slides were blocked with 0.5% BSA for 30 minutes at room temperature. A small area around tissue section was marked with a hydrophobic pen to allow even distribution of primary antibody on the tissue. Thereafter, a primary antibody prepared at 1:200 dilution in 0.5% BSA was added to the tissue section and incubated at 4°C for an hour in the dark. This was followed by three washes with 1x PBS for 5 minutes each. A secondary antibody prepared at 1:2000 dilution in 0.5% BSA was added to the tissue sections and incubated for 30 minutes at room temperature. Slides were then washed with one wash of 1x PBST (PBS containing 0.1% Triton-X 100) and two washes of 1x PBS for 5 minutes each. Slides were mounted on prolong anti-fade mounting media containing DAPI and sealed with coverslips.

Immunohistochemistry on paraffin section was done as follows. Slides were baked in an oven set at 65°C for 20 minutes to melt excess paraffin. Slides were then subjected to three serial Xylene incubations for 10 minutes each. Slides were dehydrated with a series of ethanol washes:

2 incubations in 100% ethanol, one in 95% ethanol, and then a 70% ethanol incubation for 5 minutes each. Slides were kept in cold tap water until ready for permeabilization step. Sections were permeabilized with 0.5% Triton X-100 in 1x PBS for 15 minutes at room temperature. After three 1x PBS wash for 5 minutes each, tissue sections were processed for antigen retrieval. Pre-warmed Antigen retrieval buffer (10mM Sodium citrate, 0.05% Tween-20 at pH 6.8) containing coupling jar was placed in a boiler. Slides were then boiled in Antigen retrieval buffer for 15 minutes. This was followed by three 1x PBS wash for 5 minutes each. Endogenous peroxidase activity of tissue sections was inhibited by incubating slides in freshly prepared 3% H₂O₂ for 20 minutes. After three 1x PBS wash of 5 minutes each, the area surrounding the tissue was marked with a hydrophobic pen and tissue section was incubated with 0.5% BSA for 30 minutes at 4°C in a humidified chamber. A primary antibody prepared in 0.5% BSA blocker was added to sections and incubated at 4°C for 1 hour. Slides were washed with 1x PBS three times for 5 minutes each and then incubated with secondary antibody for 30 minutes at room temperature in the dark. After three washes with 1x PBS, slides were mounted with coverslips in prolong anti-fade reagent containing DAPI, and edges were sealed with nail paint. Wheat Germ Agglutinin staining of cell membrane was done on paraffin embedded tissue sections. Tissue sections were de-paraffinized, followed by series of ethanol washes in a similar manner as described previously. Thereafter 1:200 dilution of WGA-conjugated to Texas Red-X was freshly prepared in 1x HBSS. Slides were incubated in a humidified chamber for one hour at 37°C. After a series of washes with 1x HBSS, slides were mounted with coverslips in prolong anti-fade reagent containing DAPI, and edges were sealed with nail paint. For co-staining with anti-vWF, anti-cTnT, and WGA, tissues sections were processed similarly as described above, except that primary antibodies were incubated overnight, followed by WGA incubation for one hour in humidified chamber, and 1x HBSS was used for all wash steps involved. After wash steps, slides

were incubated with appropriate isotype matched secondary antibodies. The tissue sections were mounted with coverslips in prolong anti-fade reagent containing DAPI, and edges were sealed with nail paint. High-resolution confocal imaging of slides was done using LSM 880 (Carl Zeiss) at 63x and 20x. Images were analyzed with Zen 2011 software.

H. Telomerase Repeat Amplification Protocol (TRAP) Assay

Telomerase activity in ECs was estimated using Telomerase Repeat Amplification Protocol (TRAP) assay kit (Trapeze, S770) purchased from Millipore (Billerica, MD). Non-synchronized growing ECs were stimulated with Wnt3a (50ng/ml) or Wnt signaling activator. 10^6 cells were resuspended in 200 μ l of 1x CHAPS lysis buffered provided in the kit. The cells were incubated on ice for 30 minutes. Samples were centrifuged at 12,000 g for 20 minutes at 4°C. Approximately 160 μ l of the supernatant was transferred into a fresh tube. A telomerase positive cell pellet provided with the kit was lysed using 1x CHAPS lysis buffer using the above protocol. The protein extracted was diluted 1:20 with 1x CHAPS lysis buffer. A negative control where telomerase is inactive was prepared by incubating 10 μ l of the sample at 85°C for 10 minutes prior to the TRAP assay. Telomeric repeats were amplified by setting up a PCR reaction using the following components; 5 μ l of 10x TRAP buffer, 1 μ l of 50x dNTP mix, 1 μ l of TS Primer, 1 μ l of TRAP Primer mix, 2 units of Taq polymerase, 39.6 μ l of dH₂O and 2 μ l (1.5 μ g) of protein extract. The PCR amplification cycle was as follows; 30°C for 30 minutes, 94°C for 30 seconds, 52°C for 30 seconds, 72°C for 30 seconds, 72°C for 5 minutes, with a hold stage at 4°C and consisted of 33 cycles. The TS primers serve as PCR amplification control to monitor PCR inhibition, which gives a 36 bp band (Internal control). Amplicons were separated on a vertical 12% polyacrylamide gel in 1x TBE buffer. The gel was then stained with 1:10,000 of 10mg/ml

of Ethidium bromide for 20 minutes at room temperature and de-stained for 20-30 minutes using deionized water. Images were captured using gel imaging system Fotodyne (Hartland, WI).

I. Luciferase Reporter Assay

hTERT promoter reporter constructs were custom designed by Genecopoeia (Rockville, MD). 1701bp, 1309bp and 636bp promoter regions upstream of the transcription start site (TSS) that contain 6, 1 and 0 NANOG binding elements (NBE) were cloned into a dual reporter plasmid pEZX-LvG04, which contained Gaussia Luciferase (GLuc) and constitutively active secreted alkaline phosphatase (SEAP). Viral particles containing these constructs and the negative control (vector alone) were generated by transfection packaging cell line Phoenix293, followed by puromycin (4 μ g/ml) selection of the positive clones. To generate virus, a confluent plate of transfected Phoenix cells was supplemented with EC basal media free of serum and growth factors. Media collected at 48 hours was centrifuged at 1500 rpm for 5 minutes to concentrate the viral particles. For a 6 well plate, 1ml of freshly collected viral particles was used to transduce ECs in the presence of Polybrene (4 μ g/ml) overnight. Next day, cells were replenished with complete media and incubated for an additional 30 hours. At the end of 48 hours, cells were serum starved for 3 hours followed by addition of Wnt3a (50ng/ml) for 3 hours. Luciferase activity and SEAP activity was measured using Secrete-PairTM Luminescence Assay kit (LF031, Genecopoeia). 200 μ l of culture media was collected into Eppendorf tubes and placed at room temperature. 1x GL-H buffer was prepared in distilled water. GLuc Assay working solution was prepared by adding substrate GL to 1x GL-H buffer in the ratio of 1:100 and mixed well by inverting the tube several times. GLuc working solution was incubated for 25 minutes at room temperature, capped and protected from light. The luminometer was set to a measurement of 1-2 seconds of integration. To measure luciferase activity, 10 μ l of culture medium was mixed

with 100µl of GLuc assay working solution in a luminometer tube, vortexed briefly and incubated for 30 seconds before placing in the luminometer. To measure secreted alkaline phosphatase activity (SEAP), a 50µl aliquot of culture medium in an Eppendorf tube is placed in a heat block at 65°C for 15 minutes and then placed on ice. 1x buffer AP (Alkaline phosphatase) was prepared in distilled water. SEAP Assay working solution was prepared by mixing Substrate AP with 1x Buffer AP in the ratio of 1:100 and incubated for 5-10 minutes at room temperature, away from light. The luminometer was set to 1-3 seconds of integration. 10µl of culture medium was mixed gently with 100µl of SEAP assay working solution by gently tapping several times and activity was measured using the luminometer. Fold luciferase activity was represented by normalizing Gaussia Luciferase activity over the SEAP activity.

J. Formation of Branching Point Structures and Tube Formation Assay

A day before the experiment Matrigel was allowed to thaw in 4°C refrigerator for overnight and a sterile 96 well tissue culture plate was also placed in 4°C to keep the plate cool prior to use. ECs were grown to confluency in 6 well plate. Cells were transfected with control and *NANOG shRNA* or *hTERT* cDNA in the presence of Polybrene (4µg/ml) and incubated for 48 hours. On the day of the experiment, Matrigel was placed on ice to prevent the gel from solidifying. 60µl/well of Matrigel was aliquoted in 6 wells per the condition of the 96 well plate, placed on ice. The plate was then placed in a 37°C incubator for 20-30 minutes until the gel polymerized. In the meantime, ECs were detached using 0.05% Trypsin-EDTA solution and the cell pellet was resuspended at a volume of 1.5×10^5 cells/ml in EC media. After gel had polymerized, 100µl of cells per well gently added to the solidified matrix. The plate was incubated for 1 hour at 37°C in a CO₂ incubator. Unattached cells were removed with one 1x PBS wash, and media containing Wnt3a (50ng/ml) was added. The wells were monitored every 4

hours for tube formation. At the end of 18 hours, images were captured at 5x magnification using an Axiovert 40C microscope. The extent of branch points formed was quantified with ImageJ plugin Angiogenesis Analyzer.

K. Terminal deoxynucleotidyl transferase dUTP nick end labeling (TUNEL) Staining

TUNEL staining of 5 μ m thin heart cryosections or cultured ECs grown on coverslips was done using ApopTag® Fluorescein *In Situ* Apoptosis Detection Kit (S7110) from Millipore (Billerica, MA). Tissue sections or adherent ECs were fixed with 1% PFA for 10 minutes at room temperature. This was followed by a wash in 2 changes of 1x PBS for 5 minutes each. Slides or coverslips were post-fixed in pre-cooled 2:1 ratio of Ethanol: acetic acid for 5 minutes at -20°C. Samples were washed two times with 1x PBS for 5 minutes each. Samples were incubated with Equilibration buffer for 10 seconds at room temperature. Samples were incubated with freshly prepared Working strength TdT enzyme (30% TdT enzyme in Reaction buffer) for 1 hour at 37°C in a humidified chamber. Slides were placed in working strength Stop/Wash buffer (1 ml Stop/wash buffer in 34 ml of distilled water) and agitated for 15 seconds and then incubated for 10 minutes at room temperature. To co-stain with anti-vWF or anti-VE-cadherin antibody, slides or coverslips were incubated with 0.5% BSA blocker prepared in 1x PBS for 30 minutes in a humidified chamber at room temperature. A primary antibody prepared in 0.5% BSA prepared at 1:200 dilution was incubated for 1 hour at 4°C. Slides were washed with 3 changes of 1x PBS for 5 minutes each. Secondary antibody 1:1000 and working strength anti-Digoxigenin conjugate (47% v: v in 53% v: v blocking solution) was added to samples and incubated at room temperature for 30 minutes, protected from light. Thereafter, slides or coverslips were mounted in Prolong anti-fade mounting reagent containing DAPI. Edges of the coverslip were sealed with clear nail paint. High-resolution confocal images were captured with

LSM 880 Zeiss at 63x for tissues and 20x for cells. Images were analyzed using Zen 2011 software.

L. Animal Breeding, DNA extraction, Genotyping and Isolation of ECs

Generation of *Nanog^{tm1a(KOMP)}^{Wtsi}* (*Nanog^{fl/+}*) founder mice in the C57BL6 background was produced at the University of California (Davis, CA) (CSD33934). EC-specific Cre recombinase expressing mice *Cdh5^{CreERT2}* produced by Ralf Adams were made available through a material transfer agreement (MTA) with UK Cancer Research (London, UK). *Rosa^{mT/mG}*, also known as *tdT tomato* mice, were purchased from Jackson Laboratories (Bar Harbor, MI). After a series of breeding and cross-breeding, we generated the *Rosa^{mT/mG}::Nanog^{fl/+}::Cdh5^{CreERT2}*. Generation of *Nanog^{fl/+}::Cdh5^{CreERT2}* mice is approved and covered by ACC 15-058 protocol. Generation of *Rosa^{mT/mG}::Nanog^{fl/+}::Cdh5^{CreERT2}* is approved and covered under ACC 14-160 (previous) and 17-129 (current). Genotyping of the animals was done by tail snip method and ear tags were used to record the animals of appropriate genotype. The list of primers used is indicated in **(Table II)**. Less than 1mm of the tail was collected from pups that were more than 21 days old. Tail samples were incubated in DNA digestion buffer [50mM KCl, 10mM Tris, 0.1% TritonX-100 and freshly added 0.4mg/ml proteinase K]. Eppendorf tubes containing the tail samples were vortexed briefly, caps were sealed with paraffin and placed in a 50°C water bath for overnight. The next day, after a quick vortex 700µl of Phenol: Chloroform: Isoamyl alcohol was added to the samples and placed in a nutator for 1 hour at 4°C. Samples were centrifuged at 14,000 rpm for 5 minutes at 4°C. Clear upper phase was transferred to a new Eppendorf tube and chilled 100% ethanol was added to the supernatant to precipitate the DNA. Samples were centrifuged at 14,000 rpm for 5 minutes at 4°C. The supernatant was discarded and DNA pellet resuspended in 1ml of 70% ethanol, centrifuged at 7500 rpm for 5 minutes at 4°C. Ethanol was discarded and tubes

were placed on a paper towel to air dry for 8 minutes at room temperature. 50µl of DNase free water was added and samples incubated in a heat block set at 65°C for 15 minutes. Genotyping for the presence of *Nanog* floxed allele was carried out using ThermoFisher 2X Master mix (K0171), using the following reaction volumes: 25µl of 2X PCR master mix, 16µl of PCR grade water, 4µl of primer (10 µM of Forward and Reverse Primer) and 5µl of DNA. The following PCR cycle conditions were used to amplify *Nanog (flox)* allele. 94°C for 6 minutes, 94°C for 1 minute, 53°C for 1 minute, 72°C for 1 minute 30 seconds, 72°C for 5 minutes followed by a hold stage at 4°C, and consisted of 33 cycles. For amplifying the *Cdh5^{CreERT2}* and *Rosa^{mT/mG}* allele, PCR master mix from Sigma (R4775) was used to prepare a reaction volume of 20µl; 10µl master mix, 4µl of dH₂O, 3µl of primer (10 µM of Forward and reverse primer for Tomato, 1µM of forward and reverse primer for Cre) and 3µl of DNA. PCR reaction condition for Cre was set to 94°C for 7 minutes, 94°C for 1 minute, 53°C for 1 minute, 72°C for 1 minute, 72°C for 5 minutes, followed by a hold stage at 4°C and consisted of 30 cycles. The PCR conditions for *Tomato* allele were as follows, 94°C for 5 minutes, 94°C for 30 seconds, 56°C for 30 seconds, 72°C for 45 seconds, 72°C for 5 minutes, with a hold stage at 4°C and consisted of 35 cycles. The PCR products were resolved in a (1.8-2) % Agarose gel containing Ethidium Bromide. Images were captured using Fotodyne (Hartland, WI).

To isolate CD31⁺ ECs from mice hearts, sheep anti-rat Dynabeads were coated with CD31 antibody (Clone 13.3, BD Biosciences). 200µl of sheep anti-rat Dynabeads were washed 5 times with 1x PBS, by gently pipetting several times and placing on the magnetic rack to concentrate the beads for a minute. Beads were then resuspended in 200µl of freshly prepared 0.1% BSA in PBS. 30µl of CD31 antibody was added to the magnetic beads and placed in a nutator in 4°C for overnight. Next day, antibody beads were concentrated using the magnetic rack and unbound

antibody was washed two times using 1x PBS. The CD31 coated beads were suspended in a 200µl of 0.1% BSA in PBS and stored at 4°C until use. Next, mice were sacrificed with CO₂ inhalation followed by cervical dislocation. Hearts were excised out and washed with 1x PBS two times before placing them in ice-cold plain DMEM media. Using sterile scissors and a razor blade, 5-6 hearts were finely cut and minced into smaller pieces in DMEM media. The minced heart tissues were incubated in tissue digestion medium (10mg/ml BSA, 1mg/ml Collagenase Type IV, 1 U Dispase I in DMEM media) in a 37°C incubator with mild shaking for 42 minutes. Media containing the tissue was passed through a 16G syringe every 4 minutes. Thereafter, digested tissue was passed through a 70 µm nylon filter, to remove debris and tissue matrix. Cells were pelleted by centrifuging tubes at 800 rpm for 5 minutes. Cells are washed with 0.1% BSA in PBS 2x times. Cells were resuspended in 3 ml of 0.1% BSA in PBS in a 5-ml polypropylene tube. 20µl of CD31 coated Dynabeads were added to the 3 ml of cell suspension and placed in a nutator in 4°C for 20 minutes. Beads containing CD31⁺ cells were concentrated by placing the polypropylene tube on the magnetic rack and sit for a minute. The cell-antibody-bead complex was washed 3 times with 0.1% BSA in PBS by repeating the above steps. Cells were released from the beads by incubating with 0.05% Trypsin for 3 minutes at 37°C. CD31⁺ ECs were then used for RNA extraction or protein extraction.

Table II. Primer Sequences for Genotyping

	Name	Sequence (5'-3')
1	<i>Nanog-Lox-F (Forward)</i>	5'-GAGATGGCGCAACGCAATTAATG-3'
2	<i>Nanog-R (Reverse)</i>	5'-GAAAAGATTAGCATGGCCGCACAGG-3'
3	<i>Tdtomato-Forward</i>	5'-AGCAAGGGCGAGGAGGT ATC-3'
4	<i>Tdtomato-Reverse</i>	5'-CCTTGGAGCCGTACATGAACTGG-3'
5	<i>Cdh5^{CreET2}-Forward</i>	5'-GATCGCTGCCAGGATATACG-3'
6	<i>Cdh5^{CreERT2}-Reverse</i>	5'-AATCGCCATCTTCGAGCAG-3'

M. Inducible Deletion using the Genetically Engineered Modified Mice (GEMM) System

Rosa^{mT/mG}::Nanog^{fl/+}::Cdh5^{CreERT2} is a TAM inducible genetically engineered modified mice (GEMM) system. Administration of TAM induces activation of Cre recombinase in a tissue-specific manner. EC-specific expression of *Cdh5^{CreERT2}* in the reporter *Rosa^{mT/mG}* background allowed us to visualize Cre mediated recombination in adult vascular beds, which was indicated by a change in tdTomato red protein (TdTomato red) to Green fluorescent protein (GFP) only in the endothelial compartment. To mediate TAM inducible Cre activation, approximately 8 weeks-old mice were given intraperitoneal injections of TAM. The stock concentration of TAM in corn oil was prepared at 2mg/ml and filtered using a 0.22µm filter. This was stored at -20°C for longer periods or 4°C for one week. Thereafter, using a 26G needle, mice were administered 100µl of either vehicle (corn oil) only or 100µl of TAM (2mg/ml) for five consecutive days. After which, there was a waiting period of 7 days (d7), 14 days (d14), 21 days (d21) and 30 days (d30). At d7

post-TAM administration, CD31⁺ cells from mice hearts were isolated and used either for RNA, DNA or protein extraction for downstream analysis. Endogenous expression of tdTomato red and GFP was visualized using 5µm thin cryosections prepared from the murine hearts under an epifluorescence microscope (Olympus BX51). All animal experiments are approved by ACC protocol number 17-129 (Baruah et al. 2017).

N. Echocardiography

Groups of *Rosa^{mT/mG}::Nanog^{fl/+}* and *Rosa^{mT/mG}::Nanog^{fl/+}::Cdh5^{CreERT2}* at approximately 8 weeks of age (either male and female) were injected (either with corn oil) or with TAM for five consecutive days followed by a waiting period of 30 days (d30) or 4 weeks. At the end of 30 days, mouse heart functions were evaluated with the use of echocardiography. Echocardiographic evaluation was carried out by the Cardiovascular Physiology core at the University of Illinois at Chicago and is covered under ACC protocol 17-129. In brief, the mice were initially anesthetized with etomidate (10mg/kg BW) and intubated with a 18G angiocath sleeve. Animals were maintained under inhalation anesthesia (1.5% isoflurane), which was delivered with a nasal cone connected in series to a rodent ventilator. The stroke volume was set at (0.2-0.3)ml/min and respiration rate of 135 beats per minute. The depth of anesthesia was assessed by toe pinch reflex method. The chest of each mouse was shaved and prepped with ethanol, followed by betadine solution. Transthoracic echocardiography was performed using Vevo 220 (Visual Sonics, Toronto, ON, Canada). Two-dimensional M-mode tracing and pulse Doppler measurements of the Left Ventricle (LV) was measured at the parasternal short axis and long axis at the view of the papillary muscles. The following dimensions were measured according to the American Society of Echocardiography leading edge method on the M-mode tracing; Interventricular septal, LV posterior wall thickness and LV and RV (Right Ventricle)

internal dimensions were measured at the end of diastole and systole (Baruah et al. 2017). All measurements were made from at least three consecutive cardiac cycles. Following this procedure, the mice were euthanized and hearts were harvested for post hoc analysis.

O. JC-1 Staining of Mitochondria

Live Cell staining of mitochondria with JC-1 dye. Cultured ECs grown on glass bottom culture dishes, were Untransfected (control), or transfected with *Control* and *NANOG siRNA* followed by an incubation for 48 hours. Thereafter, cells were stained with 0.5 μ g/ml JC-1 dye (T3168, ThermoFisher Scientific, Waltham, MA) for 1 hour at 37°C and Hoechst dye to stain the nucleus. Cells were imaged live with Zeiss LSM 810 confocal microscope at 63x magnification. Images were saved as. czi and analyzed with Zen software.

P. Statistics

All experiments were conducted in triplicates and repeated at least three independent times. For animal experiments, n=6 mice per group were used. Data obtained were analyzed using the statistical software GraphPad Prism version 6. For comparison between two groups, unpaired student's T-test was used. For comparison between multiple groups, data were analyzed with ANOVA followed by either Sidak's or Tukey's test or Dunnett's test. Sidak's test is used when comparison is made between a set of means. Tukey's test compares mean of a sample to every other mean. Dunnett's test compares every to a control mean. A P value of <0.05 was considered significant. The error bars represent mean \pm SD (Standard deviation).

IV. RESULTS

A. Nanog Expression in Adult Tissues and Vascular Endothelium

To analyze the expression of Nanog in adult tissues, we used the publicly available database <https://www.biogps.org>. The database has a repository of multiple tissue samples from different species including human and mouse. The data obtained is curated and represented as a histogram to indicate the expression pattern of NANOG across the tissue samples. Accordingly, we found that NANOG is expressed in a panel of human and mouse tissues (**Figure 8 and Figure 9**). To identify and localize NANOG⁺ and CD31⁺ vascular ECs in the myocardium, human heart sections from a 55-year-old donor and 3 month old murine heart sections were immunostained with anti-NANOG (red) and anti-CD31(green) or anti-vWF (green) antibodies (**Figure 10A-G**). Interestingly, in both the species, we identified a pool of CD31⁺ cells that stained positive for Nanog. This indicated that there is a subset of ECs in the adult coronary vasculature which expressed Nanog.

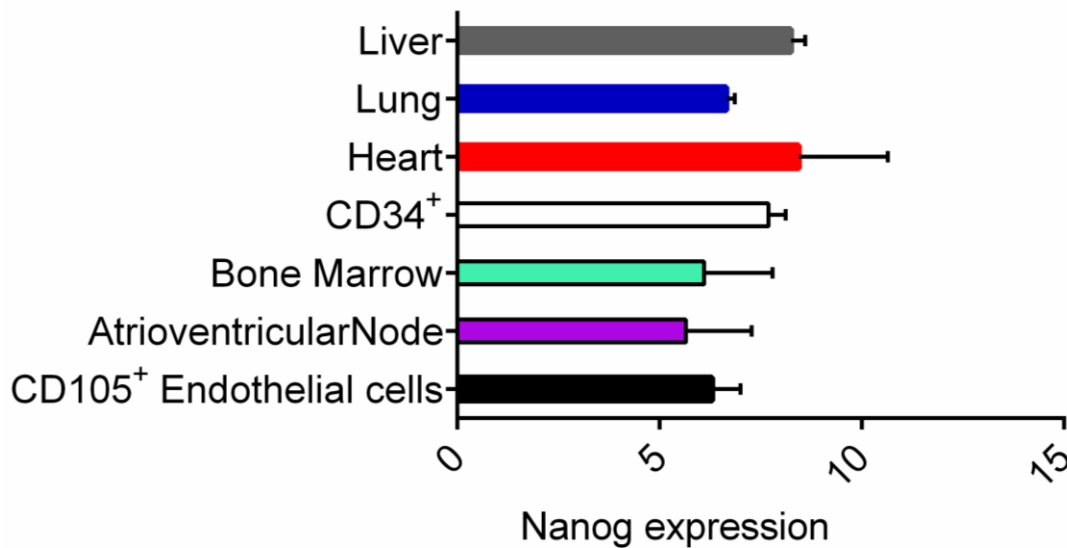


Figure 8: Expression of *NANOG* in adult human tissues. A) Differential expression of *NANOG* in a selected array of adult cells and vascularized tissues. Raw data obtained from at biogps.org. Dataset ID: GeneAtlas U133A, gcrma is plotted as a histogram using Graphpad prism software. The tissue specific mRNA expression patterned is obtained using high-density oligonucleotide array and included embryonic stem cells (ESCs) as positive control. Error bars represent mean \pm SD

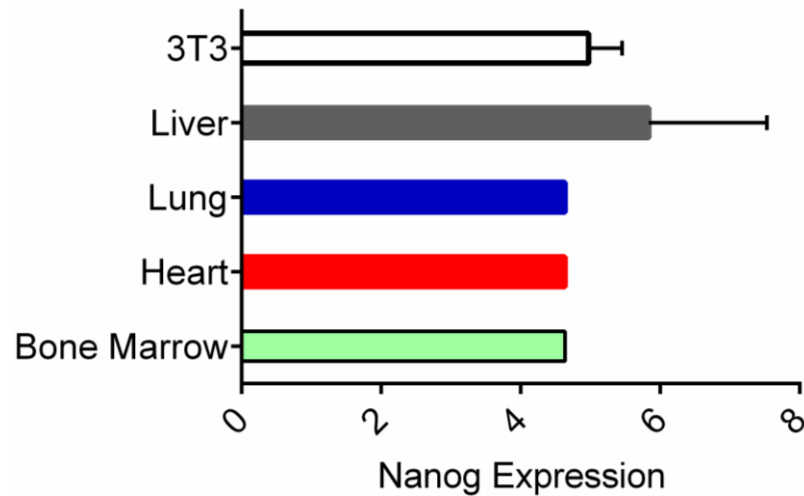


Figure 9: Expression of *Nanog* in adult mouse tissues. A) Differential expression of *Nanog* in a selected array of cells and adult vascularized tissues. Raw data obtained from at biogps.org. Dataset ID: GeneAtlas MOE430, gcrma is plotted as a histogram using Graphpad prism software. The tissue specific mRNA expression patterned is obtained using high-density oligonucleotide array and included embryonic stem cells (ESCs) as positive control. Error bars represent mean \pm Standard error of difference.

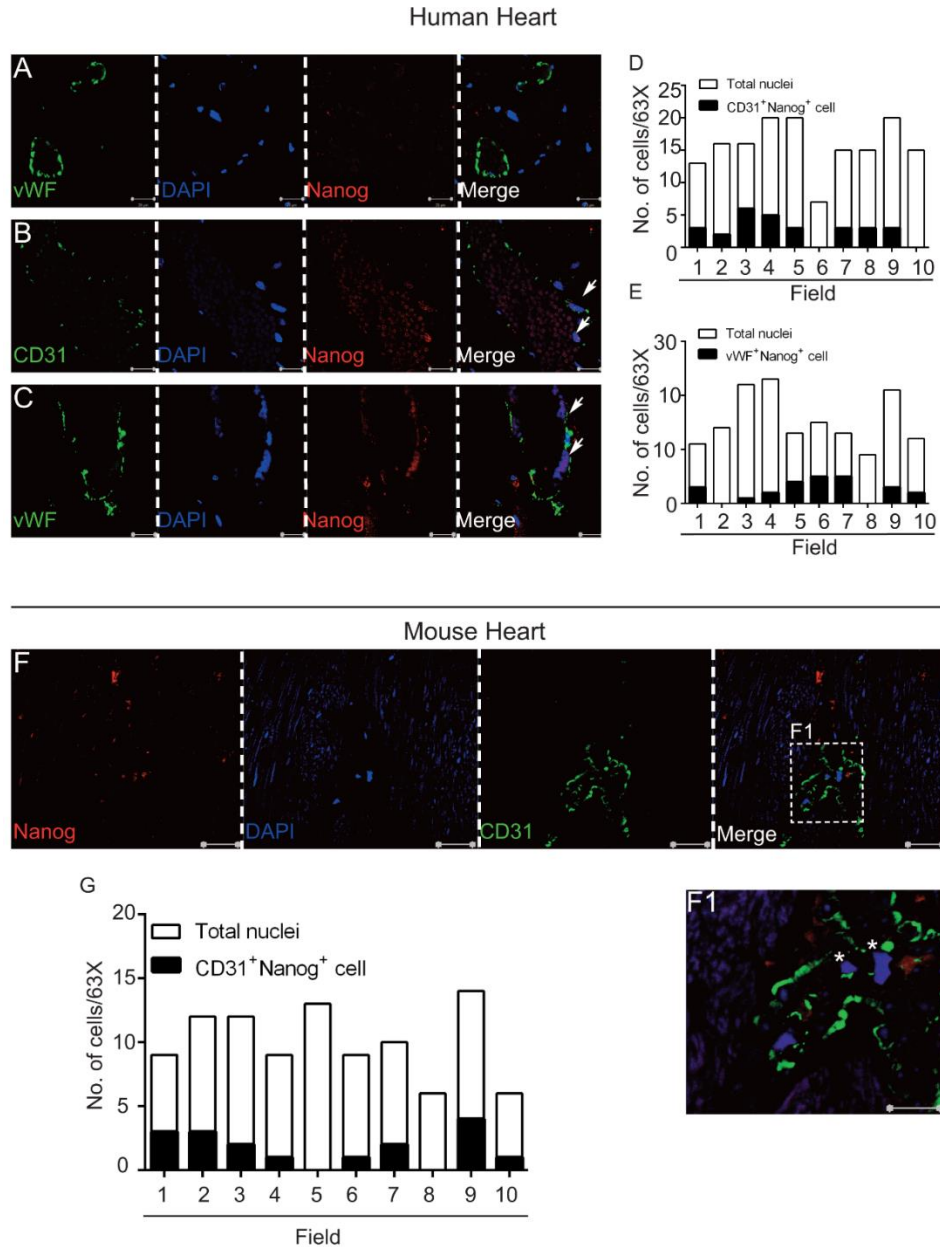


Figure 10: Microscopic analyses of Nanog⁺ cells in human and mouse heart tissues. Human heart sections obtained from a 55-year-old donor shows: A) Undetectable anti-Nanog⁺ (red) immunoreactivity in the nucleus in anti-CD31⁺ vascular structures. B) Anti-Nanog⁺ (red, nucleus) immunoreactivity in CD31⁺ (green) vascular structures. C) Anti-Nanog⁺ (red, nucleus) immunoreactivity in anti-vWF⁺ myocardial EC. White arrows indicate ECs expressing Nanog. D,E) Quantification of CD31⁺/vWF⁺ and Nanog⁺ cells in ten different fields at 63x magnification. Three (3) months old mouse heart tissue sections shows: F) the presence of Nanog⁺ (red, nucleus) in CD31⁺ (green) blood vessels. F1) Inset shows zoomed area with asterisk (*) indicating CD31⁺ and Nanog⁺ cells. G) Quantification of CD31⁺ and Nanog⁺ cells in ten different fields at 63x magnification. Scale bar as indicated. White dotted line indicates separation of panels.

B. Wnt3a Induced hTERT Expression and Telomerase Activity (TA) in Vascular ECs

To address if Wnt3a stimuli can induce expression of hTERT in ECs, a monolayer of ECs from different vascular beds was stimulated with Wnt3a (50ng/ml) for 6 hours. Control cells were left unstimulated. Thereafter, mRNA obtained from the control and stimulated cells were subjected to quantitative-real time-PCR analysis (qRT-PCR). Interestingly, Wnt3a induced expression of *NANOG* and *hTERT* genes in ECs (**Figure 11A-C**). To further assess if the increase in mRNA levels also resulted in an increase in the protein expression, total cell lysates were prepared from Control and Wnt3a stimulated ECs. The protein extracts were separated using sodium dodecyl sulfate (SDS)-Polyacrylamide gel electrophoresis (PAGE) and subjected to WB analysis. The membrane was immunoblotted with anti- β -catenin, anti-NANOG, and anti-hTERT antibodies. Anti-GAPDH was used as a loading control. In the unstimulated group, NANOG and hTERT were expressed at very low levels. Whereas Wnt3a stimuli significantly increased the expression of these proteins. We included β -catenin as a positive control to assess Wnt3a activation (**Figure 12A, B**). Using high-resolution confocal imaging, we also confirmed an increased localization of hTERT (red) in the nucleus of Wnt3a stimulated ECs compared to control groups (**Figure 12C**).

Next, we determined if increased hTERT protein expression induced telomerase activity (TA) in ECs. Quiescent or monolayer ECs do not have TA. Control (unstimulated) and Wnt3a (50ng/ml) stimulated ECs for 6 hours were used to prepare the cell extracts for highly sensitive telomerase repeat amplification protocol (TRAP) assay. The TRAP protocol utilizes endogenous hTERT activity to amplify telomere repeat products, which was then resolved using a vertical acrylamide gel electrophoresis. We found that unstimulated ECs were devoid of any TA, while Wnt3a stimuli induced TA in ECs (**Figure 12D, E**). The lanes on the right include telomerase +

cell extract as the positive control; a synthetic TSR8 template having amplicons with 6 base pair increments, and a quality control lane (**Figure 12D, E**). These results indicated that Wnt3a induced expression of hTERT and subsequently TA in otherwise quiescent ECs.

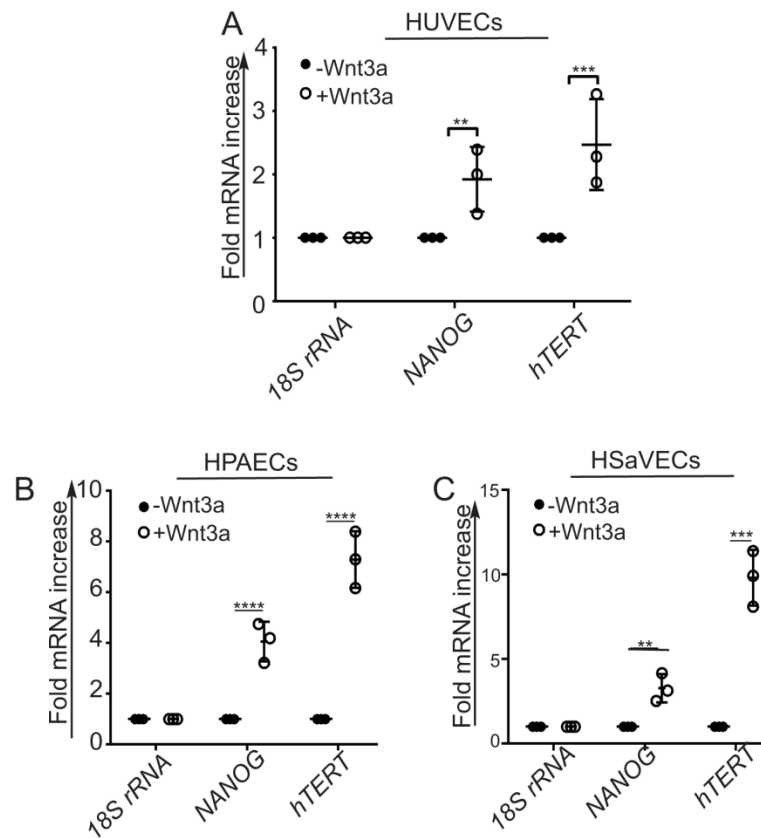


Figure 11: Wnt3a induced expression of *NANOG* and *hTERT* mRNA in arterial and venous ECs. qRT-PCR analysis of *NANOG* and *hTERT* genes with *18S rRNA* as the internal control in A) HUVECs B) HPAECs and C) HSaVECs. Error bars represent mean \pm SD.

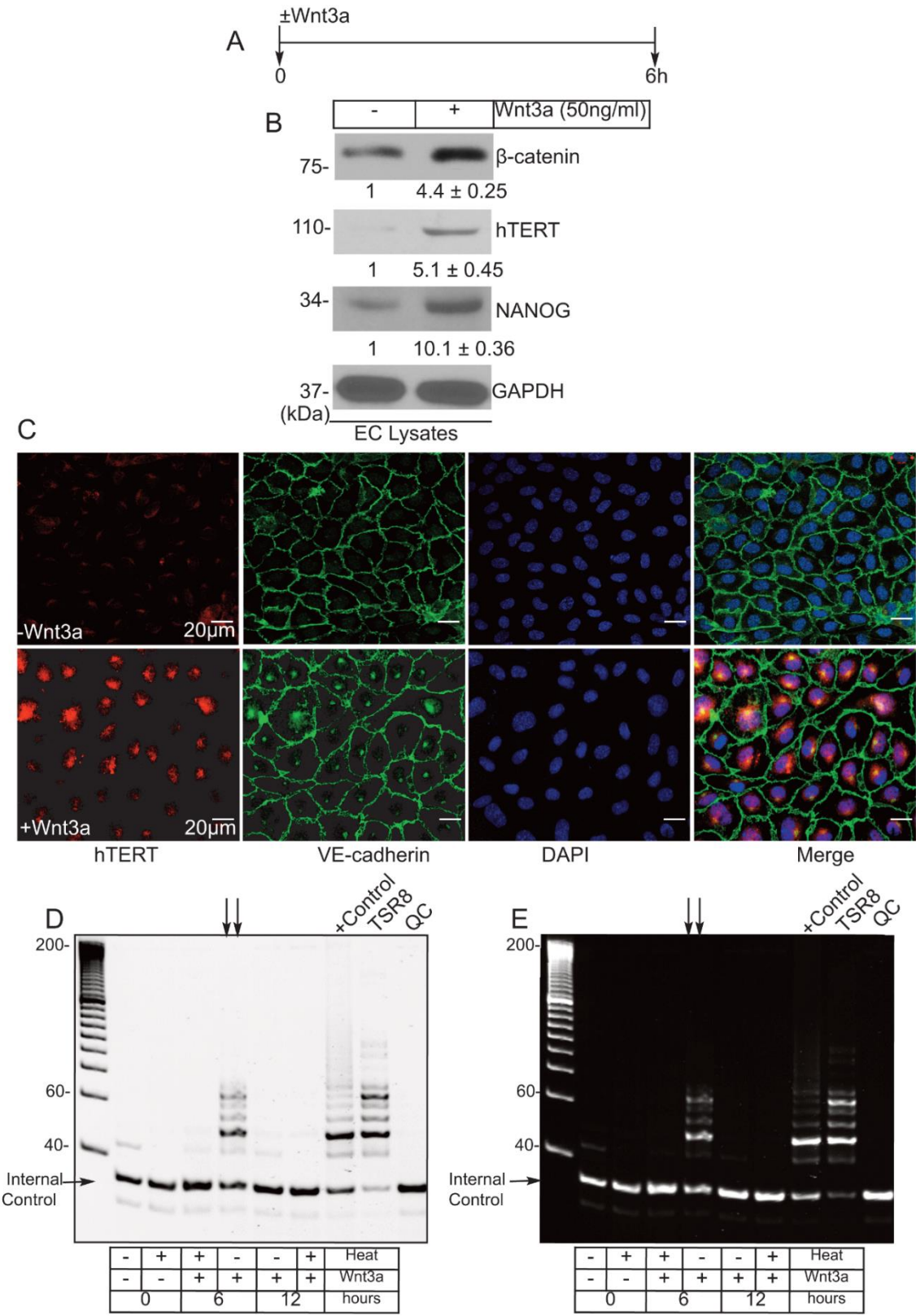


Figure 12: hTERT expression and telomerase activity in ECs. A) Timeline showing Wnt3a (50ng/ml) stimuli of cultured ECs and WB analysis of NANOG and hTERT proteins in response to Wnt3a stimuli. B) WB analysis of total cell lysates prepared from control and Wnt3a stimulated ECs, indicated the increased expression of NANOG and hTERT protein levels. β -catenin served as a positive control. Equal loading is shown by probing with anti-GAPDH. C) Immunocytochemistry of control and Wnt3a stimulated ECs, stained with anti-VE-cadherin (green) and anti-hTERT (red), indicates nuclear localization of hTERT in the Wnt3a stimulated group. Scale bar is 20 μ m. D) Inverted gel image for optimal viewing and resolution indicated telomerase activity (TA) of ECs in response to Wnt3a stimuli. Double arrows indicate TA in ECs. E) Unaltered gel micrograph indicates TA of ECs in response to Wnt3a stimuli.

C. Wnt3a Induced NANOG Binds to *hTERT* Promoter and Mediates its Transcription

To assess the mechanism underlying *hTERT* transcriptional activation, we performed a bioinformatics analysis of -3.6kb promoter DNA segment upstream of the *hTERT* transcription start site (TSS). Accordingly, we identified 16 potential NANOG binding elements (NBE) (**Figure 13A**). Using this information, we designed primers to target and amplify approximately 1.5kb region of *hTERT* promoter DNA fragment upstream from TSS, which contained eight (8) potential NBEs. In a ChIP-qPCR assay, we found that upon stimulation of cultured ECs with Wnt3a (50ng/ml), there was a significant binding of NANOG to the *hTERT* promoter DNA (**Figure 14A, B**). This interaction was not observed in control or unstimulated ECs. We further confirmed this binding by amplifying the eluted DNA with *hTERT* promoter-specific primers and resolved the amplicon in a conventional agarose gel electrophoresis (**Figure 14C**). This data suggested that Wnt3a induced NANOG bound to the *hTERT* promoter DNA regions in ECs.

In order to address if NANOG binding to the *hTERT* promoter in response to Wnt3a stimuli was functionally significant, we designed and generated three *hTERT* promoter-reporter constructs that were truncated at different sites upstream from the (+1) TSS, and contained different NBEs. Accordingly, the promoter construct one was -1701bp in length and had 6 NBE, promoter construct two was -1309 bp in length and had 1 NBE, and promoter construct three was -636 bp in length and had 0 NBE. These promoters were custom cloned into dual reporter pEZXLv04 from *Genecopia*. Lentiviral particles consisting of the promoter fragments were used to infect ECs in culture. Thereafter, cells were either unstimulated or stimulated with Wnt3a (50ng/ml) for 3 hours. The luciferase activity was normalized to constitutively secreted alkaline phosphatase (SEAP). The promoter construct containing 6 NBE showed a significant increase in

promoter activity in response to Wnt3a stimuli (**Figure 14D, E**). These results indicated that Wnt3a induced NANOG expression led to an increased *hTERT* promoter activity in ECs.

Furthermore, to precisely show the role of NANOG in the process of *hTERT* transcriptional activation, cultured ECs were co-transfected with *Control* and *NANOG shRNA* virus, and the -1701bp- *hTERT* promoter reporter fragment. The luciferase activity in NANOG depleted ECs was measured in response to Wnt3a (50ng/ml) stimuli for 3 hours. Interestingly, we observed a decrease in *hTERT* promoter activity in NANOG depleted ECs (**Figure 14F**). While NANOG depletion did not completely abolish *hTERT* transcriptional activity, this might indicate that *hTERT* promoter can be regulated by other TFs of the Wnt pathway. The data provided us with a proof of concept that Wnt3a induced NANOG bound to the *hTERT* promoter and regulated its transcription in ECs.

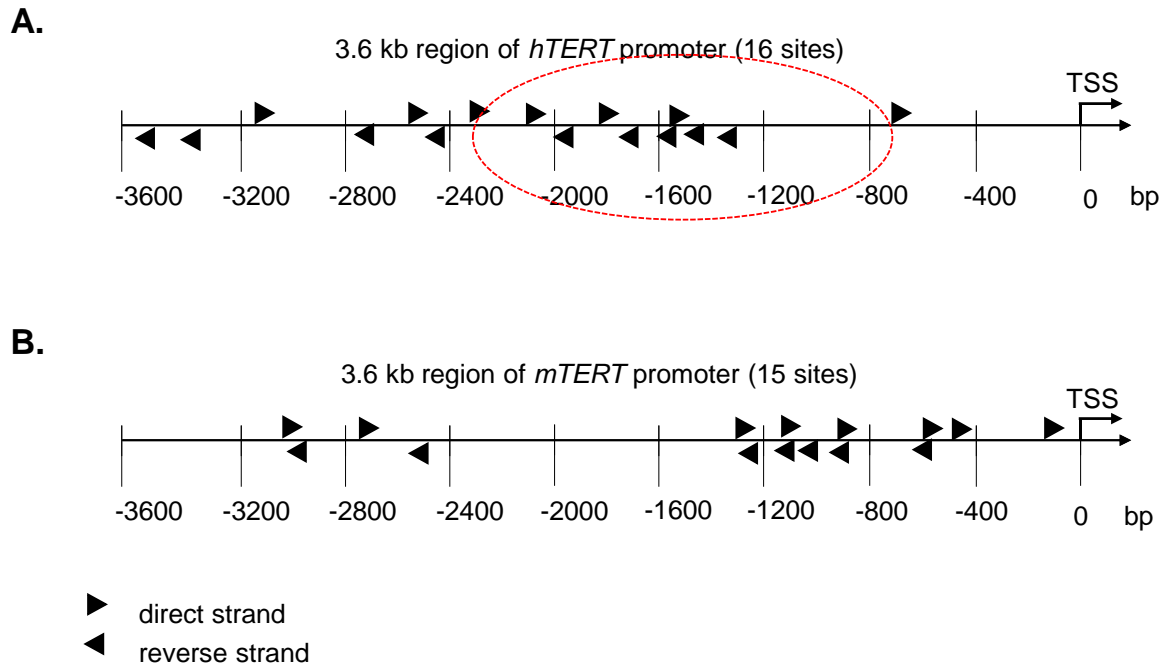


Figure 13: Scheme of human and mouse *TERT* promoters indicating NANOG binding sites. A) -3.6 kb of DNA from upstream of TSS indicate 16 NANOG binding elements (NBE) on the *hTERT* promoter. B) -3.6 kb of the mouse *Tert* promoter has 15 NBEs. Forward triangle indicates 5'-3' direction and reverse triangle indicate 3'-5' direction. The red dotted eclipse indicates region of interest used to validate NANOG binding in the ChIP assay. *Promoter sequence alignment provided in Appendix.

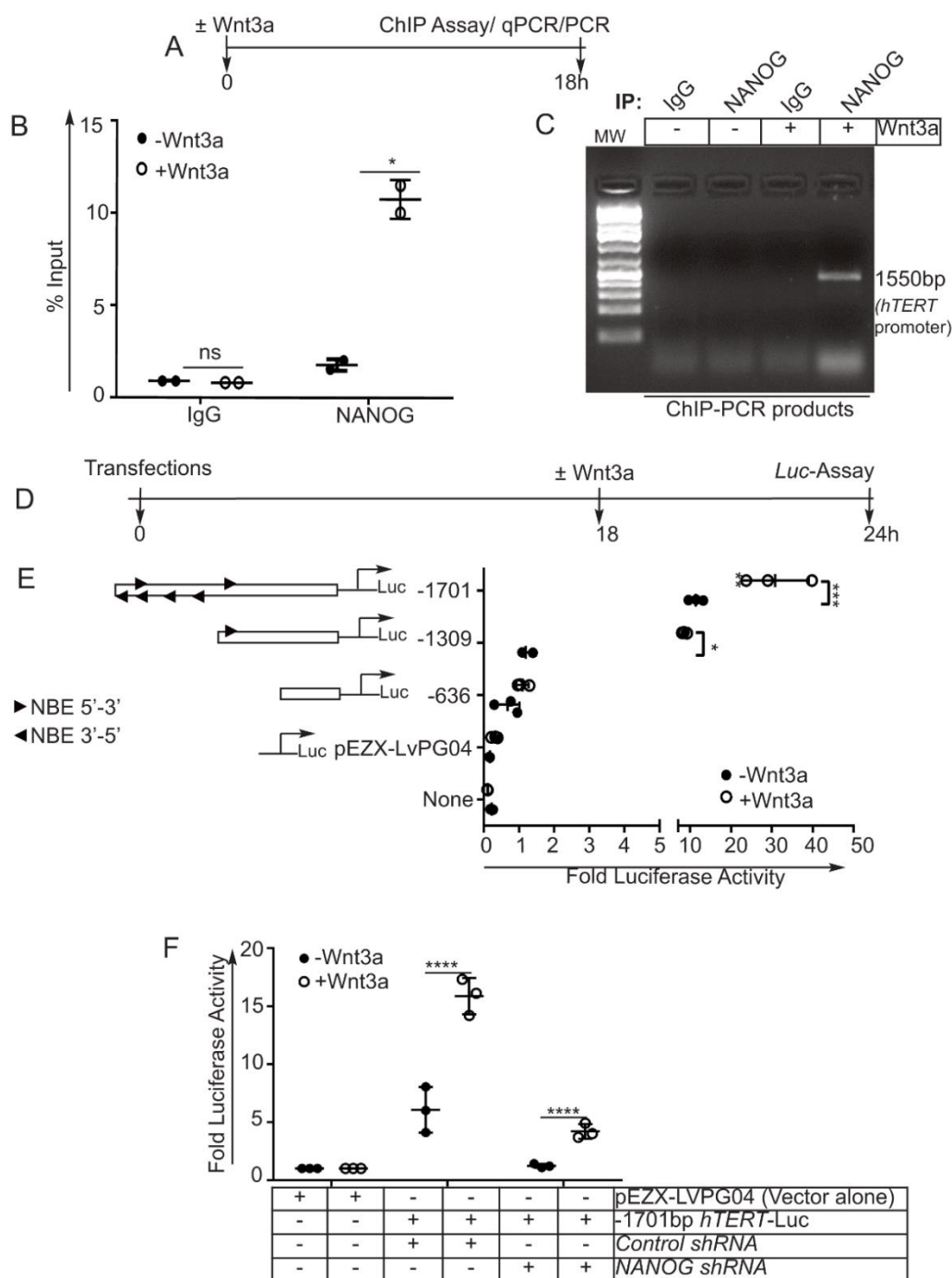


Figure 14: NANOG binds to the *hTERT* promoter region and regulates its transcription. A) Timeline of the ChIP assay followed by qPCR/PCR. B) Binding of NANOG to *hTERT* promoter in response to Wnt3a stimuli as indicated by % Input. C) Gel micrograph showing ChIP-PCR product of the *hTERT* promoter at ~1550bp. D) Transfections of ECs with promoter constructs followed by luciferase assay. E) Fold Luciferase Activity represents luciferase activity normalized over secreted alkaline phosphatase (SEAP). An increased Fold Luciferase activity of p1701-*hTERT*-Luc promoter in response to Wnt3a stimuli. F) Fold Luciferase activity of p1701-*hTERT*-Luc in *Nanog* depleted ECs, indicated a reduction in activity compared to controls. Error bars represent mean \pm SD.

D. Loss and Gain-of-NANOG Expression in ECs Alters hTERT Expression

Based on our ChIP and promoter activity data, we next examined the effects of NANOG depletion on hTERT expression in ECs. ECs were transfected with *Control* or *NANOG shRNA*, after 48 hours total mRNAs obtained from the two groups were subjected to qRT-PCR analysis. At the basal state, NANOG depletion resulted in a decreased expression of hTERT, along with NANOG target genes *CYCLIN-D1* and *VEGFR2* (**Figure 15**). To show that NANOG depletion altered hTERT expression in the presence of Wnt3a stimuli, ECs were transiently transfected with *Control* and *NANOG shRNA*, followed by a Wnt3a (50ng/ml) stimuli for 6 hours (**Figure 16A**). The total mRNAs obtained from *Control* and NANOG depleted ECs with or without Wnt3a stimuli were analyzed for the expression of *NANOG*, *hTERT*, *CYCLIN-D1* and *VEGFR2* genes. Interestingly, NANOG depletion significantly reduced the expression of hTERT in ECs even in the presence of Wnt3a (**Figure 16B**). A similar pattern was observed for the known NANOG target genes, *CYCLIN-D1* and *VEGFR2*. This data surmised that loss of NANOG resulted in a reduced expression of *hTERT* in ECs.

We further confirmed the mRNA studies by complementing with biochemical studies. Here, using the similar approach, ECs were transfected with *Control* or *NANOG shRNA* virus for overnight, followed by an incubation in complete media for additional 30 hours. Thereafter, cells were stimulated with or without Wnt3a (50ng/ml) for 6 hours. The total cell lysates prepared from *Control* and NANOG depleted ECs were subjected to WB analysis. The NC membrane was immunoblotted with anti-NANOG and anti-hTERT antibodies, with anti-GAPDH used to determine equal loading across all lanes. We observed that Wnt3a induced expression of NANOG and hTERT in ECs, while NANOG depletion resulted in a significant reduction of hTERT polypeptide levels in ECs (**Figure 16C, D**). This corroborated our previous observation

that Wnt3a induced NANOG expression efficiently regulated the expression of hTERT protein in primary ECs.

In an adjunct experiment, we exogenously expressed HA-tagged NANOG in cultured ECs and subjected the total lysates to WB analysis. The membrane was immunoblotted with anti-VEGFR2, anti-hTERT, anti-HA, anti-CYCLIN-D1, and anti-GAPDH antibodies. Interestingly, overexpression of NANOG in ECs led to a marked increase in the protein levels of hTERT, as well as VEGFR2 and CYCLIN-D1 (**Figure 16E, F**). Exogenous NANOG expression in the cells was confirmed by probing with an anti-HA antibody, which was absent in the control cells. These results demonstrated that by bypassing addition of Wnt3a, exogenously added NANOG led to a robust increase in the hTERT protein levels. This in turn highlighted the precise role of NANOG in regulating the expression of hTERT in ECs.

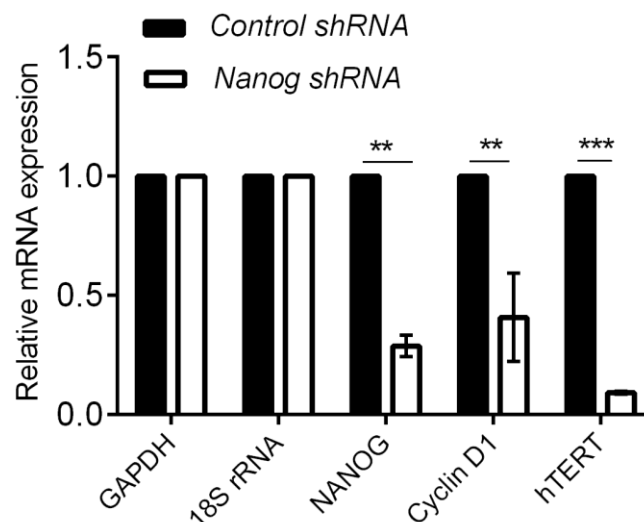


Figure 15: NANOG knockdown decreases *hTERT* expression in ECs. qRT-PCR analysis of *Control* and *NANOG* depleted ECs, indicate a reduced expression of *hTERT* and *CYCLIN-D1* genes in basal state. Error bars represent standard error of difference.

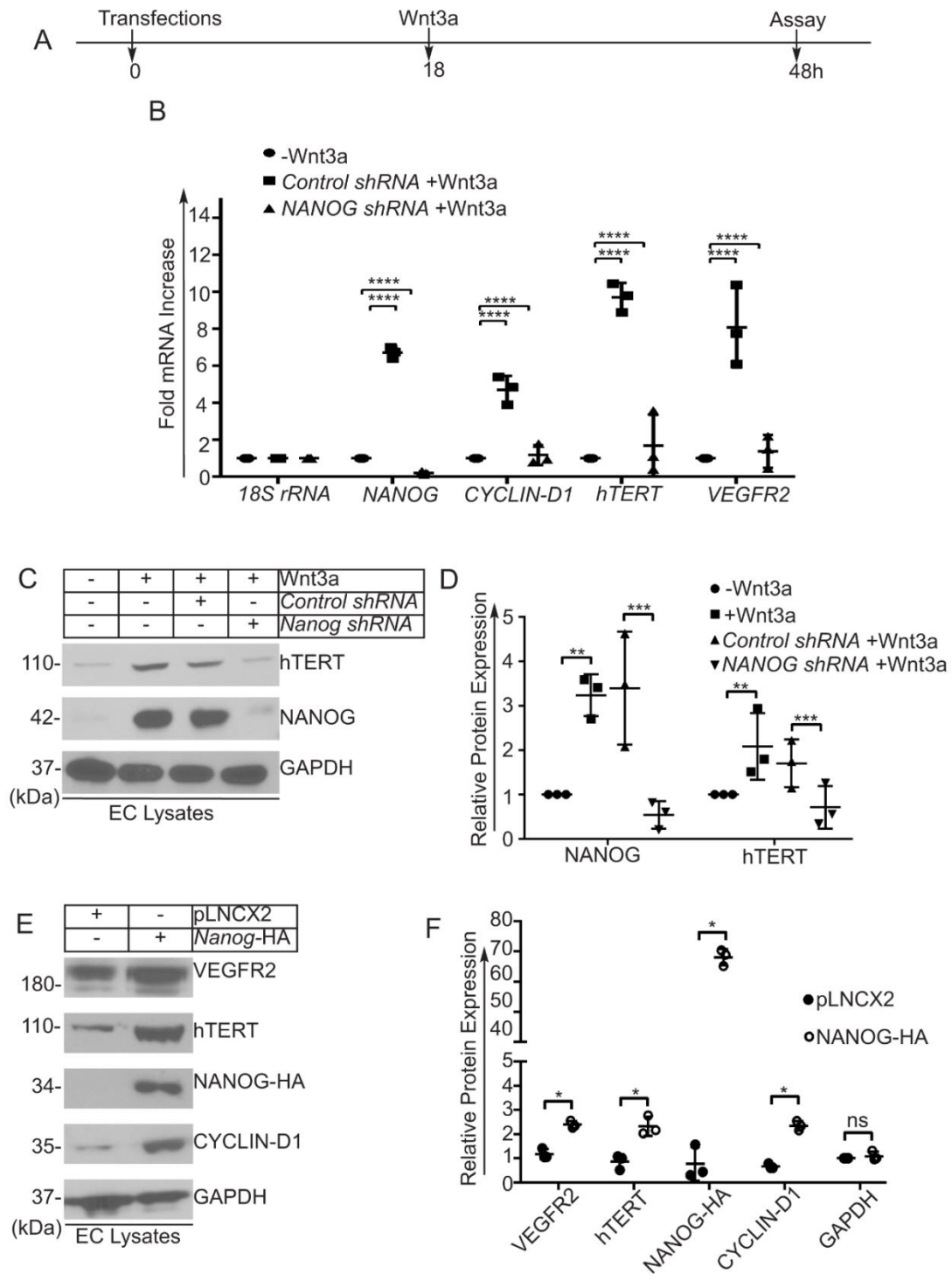


Figure 16: NANOG mediates expression of hTERT in ECs. A) Timeline of transfections. B) qRT-PCR analysis of *NANOG*, *hTERT*, *CYCLIN-D1* and *VEGFR2* genes in the presence or absence of Wnt3a. C) Immunoblots indicate depletion of NANOG proteins and reduced the expression of hTERT in ECs. D) Quantification of relative protein expression of NANOG and hTERT. E) Representative Immunoblots of control and HA-tagged NANOG transfected ECs, indicate the increased expression of VEGFR2, hTERT, CYCLIN-D1 proteins. F) Quantification of relative protein expression between control and HA-tagged *Nanog* groups. Error bars represent mean \pm SD.

E. Generation of Timed Inducible Single *Nanog* Allele Deletion Mice

To delineate and understand the functional significance of the NANOG>hTERT signaling axis *in vivo*, we generated the TAM inducible endothelial cell-specific *Cdh5^{CreERT2}* single *Nanog* allele knockout mice in a *Rosa^{mT/mG}* reporter mice background (**Figure 17A**). Due to the fact that *Nanog* homozygous loss of *Nanog* is embryonic lethal and majority of the cardiovascular phenotype resulted from mutations in a single copy of the gene, we engineered our mouse model that potentially mimicked a clinically relevant system and allowed us to address the loss of a single *Nanog* allele in adult vascular compartments of the heart (Yamaguchi et al. 2009; Chen et al. 2012; S. Oka et al. 2011; Yuldasheva et al. 2014; Theodoris et al. 2017). After a series of breeding and cross-breeding, groups of *Rosa^{mT/mG}::Nanog^{fl/+}::Cdh5^{CreERT2}* (*EC Nanog^{-/+}*) and *Rosa^{mT/mG}::Nanog^{fl/+}* (*Control*) mice were used for all *in vivo* experiments. *Nanog^{fl/+}* mice were produced in collaboration with UC Davis KOMP project as outlined in materials and methods. *Cdh5(PAC)-CreERT2* or *Cdh5^{CreERT2}* mice generated by Ralf H Adams were obtained through a material transfer agreement (MTA) from the UK Cancer Research Foundation. In this mouse system, Cre-ERT2 fusion protein is regulated by the EC-specific *Cdh5* promoter. Low-dose of TAM activates and leads to nuclear translocation of Cre-ERT2 protein enabling TAM-induced Cre recombinase activity only in the vascular ECs. The Cre activity thereby mediates recombination of lox-P elements flanking target gene resulting in knockout, knockin or transgene activation precisely in the vascular ECs. Absence of TAM treatment in *Cdh5^{CreERT2}* mice do not demonstrate Cre recombinase activity, while TAM-injected *Cdh5^{CreERT2}* mice demonstrate approximately 95% penetrance in vascular ECs. All animal experiments have been approved and covered by ACC protocol 17-129. The representative genotyping data indicated the presence of single *Nanog* *flox* allele, *Cdh5^{CreERT2}* allele, and *Rosa^{mT/mG}* allele (**Figure 17B-E**).

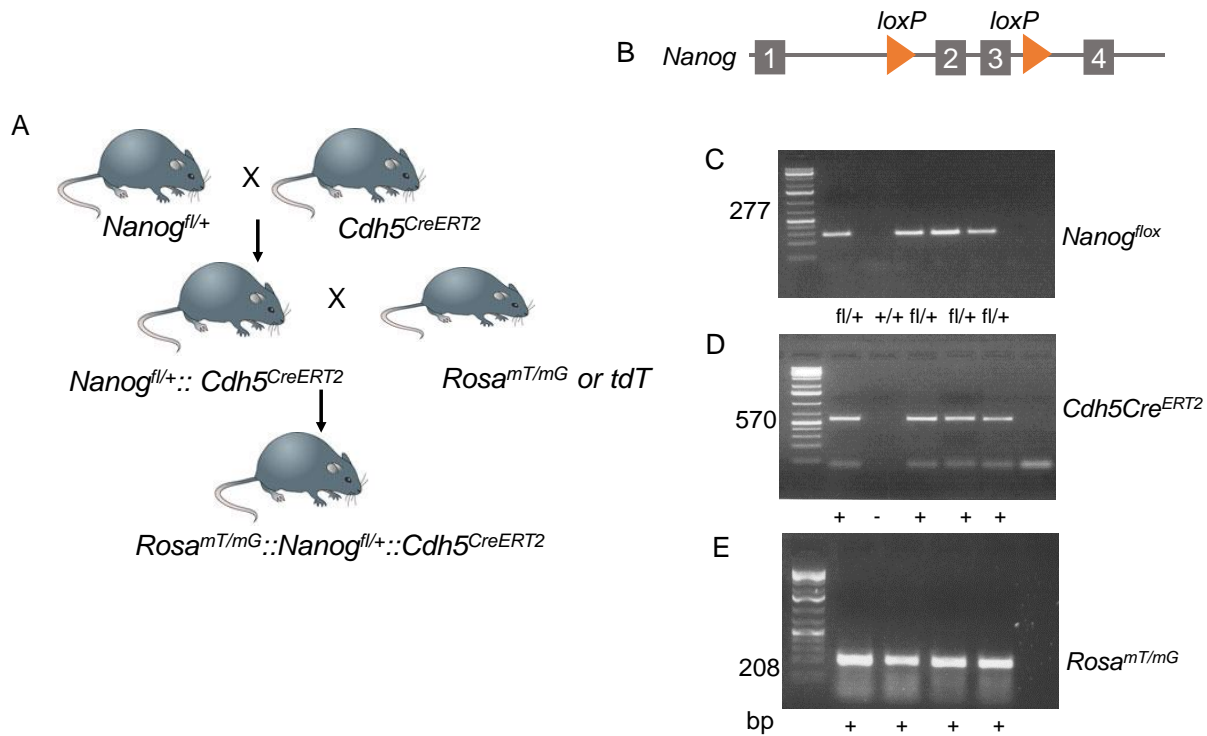


Figure 17: Generation of the *Rosa^{mT/mG}::Nanog^{fl/+}::Cdh5^{CreERT2}* mice. A) Scheme of generating *Rosa^{mT/mG}::Nanog^{fl/+}::Cdh5^{CreERT2}* mice. B) Scheme of the mouse *Nanog* gene indicate presence of loxP elements flanking the exon 2 and exon 3. C) Representative diagnostic genotyping PCR product confirm the presence of *Nanog^{fl/+}* allele. D) Representative diagnostic PCR-genotyping image confirm the presence of *Cdh5^{CreERT2}* loci. E) PCR product confirm the presence of *Rosa^{mT/mG}* allele. On left, the PCR product sizes (bp) are as shown. fl/+ : flox/wt ; + : presence; - : absence. Mouse image source: *Nature.com*.

F. Deletion of Endothelial Single *Nanog* Allele Reduces mTERT Expression *in vivo*

Similar to the human *TERT* promoter, a region of -3.6 kb mouse *Tert* promoter upstream of the Transcription Start Site (TSS) also harbors 15 potential NBEs (**Figure 13B**). This analysis provided us with the impetus to analyze the expression of *Tert* in response to single *Nanog* allele deletion in the coronary vasculature. To examine this, approximately 8 weeks old mice of the genotype *Nanog*^{fl/+}::*Cdh5*^{CreERT2} and *Nanog*^{fl/+} were given the intraperitoneal administration of low dose Tamoxifen (TAM) (2mg/BW) for five consecutive days or vehicle (corn oil) (**Figure 18A**). After a waiting period of 7 days, CD31⁺ cardiac ECs were isolated from the whole hearts and subjected to qRT-PCR analysis. There was a significant reduction in the mRNA levels of *Tert* along with *Vegfr2* in the cardiac ECs (**Figure 18B**). As expected, *NANOG* expression was reduced by approximately 50%, also confirmed at the protein level. CD31⁺ cardiac ECs were pooled from two mice hearts and total lysates were subjected to WB analysis. The membrane was immunoblotted with anti-Nanog, anti-Tert, anti-Vegfr2 and anti-Gapdh antibodies. As observed with the mRNA levels, there was a similar and significant reduced expression of Nanog and Tert protein in cardiac ECs (**Figure 18C, D**).

To further visualize and *in vivo* fate map single *Nanog* allele deletion in the coronary vascular endothelium, thin myocardium cryosections prepared from vehicle or TAM injected *Rosa*^{mT/mG}, Control and EC *Nanog*^{-/+} mice were analyzed with high-resolution confocal microscopy for endogenous expression of tdTomato red and green fluorescent protein (GFP) proteins. Administration of TAM activated *Cdh5* specific cre in the vascular endothelium leading to the conversion of tdTomato red protein to GFP. In control mice hearts, tdTomato red was expressed in a pan cellular manner, whereas in EC *Nanog*^{-/+} mice large coronary vessel and microvessel expressed GFP (**Figure 18E, F**) which indicated the efficiency of the system. This

data highlighted the efficiency of our GEMM system in mediating single *Nanog* allele deletion in target tissue such as the adult mouse myocardium.

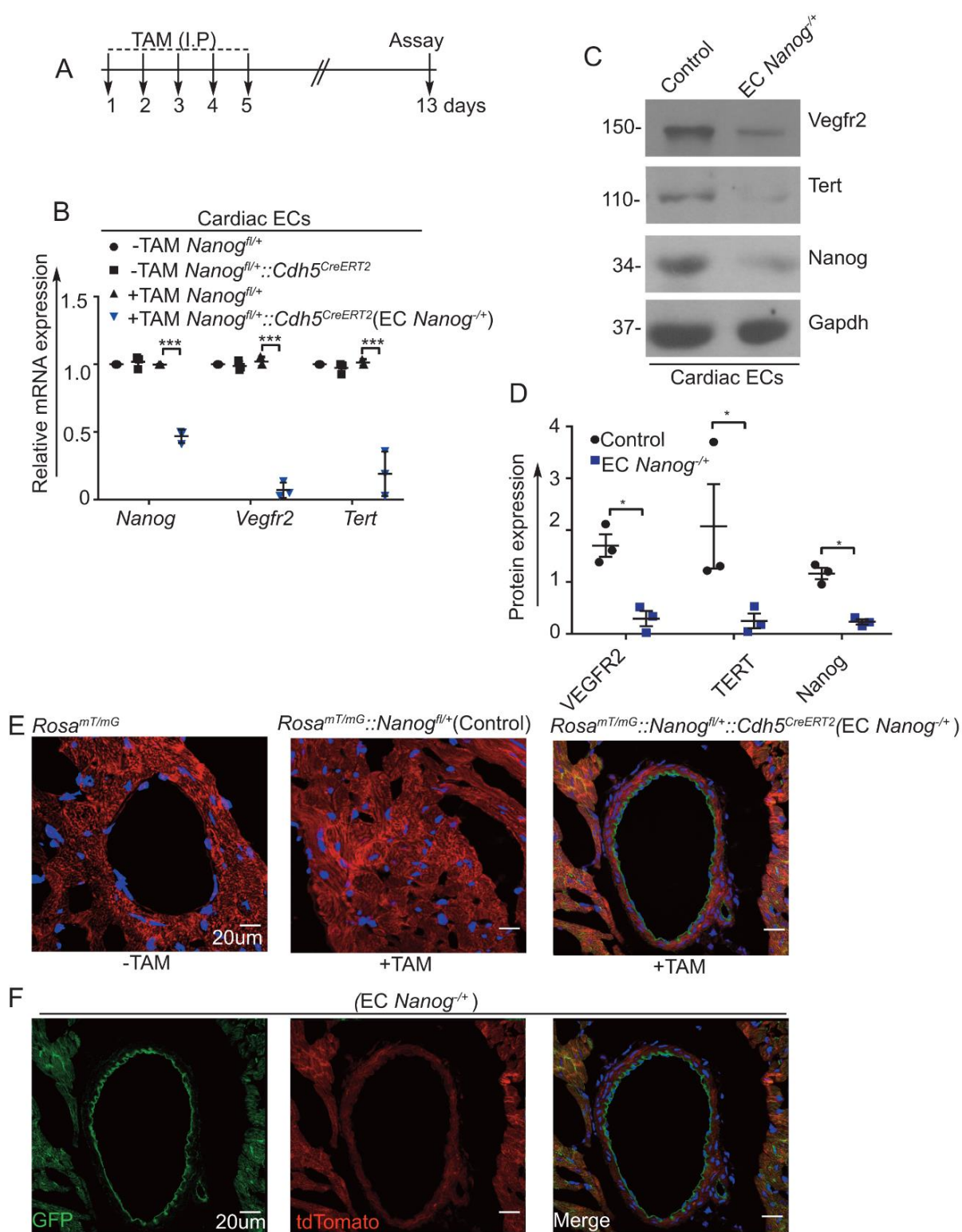


Figure 18: *Cdh5^{CreERT2}* mediated timed-inducible deletion of single *Nanog* allele in adult mouse hearts. A) Timeline of TAM administration. B) qRT-PCR analysis of CD31⁺ cardiac ECs, confirmed the deletion of single *Nanog* allele, along with a reduced expression of *Vegfr2* and *Tert* genes in EC *Nanog*^{-/+} mice versus control groups. C) WB analysis of pooled CD31⁺ Control and EC *Nanog*^{-/+} cardiac ECs indicated reduced expression of *Vegfr2* and *Tert* proteins. D) Quantification of protein expression of *Vegfr2*, *Tert* and *Nanog*. E) Thin myocardial sections were analyzed with high-resolution confocal microscopy indicate pan-cellular expression of tdTomato (red) protein in control groups, whereas green fluorescent protein (GFP) expression was localized to the vascular endothelial compartments in EC *Nanog*^{-/+} groups. Blue indicate nucleus stained with DAPI. F) Split channel images of dTomato, GFP and merged images. Scale bar is 20 μ m. Error bars represent mean \pm SD.

G. *Nanog* Haplo-insufficiency in ECs Results in Apoptosis of Vascular and non-Vascular Cells of the Heart

Next, we sought to characterize the phenotype resulting from inducible loss of single *Nanog* allele in the murine hearts in a time-dependent manner. Control and EC *Nanog*^{-/+} mice were administered intraperitoneal TAM (2mg/BW) injections for 5 consecutive days, followed by a waiting period of 7 days (d7), 14 days (d14), 21 days (d21) and 30 days (d30). Thin sections prepared from groups of mice were co-stained with anti-von Willebrand factor (vWF), an EC marker in magenta and TUNEL in green. Interestingly, there was a significant increase in EC and non-EC cell death in a time-dependent manner (**Figure 19B, C**). In addition, depletion of EC-specific NANOG resulted in an increased apoptotic cell death. Because cells were serum and growth factor starved overnight, basal cell death remained at 20% (**Figure 20**).

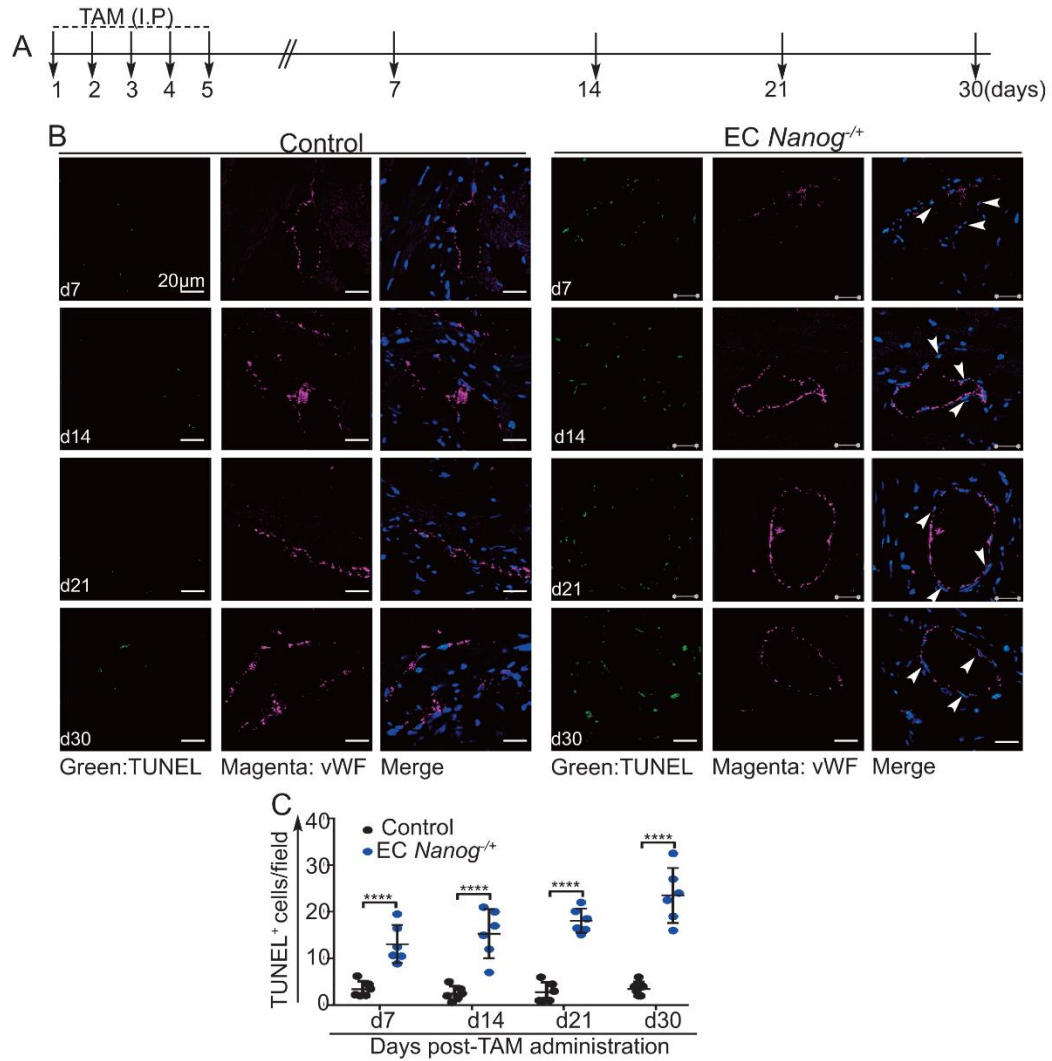


Figure 19: Characterization of Apoptotic (TUNEL⁺) cells in vWF⁺ vessels in mice myocardium. A) Timeline of TAM administration on control and EC *Nanog*^{+/+} mice groups. B) Representative immunohistological analysis of thin myocardial sections stained with anti-vWF (magenta) and TUNEL (green) indicate endothelial cell death along with non-endothelial cell death in a time-dependent manner. White arrows indicate vWF and TUNEL positive structures. C) Quantification of TUNEL⁺ cells in the myocardial sections. Scale bar is 20 μ m. n= 6 mice/group. Error bars represent mean \pm SD.

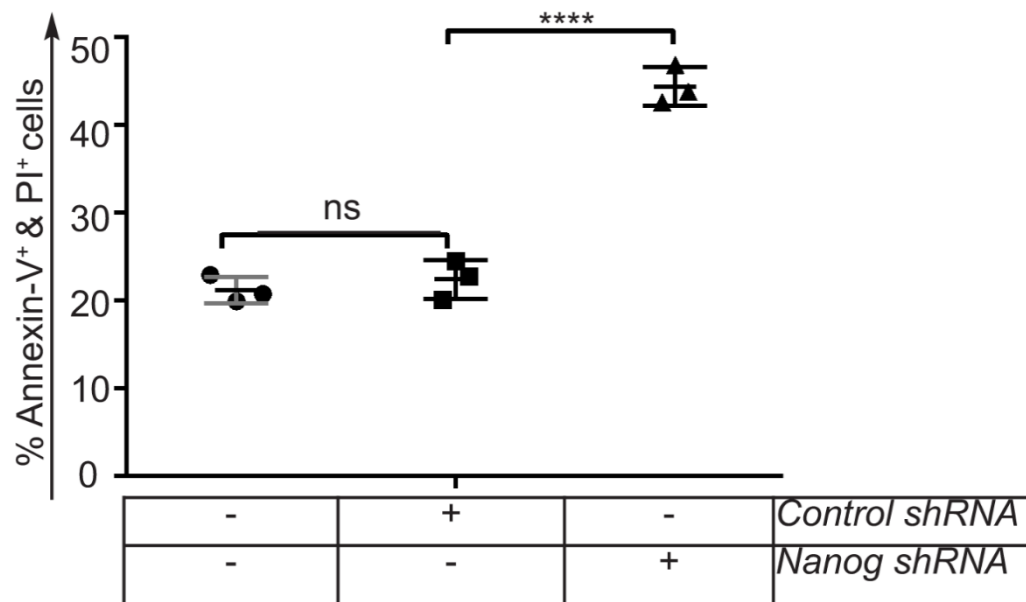


Figure 20: *NANOG* knockdown induces apoptosis in ECs. Untransfected (Control), *Control shRNA* and *NANOG shRNA* transfected ECs were labeled with Annexin-V (early apoptotic marker) and Propidium Iodide (PI) (necrotic marker) thereafter subjected to FACS analyses. *NANOG* knockdown resulted in a significant increase in Annexin-V⁺ and PI⁺ cells. Error bar represent mean \pm SD.

H. *Nanog* Haplo-insufficiency in ECs Results in Vascular and Perivascular Fibrosis

Apoptosis of ECs can trigger the release of inflammatory molecules, which in turn attract inflammatory, immune, and fibroblast cells. Therefore, to examine the extent of fibrosis in the EC *Nanog*^{-/+} mice hearts, we followed the similar regime of TAM administration on Control and EC *Nanog*^{-/+} groups and waited for 7, 14, 21 and 30 days. Paraffin-embedded thin sections were prepared from the mouse hearts, which were then subjected to Masson's trichrome staining to reveal the extent of fibrosis or collagen deposit (blue). Interestingly, we observed an increased fibrotic lesion in an around the vascular structures of the myocardium (**Figure 21A-C**). This data indicated that loss of single *Nanog* allele in the endothelium of adult hearts resulted in an increased fibrosis of the vascular compartments.

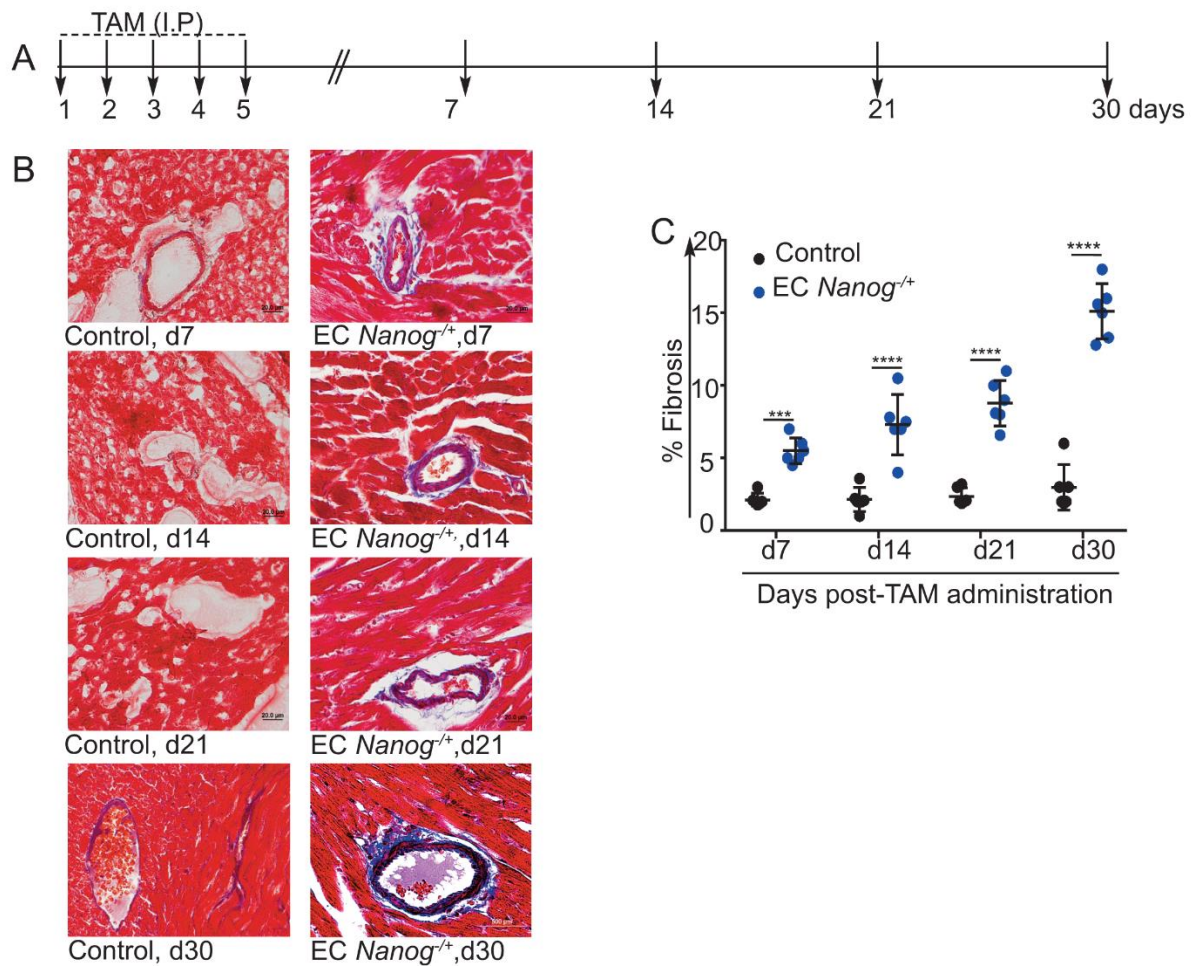


Figure 21: Visualizing fibrotic lesion in EC-single *Nanog* allele deleted mouse hearts. A) Timeline of tamoxifen (TAM) administration on control and EC *Nanog*^{-/-} mice groups. B) Representative immunohistological analysis of thin myocardial sections from control and EC *Nanog*^{-/-} mice groups stained with Masson's Trichrome staining (blue) indicate an increase in vascular and perivascular fibrotic lesion in a time dependent manner. C) Quantification of % fibrosis in the myocardial sections. Scale bar is 20 μ m. n= 6 mice/group. Error bars represent mean \pm SD.

I. Loss of single EC-*Nanog* allele Mice Hearts Displays Cardiac Hypertrophy like Phenotype

Because we observed profound apoptotic cell death and fibrosis of the vascular compartments in the hearts, next we conducted an echocardiographic evaluation of the hearts at d30 post-TAM administration. Accordingly, Control and EC *Nanog*^{-/+} mice hearts were injected with TAM (2mg/BW) for 5 consecutive days followed by a waiting period of 30 days (d30). Thereafter, mice hearts were analyzed with high-resolution echocardiography to evaluate cardiac parameters and function. Three representative M-mode tracing of the mice hearts at d30 post-TAM administration are shown (**Figure 22β**). Interestingly, EC *Nanog*^{-/+} indicated a significant increase in diastolic parameters; Left Ventricular Diameter at diastole (LVDd) in mm and Left Ventricular Volume at Diastole (LVVd) in μ l (**Figure 22C1, C2**), compared to Control hearts. The EC *Nanog*^{-/+} hearts had a decline in heart rate (**Figure 22C3**) compared to Control group. However, there was a significant increase in Cardiac Output (CO) (**Figure 22C4**) and Stroke Volume (SV) in μ l (**Figure 22C5**) in EC *Nanog*^{-/+} mice. To our surprise, EC *Nanog*^{-/+} hearts not only displayed LV hypertrophy and increased LV mass, but also a significant Right Ventricular Hypertrophy (RVH) (**Figure 22C6-C8**).

We further validated this by evaluating thin sections prepared from Control and EC *Nanog*^{-/+} mouse hearts with H and E staining and Wheat Germ Agglutinin (WGA) (**Figure 23**) staining to assess the cardiomyocyte area. H and E staining showed pan tropic presence of larger nuclei in EC *Nanog*^{-/+} mice compared to Control myocardium (**Figure 24B**). Moreover, whole hearts freshly excised and imaged revealed a significantly increased heart size of the EC *Nanog*^{-/+} group (**Figure 24D, E**). At the molecular level, there was a significant increase in genetic markers associated with CH, such as *Anp*, *Bnp*, *Myh7*, and *Et-1* in the EC *Nanog*^{-/+} versus

Control, indicating that disruption of EC homeostatic function via single *Nanog* allele deletion resulted in a cardiac hypertrophy like phenotype. **(Figure 24F)**.

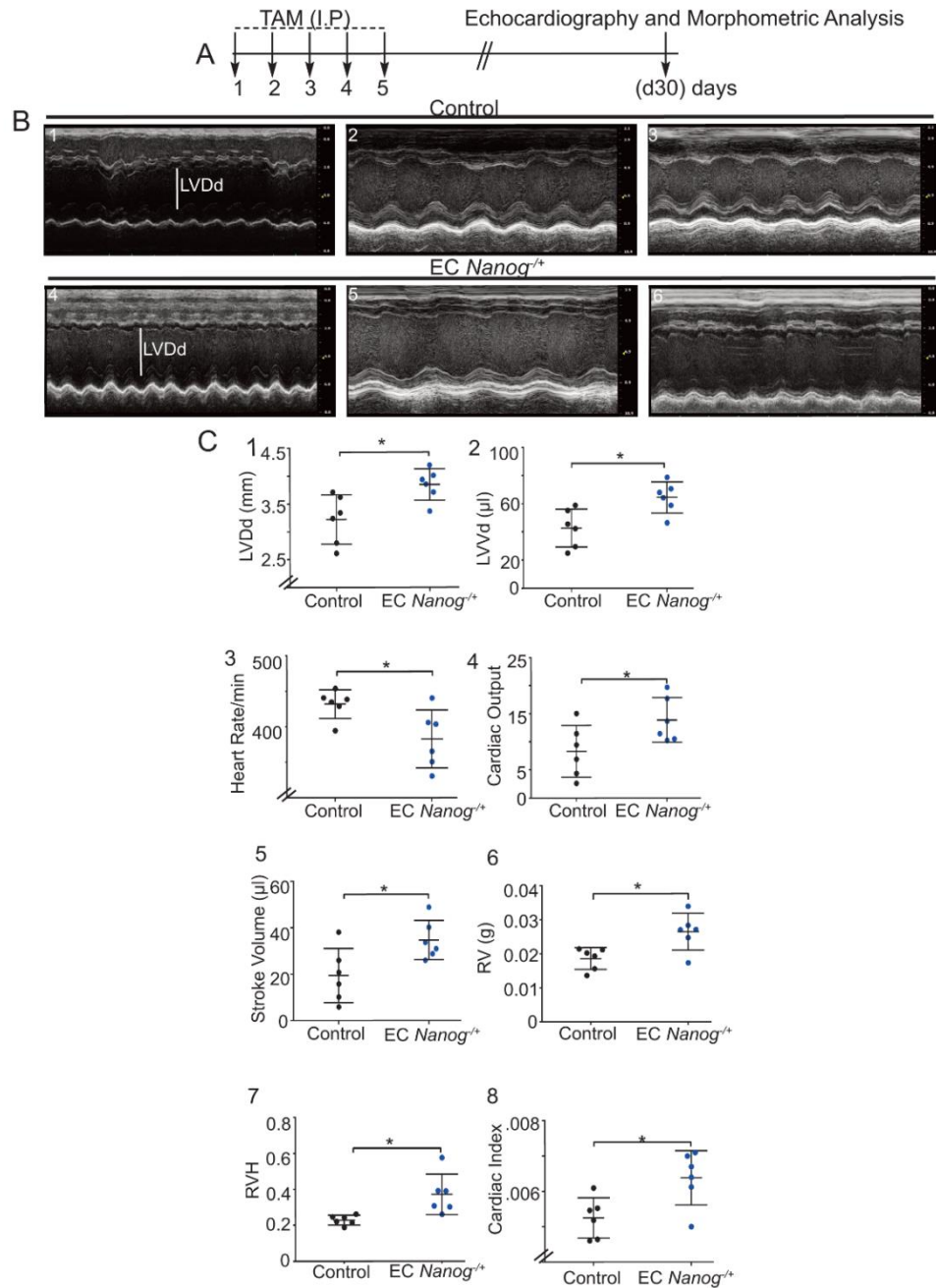


Figure 22: Echocardiographic evaluation of EC-specific single *Nanog* allele deletion in the mouse hearts. A) Timeline of TAM administration. B) Panel 1-3 show three representative M-mode tracing of the cardiac chambers of Control mice. Panel 4-5 show three representative M-mode tracing of cardiac chambers of EC *Nanog*^{+/+} mice. C) Quantification of left ventricular (LV) parameters at diastole in control vs EC *Nanog*^{+/+} mice. C1. Left ventricular diameter at diastole (LVDd) in mm. C2. Left ventricular volume at diastole (LVVd) in μl. C3. Heart rate per min C4. Cardiac output. C5. Stroke Volume in μl. C6. Right ventricular (RV) weight in grams. C7. Right ventricular hypertrophy (RVH): Ratio of RV weight to total weight of Left ventricle and septum. C8. Cardiac index: Ratio of wet heart weight/ body weight. n= 6 mice/group. Scale bar is 50μm. Error bars represent mean ± SD.

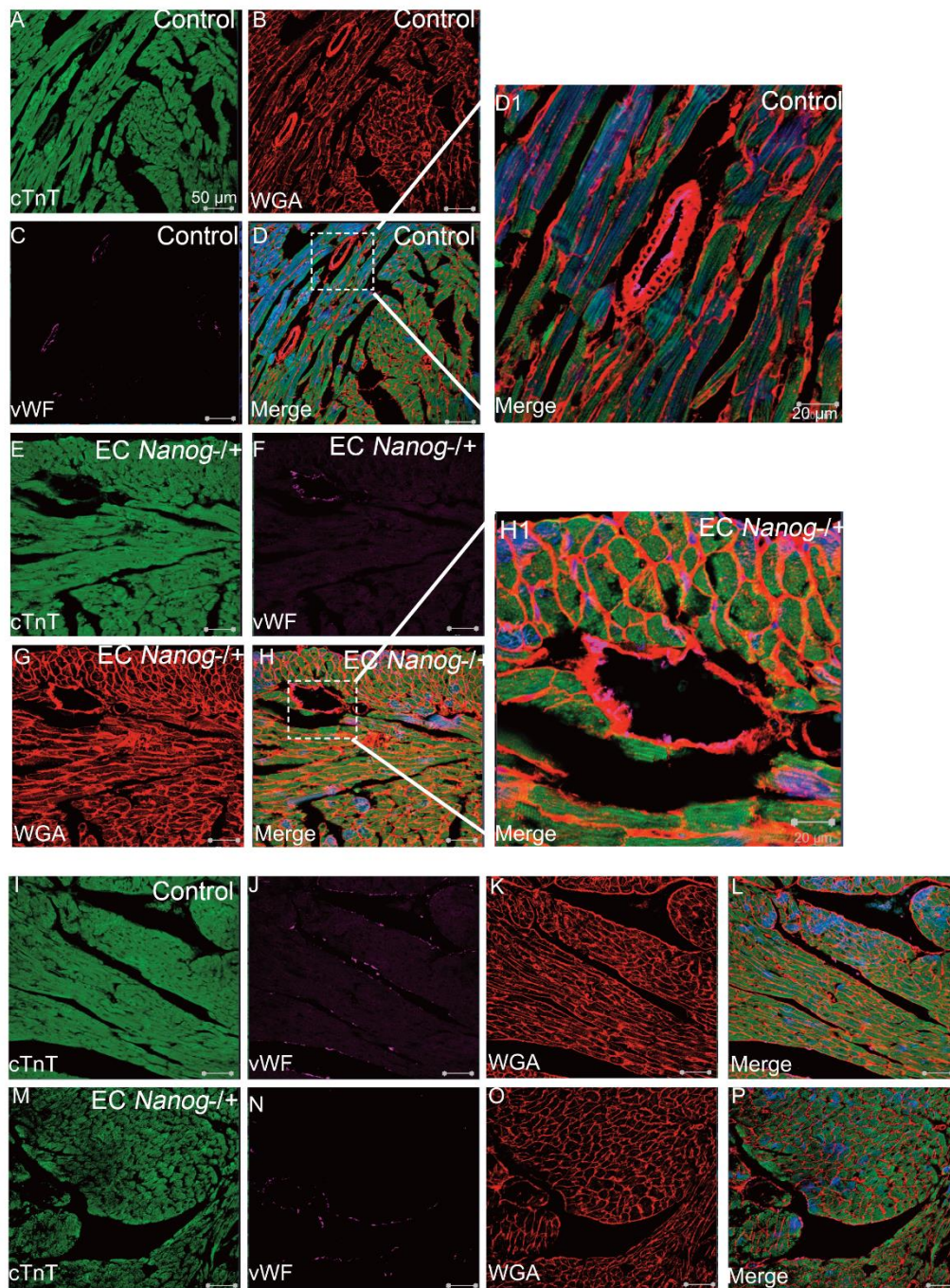


Figure 23. Phenotypic analyses of cardiomyocytes and the cardiac vasculature. A-D. Heart sections prepared from indicated mice were stained with anti-cardiac Troponin T (cTnT, green), EC marker (vWF, magenta), and lectin (red, WGA). D1) Inset indicates zoomed area highlighting the co-staining of EC membrane with WGA in vWF⁺ vascular structure. E-H) Heart sections prepared from indicated mice were stained with anti-cardiac Troponin T (cTnT, green), EC marker (vWF, magenta), and lectin (red, WGA). H1) Inset indicates zoomed area highlighting the co-staining of EC membrane with WGA in vWF⁺ vascular structure. I-L) Representative Control and M-P) EC *Nanog*^{-/-} mouse hearts from additional fields. Scale bar as indicated.

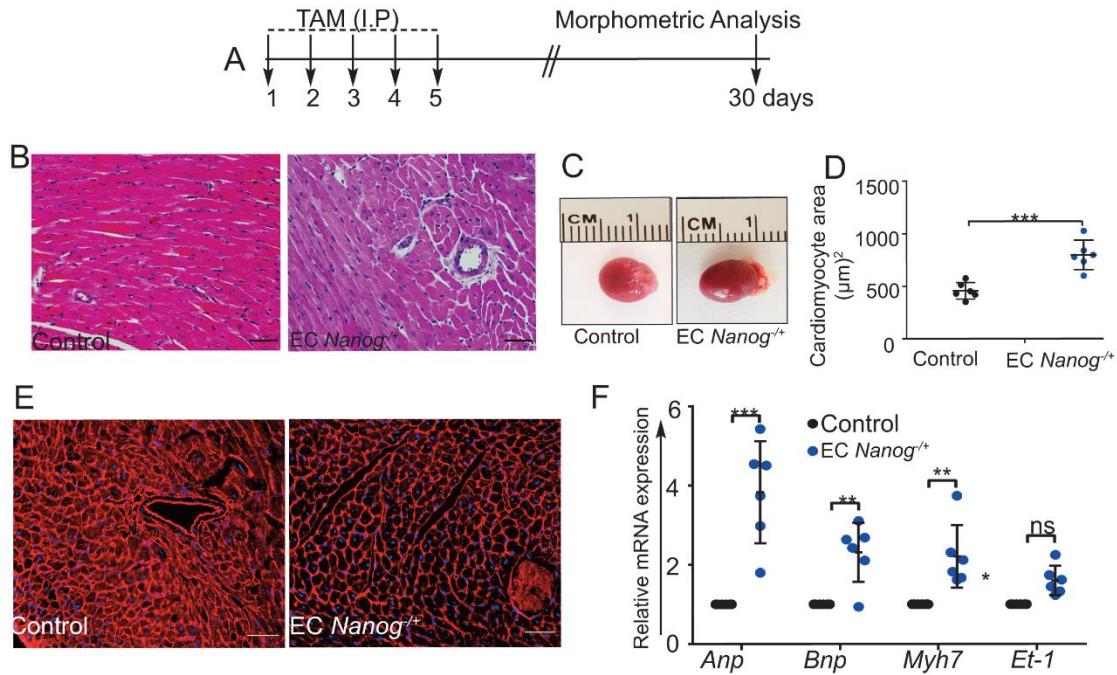


Figure 24: Cardiac hypertrophy as a result of EC-*Nanog* haploinsufficiency. A) Timeline of TAM administration. B) H and E stained myocardial sections from Control and EC *Nanog*^{+/-} mice show presence of larger nuclei in EC *Nanog*^{+/-} mice. C) Whole hearts excised and imaged at d30 indicate EC *Nanog*^{+/-} mice hearts to be larger in mass compared to Control. D) Quantification of cardiomyocyte cross-sectional area in Control and EC *Nanog*^{+/-} mice. E) Representative Wheat Germ Agglutinin (WGA) staining of ECs to assess cardiomyocyte area in Control and EC *Nanog*^{+/-} mice indicate an increase in cardiomyocyte area in EC *Nanog*^{+/-} mouse groups. F) qRT-PCR analysis of total mRNA extracted from whole hearts indicate an increase in molecular markers associated with cardiac hypertrophy, *Anp*, *Bnp*, *Myh7*, and *Et-1* in the EC *Nanog*^{+/-} mice group *versus* Control. n= 6 mice/group. Scale bar is 50μm. Error bars represent mean ± SD.

J. NANOG>hTERT Axis is Necessary for Preventing Apoptosis and Angiogenesis

Inhibition of apoptosis, cell proliferation, and ultimately forming the capillary network are essential during neovascularization involved in pathological or physiological angiogenesis. To show the precise role of Wnt3a induced NANOG/hTERT signaling in angiogenic activities, we designed *in vitro* rescue experiments where hTERT was exogenously expressed in NANOG depleted ECs and assessed cell proliferation, survival, and ability to form capillary-like networks in a 2D Matrigel assay (**Figure 25A**). We observed an increased cell proliferation measured by the extent of BrdU incorporation in nuclei of ECs in response to Wnt3a stimuli, which was significantly reduced in NANOG depleted ECs (**Figure 25B**). Interestingly, re-expressing hTERT into NANOG depleted ECs partially restored cell proliferation (**Figure 25B, C**). Using a similar scheme, we then performed a co-immunostaining of ECs with VE-cadherin and TUNEL staining to quantify the extent of cell death in NANOG depleted ECs and *hTERT* re-expressed ECs. NANOG depletion showed increased cell death as quantified by TUNEL⁺ cells per nuclei, while re-expression of hTERT in NANOG depleted ECs showed significantly reduced TUNEL⁺ cells (**Figure 25D, E**). Finally, to show that NANOG>hTERT axis is necessary during tube formation, control ECs (Untransfected); *Control* and *NANOG shRNA* transfected, and *NANOG shRNA* and *hTERT cDNA* co-transfected ECs were plated onto a 2D Matrigel matrix with Wnt3a stimulus overnight. In line with our previous observation, *Nanog* depleted ECs had reduced branch point structures compared to control group, the effect of which was partially restored in the *hTERT*-cDNA transfected ECs (**Figure 25F, G**). WB analysis confirmed the efficiency of NANOG depletion and TERT expression in ECs (**Figure 25H**). These results showed the precise role of NANOG>hTERT signaling axis in angiogenic activities.

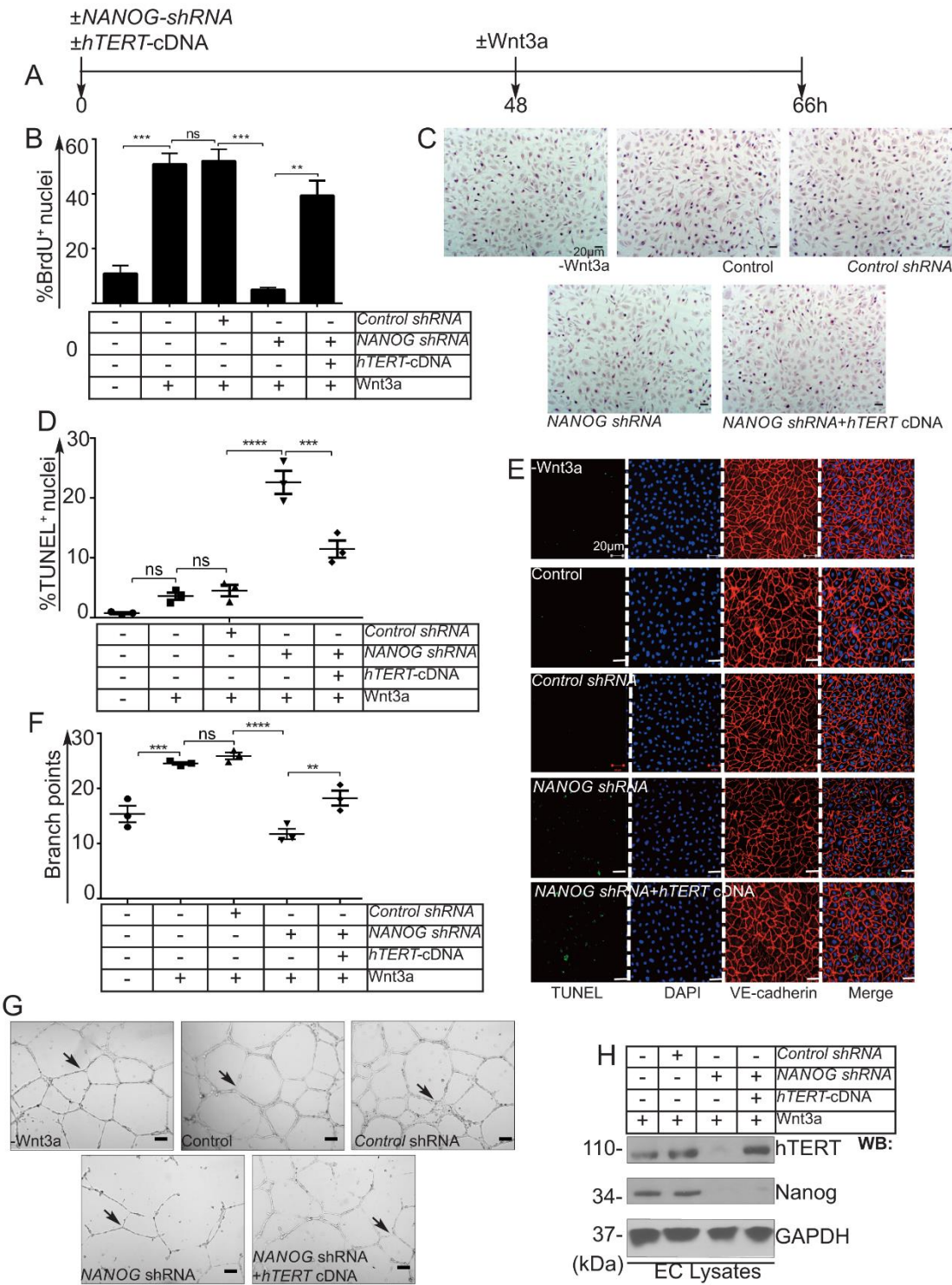


Figure 25: hTERT expression is required for NANOG mediated angiogenic activities of ECs. A) Timeline of transfections. B) Quantification of BrdU⁺ nuclei. C) Representative images indication presence of BrdU⁺ nuclei in –Wnt3a, Control, NANOG depleted, and *hTERT*-cDNA expressing groups. Scale bar is 20 μ m. D) Quantification of TUNEL⁺ nuclei in Control, *Nanog* - shRNA and *hTERT*-cDNA transfected groups. E) Representative high resolution confocal images of cultured ECs stained with anti-VE-cadherin (red) and TUNEL (green) indicate increased TUNEL⁺ cells in the *Nanog* depleted group. Re-expression of *hTERT*-cDNA into *Nanog* depleted groups reduced the extent of TUNEL⁺ cells. Scale bar is 50 μ m. F) Quantification of branch point structures in response to NANOG depletion and *hTERT* re-expression in ECs. G) Representative images of branch point structures indicated with black arrows show the formation of capillary tube-like structures in response to NANOG depletion and *hTERT* re-expressing ECs. H) Efficiency of NANOG-depletion and *hTERT*-re-expression in ECs. Scale bar is 50 μ m. Error bars represent mean \pm SD.

K. NANOG Depletion in ECs Results in a Hyperpolarization of the Mitochondria

Loss of NANOG and hTERT leads to apoptotic cell death. In addition, a decline in TA leads to a metabolic compromise altering mitochondrial function. To determine the effects of NANOG depletion on the mitochondria in ECs, we used *siRNA* mediated transient knockdown of *NANOG* in ECs and examined the polarization of mitochondria using JC-1 dye (**Figure 26A**). Accordingly, in control groups we observed basal accumulation of JC-1 monomer (green), indicating the polarity of mitochondria. However, in response to NANOG depletion, we observed an increased shift from monomer (green) to aggregate (red) form of JC-1 dye (**Figure 26B, C**). These results indicated that *NANOG* knockdown resulted in hyperpolarization of mitochondria.

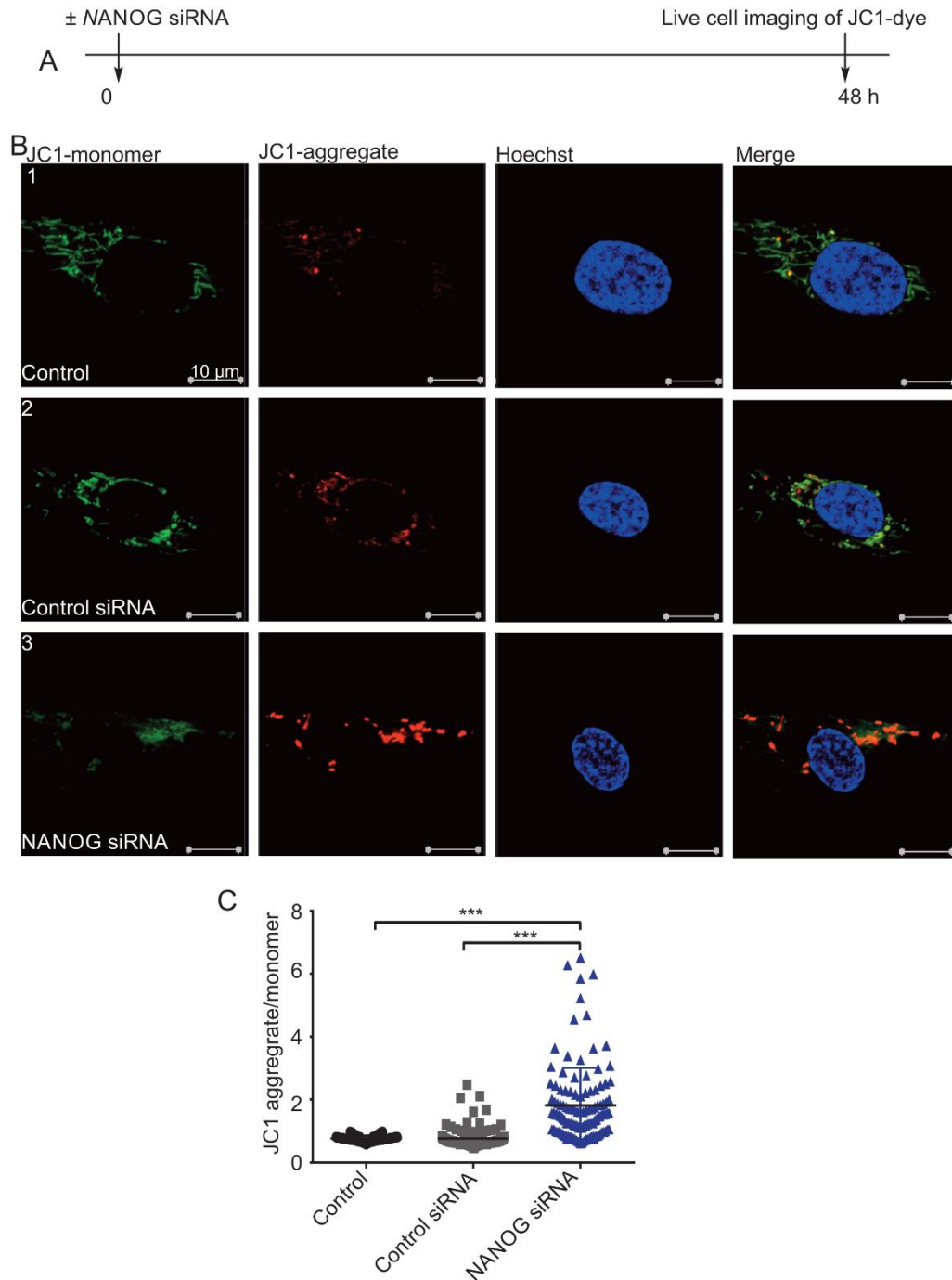


Figure 26: Assessing mitochondrial polarization state in response to NANOG depletion in ECs. A) Timeline of transfections and live cell imaging with JC-1 dye. B) Representative live cell images of mitochondria in Control and NANOG depleted groups. JC-1 monomer in green and JC-1 aggregate in red, indicate presence of JC-1 monomer in basal conditions. In response to NANOG depletion, an increase in JC-1 aggregate resulting from mitochondrial hyperpolarization. C) Quantification of JC-1 aggregate/monomer ratio in ECs. Scale bar is 10 μ m. Error bars represent mean \pm SD.

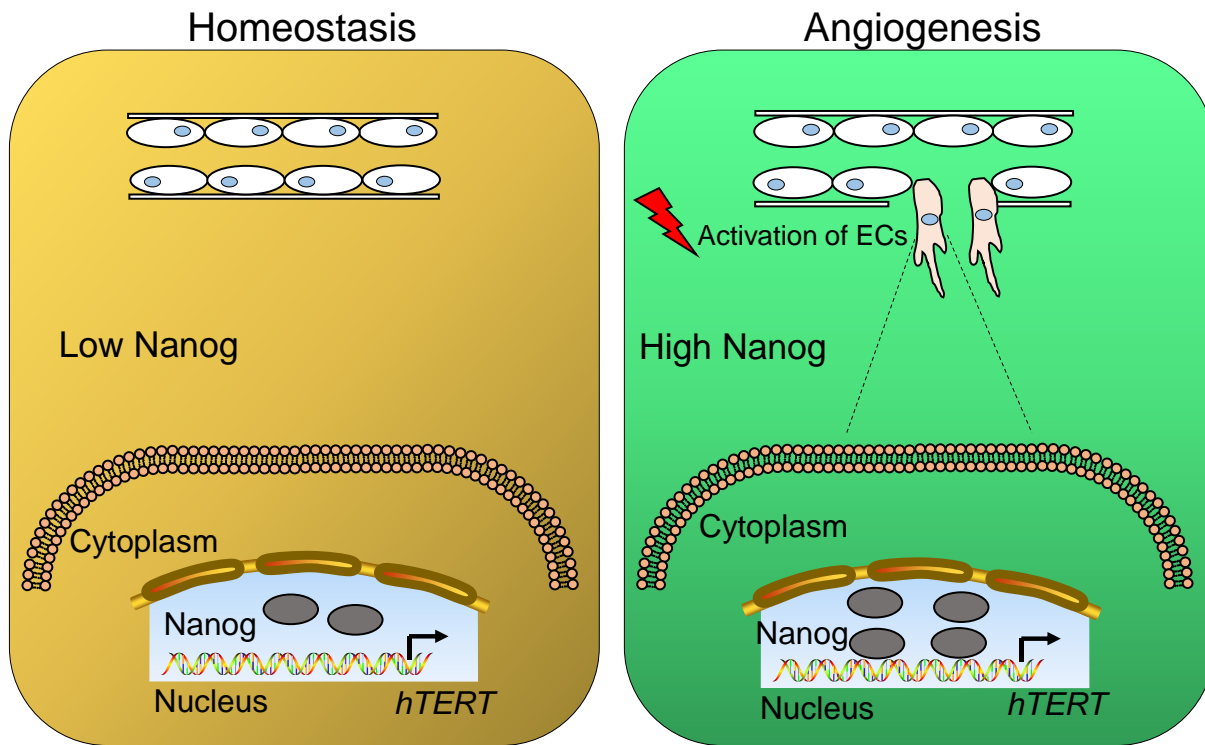


Figure 27: Summary Model. Low level NANOG in the adult vasculature is essential to maintain the homeostatic function of the endothelium. Angiogenesis, an adaptive biological response that mediates reparative events following injury, entails Wnt mediated increased and coordinated expression of NANOG, thereby amplifying the activities of hTERT in ECs.

Table III: Cardiac Parameters in Control and EC *Nanog*^{-/+} Mice

Physiological end-points	Control (n=6)	EC <i>Nanog</i>^{-/+} (n=6)	P value
Ejection Fraction (EF)%	50. 29 ± 8. 593	54. 04 ± 3. 462	0. 6942
Fractional Shortening (FS)%	26. 49 ± 5. 964	27. 70 ± 2. 216	0. 8533
LVDs* (mm)	2. 441 ± 0. 2693	2. 783 ± 0. 1183	0. 2715
LVVs** (μl)	23. 28 ± 5. 133	29. 74 ± 2. 939	0. 3001

*LVDs, Left Ventricular Diameter at systole; **LVVs, Left Ventricular Volume at systole

V. DISCUSSION

The robust homeostatic activities at the level of endothelial cells regulates the normal contractile myocardial behavior. However, the signaling mechanisms involved in these processes is not completely understood. Our published studies (Kohler et al. 2011; Kohler et al. 2014; Baruah et al. 2017) and data presented in this dissertation demonstrate that the stem cell transcription factor (TF) Nanog plays a crucial role in preventing EC apoptosis in the vascular endothelium of the heart, which I propose in part is regulated by the activity of hTERT. We posit that apoptosis of vascular ECs and non-vascular cells likely mediated induction of hypertrophy of the cardiomyocytes. I provide a comprehensive discussion of the results in support of this hypothesis and put forward additional directions which should be addressed in future studies.

In my dissertation research, I demonstrate that i) adult vascular ECs express transcription factor Nanog, ii) Wnt3a induced expression of NANOG regulates transcription of hTERT in ECs, iii) Inducible loss of single Nanog allele in the adult vascular ECs resulted in apoptotic cell death and fibrosis in mouse myocardial tissues, iv) Haploinsufficiency of the EC Nanog allele induced a CH like phenotype, and finally, v) NANOG induced hTERT expression prevents apoptosis and restores the ability to form capillary-like structures in vitro.

We began by investigating the expression of Nanog in adult vascular endothelium. To our surprise, we found that there was a heterogeneous expression of Nanog in the cardiac microvasculature of both human and mouse heart tissues. We localized and identified CD31+ and Nanog+ ECs in the myocardial sections by conducting high-resolution confocal imaging. Interestingly, not all CD31+ ECs stained positive for Nanog. This could imply that expression of Nanog is heterogeneous in vivo and only a subset of ECs in the vascular endothelium of the heart tissue actively synthesize Nanog. This result confirms multiple reports of EC heterogeneity in

vivo and within tissues (Aird 2012; Dejana et al. 2017). Most importantly, Wnt/ β -catenin signaling, which regulates expression of Nanog in ECs, is active in the vascular endothelium of heart tissues and partly explains the heterogeneous expression of Nanog in ECs.

After confirming expression of Nanog in adult ECs in vivo, our goal was to investigate the NANOG transcriptional axis in ECs. Primary ECs in culture express very low levels of NANOG, expression of which is amplified in response to exogenous stimuli such as the Wnt3a. To identify downstream targets of NANOG in ECs and mimic our in vivo observation, we used Wnt3a (50ng/ml) ligand to activate canonical Wnt signaling in cultured ECs. Upon stimulating ECs from different vascular beds (HUVECs, HSAVECs, and HPAECs) with Wnt3a for 6 hours, we observed increased transcripts of NANOG and hTERT. Although there was variation in the levels of hTERT mRNA among the ECs from the different vascular beds, we observed a consistent increase across all subtypes. These results indicated that upon Wnt3a stimuli, venous and arterial ECs accumulate hTERT transcripts in culture. We further validated the increase in protein levels of NANOG and hTERT using WB analysis and confirmed an increase in nuclear accumulation of hTERT using microscopy. The primary role of hTERT entails the addition of telomere DNA to the ends of chromosome via its telomerase activity (TA). Therefore, to test whether an increase in the hTERT proteins accounted for its activity, we utilized the highly sensitive TRAP assay protocol to determine TA in EC extracts stimulated with or without Wnt3a. It is well established that ECs in culture do not possess TA. Accordingly, we did not detect any TA in an unstimulated group of ECs. However Wnt3a stimuli induced TA in ECs. These results gave us the impetus to delineate if there is a possible correlation between the expression of NANOG and hTERT in ECs resulting from stimulation with Wnt3a.

Independent studies have reported that NANOG and hTERT are targets of the Wnt/ β -catenin signaling pathway. Using this information, we first sought to determine if NANOG can potentially regulate transcription of hTERT. We previously identified the ATTA nucleotide sequence as the minimal binding site to which NANOG can bind to target DNA regions. Interestingly, we found 16 potential NBEs in a -3.6 kb of the hTERT promoter upstream of its transcription start site (TSS). ChIP-qPCR and ChIP-PCR experiments confirmed that in response to Wnt3a stimuli, there was increased binding of NANOG to the hTERT promoter DNA segment. This is the first time we show that in primary ECs, Wnt3a induced NANOG binds to the promoter regions of hTERT. Using the luciferase promoter reporter activity assay, we confirmed that Wnt3a induced NANOG binds to hTERT promoter and mediates its transcription. Interestingly, in an additional experiment when Nanog levels were depleted in ECs, hTERT promoter activity was significantly reduced but not abolished. While this data suggests the primary role of NANOG in mediating hTERT transcription, it is possible that other downstream factors of the Wnt/ β -catenin pathway might regulate hTERT expression. Another important consideration is whether or not NANOG-hTERT protein interacts. In several attempts, using validated antibodies we performed a co-immunoprecipitation assay to examine the interaction of NANOG with hTERT protein and vice-versa. We did not detect a complex formation between NANOG and hTERT in ECs. Nevertheless, the ChIP assays combined with promoter activity studies provided us with a proof of concept that Wnt3a induced NANOG expression mediates hTERT transcription in ECs.

Expanding on the idea that Wnt3a induced expression of NANOG mediated hTERT transcription, we conducted in vitro loss and gain-of-function studies. Loss of NANOG in basal conditions or Wnt3a stimulated conditions resulted in reduced expression of hTERT at the

mRNA and protein levels. Accordingly, the addition of exogenous NANOG resulted in a robust increase in hTERT protein levels. These results showed that exogenous expression of NANOG in the absence of Wnt3a resulted in similar expression of hTERT in ECs, which suggested NANOG mediates hTERT transcription. It will be interesting to see if the addition of exogenous NANOG can replicate the regulatory effect on the hTERT promoter, which was not addressed in this study.

In this study, we report expression of Nanog in the vasculature of the mouse heart. Importantly, human and mouse Nanog share approximately 85% homeodomain similarity (Hart et al. 2004). Interestingly, Richardson et al. (2012) have demonstrated that mouse heart tissues also harbor a heterogeneous population of CD31⁺ cells that have telomerase expression (Richardson et al. 2012). To substantiate our in vitro studies and to determine the functional relevance of Nanog induced Tert transcriptional axis in vivo, we utilized a GEMM system that enabled us to inducibly delete a single allele of Nanog in the vascular compartment in a temporal manner and conducted a phenotypic characterization resulting from this event. Prior to this, we also conducted a bioinformatics analysis of the mouse TERT promoter and found that similar to the human TERT promoter, a -3.6kb of mouse TERT promoter harbors 15 potential NBEs. Alignment of human and mouse Tert promoter DNA sequences revealed approximately 50% identity between the species. (**Appendix A and B**). Accordingly, Control and EC *Nanog*^{-/+} groups of mice approximately 8 weeks old were administered low dose TAM to induce Cdh5 mediated expression of Cre, and thereby deletion of a single allele of Nanog in the vascular compartment of the mouse heart. mRNA and protein expression analysis conducted on the CD31⁺ cardiac ECs isolated from Control and EC *Nanog*^{-/+} mice revealed a significantly reduced *Tert* expression, along with *Vegfr2*, a known target of Nanog. The efficiency of our

system was further validated by conducting high-resolution confocal imaging on mouse myocardial sections. After TAM administration, *Cdh5^{CreERT2}* mediated expression of GFP was confined to the vascular compartment in these mice. These results demonstrate the efficacy of our GEMM system and highlighted the role of Nanog in regulating expression of *Tert* in vivo.

Nanog and Tert proteins have been implicated in cell survival activities (Yamaguchi et al. 2009; Piazzolla et al. 2014; Bar et al. 2014). Thus, we characterized the phenotype resulting from inducible deletion of a single Nanog allele in mouse hearts in a time-dependent manner. Using the highly sensitive TUNEL assay combined with co-immunostaining with anti-vWF, an EC marker, we detected increased TUNEL⁺ and vWF⁺ cells in the myocardium of EC *Nanog*^{-/+} at day 7, 14, 21 and 30 following TAM injections. What was interesting is that we also observed a subset of vWF⁻ cells that were positive for TUNEL staining. This was a surprising and unexpected phenotype. One potential interpretation of this phenotype could be a paracrine effect emerging in the vascular compartments when a single Nanog allele was deleted. Our current study does not delve into this aspect and will require further analysis. Since we observed profound cell death in EC *Nanog*^{-/+} mouse hearts, we next examined the extent of collagen deposits in the mouse heart tissues at similar time points. Interestingly, we observed a significant amount of collagen deposit (fibrosis) on large vessels and in peripheral regions of large and small vessels. We believe that apoptotic cell death might be a potential trigger for inducing fibrosis in vascular and perivascular compartments in EC *Nanog*^{-/+} mouse hearts.

To reiterate, apoptosis and fibrosis may be two key factors associated with the progression of a CVD phenotype (Kockx and Knaapen 2000; Segura et al. 2014). Therefore, we examined heart function in Control and EC *Nanog*^{-/+} mouse hearts using high-resolution echocardiography. CH can begin by remodeling of the LV wall which in turn alters cardiac

parameters. Our data suggested that EC *Nanog*^{-/+} mouse hearts had increased LV diameter and volume during diastole. This indicated that the chambers were dilated and there was a decline in the number of heart beats per min. The EC *Nanog*^{-/+} mouse showed an increased cardiac output (CO) and stroke volume (SV). An increase in these two parameters reflected an increase in cardiac performance potentially resulting from a hypertrophic growth of the cardiomyocytes. Accordingly, we assessed the left and right ventricular hypertrophy and found a significant increase in EC *Nanog*^{-/+} mice versus Controls. To our surprise the cardiac contractility parameters of ejection fraction (EF) and fractional shortening (FS) showed an insignificant increase in EC *Nanog*^{-/+} mice compared to controls (**Table III**). These data collectively highlight the phenotype of a typical failing heart with preserved EF and FS. A detailed analysis of additional cardiac parameters at later time points will be required to confirm the resultant phenotype.

In addition to the echo data, immunohistological analysis of Control and EC *Nanog*^{-/+} heart sections revealed hypertrophy of cardiomyocytes. Whole hearts excised at day 30 also indicated a significant increase in mass compared to the Control group. qRT-PCR analysis of molecular signatures associated with CH such as *Anp*, *Bnp*, *Myh7* and *Et-1* were significantly upregulated in EC *Nanog*^{-/+} mouse hearts.

Based on our *in vivo* observations, we designed an *in vitro* rescue strategy to elucidate the role of hTERT in NANOG mediated cell survival, proliferation, and capillary formation. Accordingly, NANOG depletion resulted in apoptotic cell death of ECs, while hTERT rescue with *hTERT* cDNA partially reduced the extent of cell death. Because the primary role of ECs is forming blood vessels via proliferation and migration, rescue experiments conducted with *hTERT* cDNA partially restored cell proliferation and the ability to form capillary-like structures

in a 2D Matrigel assay. This data sheds light on the role of NANOG induced hTERT signaling axis in maintaining a survival phenotype and thereby mediating angiogenic activities of ECs, as summarized in **(Figure 27)**. Although our data suggest that the loss of EC-specific single *Nanog* allele mediated hypertrophy of cardiomyocytes, currently it is unclear how cardiac EC-apoptosis give rise to CH. One could surmise that the loss of single *Nanog* allele could downregulate the level of EC genes/paracrine factors required to maintain the normal contractile function of cardiomyocytes, e.g., downregulating EC-Nitric oxide synthase (EC-NOS) could decrease the bioavailability of nitric oxide (NO), a known regulator of vasodilation. However, further study will be necessary to unravel the role of EC-*Nanog* regulatory networks in the mechanism of contractile function of cardiomyocytes and cardiac hypertrophy.

VI. FUTURE DIRECTIONS

Although the data presented in this dissertation represent a step forward in understanding a novel mechanism by which the cardiac endothelium might play a role in maintaining the form and function of the mouse hearts, there are several unanswered questions that need further investigation.

Wnt/ β -catenin signaling activates multiple genes, and in our *in vitro* studies with Wnt3a stimuli, we observed increased expression of *hTERT* in HUVECs, HPAECs, and HSAVECs, along with *NANOG*, *VEGFR2*, and *CYCLIN-D1*. While these are only a subset of the genes from the diverse pool of WNT responsive genes, it will be important to conduct a detail analysis of Wnt3a responsive genes in ECs isolated from the cardiac microvasculature, such as human cardiac microvascular ECs or human coronary artery ECs. This will not only help validate but also substantiate the findings of *NANOG* and *hTERT* expression in the ECs from these cardiac vascular beds. It may also be useful to conduct an RNA-seq analysis of ECs isolated from EC *Nanog*^{-/+} mouse hearts. By flow sorting GFP⁺ cells that are depleted of a single *Nanog* allele can be used to determine the genetic profile of these ECs. The RNA-seq data should provide useful information into the NANOG transcriptional axis *in vivo* in the cardiac microvasculature.

While our ChIP data combined with loss and gain-of-NANOG expression studies confirmed NANOG binding to the *hTERT* promoter, it will be interesting to examine if certain NANOG Binding Elements (NBE) on the *hTERT* promoter bind NANOG differentially. Even though we found 16 NBE on *hTERT* promoter, it is possible that based on the location of NBE from the TSS, NANOG may act as an enhancer or repressor. Site-directed mutagenesis of the NBE on *hTERT* promoter coupled with an electrophoretic shift in mobility assay (EMSA) and

promoter activity assay with the mutant promoter constructs will aid in understanding this interaction and transcriptional regulation of *hTERT* in ECs.

We further went on to characterize the phenotype resulting from single *Nanog* allele deletion in adult mouse hearts and found increased apoptosis and fibrosis. While it is evident that inducible haploinsufficiency of *Nanog* resulted in cell death and fibrosis in mouse hearts, it is unclear whether these two phenotypes are mutually exclusive or related. In other words, whether apoptotic cell death leads to secondary events such as fibrosis, or vice versa. To help understand this, one can use the information obtained from RNA-seq data obtained from a timed deletion of *Nanog* *in vivo*. The differential expression should be evaluated with bioinformatics tools to understand the regulatory networks involved in CH. The expression analysis data might reveal clues to whether *Nanog* loss primarily results in apoptosis or upregulates a cascade of genes involved in fibrotic remodeling. In addition, we also observed cell death in the non-EC population. It is unclear how the loss of an EC single *Nanog* allele resulted in cell death of non-EC population. Currently, the identities of the cell types involved in CH remains unknown, i.e., whether these are myofibroblasts, cardiomyocytes, circulating or tissue-resident stem cells. This issue could be examined using immunohistochemistry analysis, where myocardial sections from Control and EC *Nanog*^{-/+} mouse can be co-stained with a cardiomyocyte marker such as Troponin T (TnT), a fibroblast marker such as secreted Frizzled related protein-1 (Sfrp1), or pericyte marker such as alpha smooth muscle actin (α SMA), and TUNEL. This analysis should provide visual confirmation of the type cells undergoing cell death and can be complemented with flow-cytometry based assays. Further, it is not known how EC-apoptosis triggers cell death in adjacent cell types. If the action is due to a paracrine loop, co-culture of ECs with non-EC populations (such as cardiomyocytes or fibroblasts) can be done using the trans-well chamber

dishes. A subsequent *Nanog* knockdown in ECs followed by ELISA should provide an insight into the paracrine factors released by ECs that leads to activation of apoptotic cascade in non-EC population.

Because *Nanog* is known to regulate pluripotency and maintain cells in an undifferentiated stage, it might be possible that single allele *Nanog* deletion in ECs induced endothelial to a mesenchymal (EndMT) transition. This event could induce collagen deposition from activated fibroblast cells. One could address this by utilizing the lineage tracing ability of our GEMM system. Because of the presence of *Rosa^{mT/mG}* reporter elements, one can trace the fate of ECs with single *Nanog* allele deletion. Combining fluorescent activated cell sorting (FACS) and immunohistochemistry, one can precisely identify the characteristics of these cells.

The apoptotic cascade is initiated in the mitochondria of a cell and I have found that depletion of NANOG in ECs resulted in mitochondrial hyperpolarization (**Figure 26**). A decline in TA in aging ECs alters mitochondrial function which is associated with increased incidence of cardiovascular disease. Therefore, it will be interesting to dissect the role of *Nanog* in the mitochondrial function of ECs. Furthermore, to precisely understand the role of endothelial telomerase in preventing apoptosis and thereby attenuating CH, transgenic mice overexpressing telomerase under the *Tie2* promoter (*Tie2^{TERT}*) can be generated and crossed with *Rosa^{mT/mG}::Nanog^{fl/+}::Cdh5^{CreERT2}* mice. The results obtained from timed deletion of single *Nanog* allele in (*Rosa^{mT/mG}::Nanog^{fl/+}::Cdh5^{CreERT2}::Tie2^{TERT}*) should reinforce the role of the *Nanog*>*Tert* signaling axis in attenuating the progression of CH.

The focus of my study was limited to elucidating the role of quantitative changes in *Nanog* expression in adult ECs in relation to pathophysiology of the heart. Using newly created *Rosa^{mT/mG}::Nanog^{fl/fl}::Cdh5^{CreERT2}* mice, it would be interesting and rewarding endeavor to

investigate: A) the role of Nanog in aged mice and B) the role of gender, i.e male versus female. In addition, it is likely the epigenetic changes in adult ECs could mediate altered expression of Nanog, it would be important to examine the epigenetics regulation of Nanog expression in the mechanism of vascular aging and EC-dysfunction that perturbs EC-homeostasis, events that could precipitate into many maladies of the blood vessels including heart failure.

Sbjct	603	AAAATGAAGGAGGGGTA--GATGGGTCAAGTAGAAAATAGCATAGGAAACGAGTCAAGTA	660
Query	599	AAGGGCAGG--GCAGGCACGAGTGATTTTATTTAGCTATTTTATTTTATTACTTACTTT	656
Sbjct	661	TAGAAGAGGTGGTAGTAACCAG--ATCATGCAGAAGGACTCAAGGCCATCTCCTCACAGT	718
Query	657	--CTGAGACAGAGTTATGCTCT--TGTTGCCCAGGCTGGAGTGCAGCGGCATGATCTTGG	712
Sbjct	719	GGCTTAGGTAGGCCT-TCCTCTGCTCTTGAGCAGGG-GCAGAGTTGCCGCTTTAAGGAGG	776
Query	713	CTCACTGCAACCTCCGTCTCCTGG--GTTCAGCAAT--TCTCGTGCCTCAGCCTCCCA	767
Sbjct	777	GGATCAGTCACCTTTAAGAACTGAAAAGCTGAA-CAGTCTTCTCAAG--TCAGAAGCC--	831
Query	768	AGTAGCTGGGATTTTCAGGCATGCACCACCACACCCGGCTA---ATTTTGTATTTTATAGTA	824
Sbjct	832	AGTGGCTTC-ATCTTACACCT-CTCTTCCTTCCCTTGCTACTCATATTGGATCT-----	883
Query	825	GAGATGGGCTTTCACCATGTTGGTCAAGCTGATCTCAAAATCCTGACCTCAGGTGATC-C	883
Sbjct	884	--GATGA--TTTGCCCAACTTGGA-AGAAACATCTC----TTCTGA----AGGGTTTCAC	930
Query	884	GCCCACTCAGCCTCCC---AAAGTGCTGGGATTACAGGCATGAGCCA---CTGCACCT-	936
Sbjct	931	AGACACCCCATCTTTCCGAGAAAGGACCGC-AT---AGGC-TG-GCCATCCCTGTGCTTA	984
Query	937	-----GGCCTATTTAACCATTTTAAAACTTCCCTGGGCTCAAGTCACACCCACTGGTAAG	991
Sbjct	985	CAAAAGGAATAATTAAGAACTTAA---TTCCATAAGC--AAAT-ACAACCTTTC-AAG	1037
Query	992	G----AGTTCATGGAGTTCAATTTCCCCTTTA-----CTCAGGAGTTACCCTCCTTTG	1040
Sbjct	1038	CCCCAAGTGGATG-ATTTTATCTTACTGTTTTTTTATATCTCATCAAATAACTTCCAAGG	1096
Query	1041	-----ATATTTTC-----TGTAATT-----CT-----TC-GT-----AGAC-TGGGGATA	1073
Sbjct	1097	GCTCAAAAATCCAAAGATGTAAAAAAGGAAGTGAAGTCTGTTTGCCAAGCCATGAGGATT	1156
Query	1074	CACCGTCTCTTGACATATTCACAG---TTTCTGTGACC-----ACCTGTTATCC-----C	1120
Sbjct	1157	AAA----TAATGACAT--TCAAAGAGATTTTTGTGCCCTAAGTACTTTTTATTGGTTTTTC	1210
Query	1121	ATGG--GACCCACTG--CAGGG-GCAGC-----TGGGAG-GCT----GCA-GGCTT	1160
Sbjct	1211	ATAGATGGTTTAAATGTGCAAGATGAAGCAAACAGAGATGGGAGTGGTATCAGCATGGATT	1270
Query	1161	CAGGTCCCAGTGG---GGTTGCCAT-CTGC-----CAGTAGAA----ACCTG---ATGTA	1204
Sbjct	1271	AAGGTGGCAGTTGTGAGGGAGGGGTACTGAGAGAACAGGACAAGGTAACCTATCTAAGGA	1330
Query	1205	GAATC--AGGGCGCGAGTGT---GGACA-CT--GTCCTGAATCT---CA-ATGTCTCAG	1251

```

      || | || ||| ||| || | || || | || ||
Sbjct 1331 GAGGCCAAGTTGGCAAGTGCCAGGGACTTCTAAGCCCAGAA-CTAGTACACATTCCCTTAG 1389
Query 1252 TGTGTGCTGAAACATGTAGAAATTAA---AGTC--CATCCCTCCTA-CTCTACTGG-GAT 1304
      ||||| | | | | | ||| || | | | || | | |
Sbjct 1390 ---GTGCTG-----TTTGGGAAGTCAGGGAGTCACCAGCCTTGGGATCTATAAAAGTGCA 1441

Query 1305 TGAGCCCCTTCCCT---ATCCCCCCCCAGGGGCA-----GAGGAGTTCCTC----TCA 1350
      || | ||| || | | | | | | || | || | | |
Sbjct 1442 TGGTGGCATTCACTCACATACTTCCTGAGCTGTTTCGATGTTGATGAAGTCGTGGGTATGA 1501
Query 1351 --CTCCTGTG-----GAGGAA----GGAA-TGATACT--TTGTTAT--TTTTCACTGCTG 1394
      || |||| | | | | | | ||| | | || | ||
Sbjct 1502 GACTGTTGTGTGTCAGTGACAACTATGTAAATGAGAATGATTGTTTCCATCTTGACCACTA 1561
Query 1395 GTACTGAATCCACTGTTTCATTTGTTGGTTTGTGTTTGTGTTTGTGTTTGTG--AGAG--GCAGTT 1450
      || || | ||| || | | | || | | | ||| ||||
Sbjct 1562 AGACGTAAACCG--GTTCCAGTGATCTCCAAACATGGCAAGCTACAGCAGAGCAGCAGCC 1619
Query 1451 TCACTCTTG----TTGCTCAGG--CTGGA---GGGAG--TGCAATGG-----CG----- 1488
      || || | |||| | || || | |||| | || || | ||
Sbjct 1620 CCA-TCCAGAGCCTTGCCCTGGTTCTGAATGGGGGAGAATCCAGTGGGAGTCGGTTGCTG 1678
Query 1489 CGATC---TTGGCTTACTGCAGCCTCT-GCCTCCCAGGTTCAAGTGATTCTCCTGCTTCC 1544
      | | | |||| | | | | | | |||| | | | | |||||
Sbjct 1679 CCAGCATGTTGGGGTA--GAAGGCTGGAGCATGACAGGTCCCCGAGGATTTCTGCTTCC 1736
Query 1545 GCCTCCCATTGCTGGGATTAC---AGGCACCCGCCACCA-----TGCCCAGCTAATTT 1596
      || || | || ||| || | | | | | || | || |
Sbjct 1737 T-----ATATGGGTAGGGATACTTGAGGTCTCTCTTCTACCTCCTTCCCTGCAGGGTT 1790
Query 1597 TTTGTATTTTGTAGTAGACGG-----GGG-TGG-----GGGTGGGGT---TCACCATG 1641
      | | | | | | | | | || | | |||| | || ||
Sbjct 1791 TATA-ACCTCTACCACTGTCTGTCTCTGGGATAGCTCCTAGGGTGACCCCCCTCCCCAAA 1849
Query 1642 TTGGCCAGGC--TGGTCTC-----GAAC----TTCTGACCTCAGA--TGATCCAC 1683
      |||| | ||| || |||| |||| | || | || | ||
Sbjct 1850 AAGGCCTCTCCCTGGCCTCATGTCTCTAAGAACAGCTTTCTAAAG-CAGGCCTGTTACAC 1908
Query 1684 -----CTGCCTCTGCCTC-CTAAA--GT-GCTGGGA-----TTACAGGTGTGAGCCAC- 1727
      || || | || | | | |||| | || | || ||||
Sbjct 1909 AAAGGCTCCCTTTTCTGCTTCATCGTTGCTGGTAGACAACCTCCACTCGTTTCCACT 1968
Query 1728 -CA-TGCC--CAGCTCAGA----ATTT-ACTCTGTT--TAGAAACATCTGGGTC-TGAGG 1775
      || | | | ||| | |||| | |||| | || | | |||| |
Sbjct 1969 TCAGTTTCTTCTACTCTGTTGTTATTTGATTCTGATGCTTGAACC--CAGGGTTGTGTAG 2026
Query 1776 T-AGGAAG--CTCACCCTCAAGTGTTGT--GGTGTTTTAAGCCAATGATAGAATTTT 1830
      | || || | |||| | | | | | | |||| || | | ||||
Sbjct 2027 TCAGCAAGTGCTACCCCTCCCTCCTCTTCTTGTGTTTTTTTGGAGCAGGG-TCTCATTTT 2085
Query 1831 TTTATTGTTGTTAGAACACTCTTGATGTTT-TACACTG----TGA-TGACTAAGACATCA 1884

```

```

          || |   ||  ||  ||||  |   |||   ||| || ||   ||||
Sbjct  2086  GCCCAAGTGGACCTAAATTTTCAGCATGTAGCTGGCCTGGTTTTGAATGCCTTCT-CATCC  2144
Query  1885  T-CAGCT--TTTCAAAGACACACTAAC-----TGCACCCATAATACTGGGGTGTCTTCTG  1936
          | |  ||  || | ||||  || ||  ||||| |  || |  |  ||||
Sbjct  2145  TGCCTCTACTTCCCAAGAGTAGCTTACAAGTGTGCACC-ACCATGCCCCGCGATATTCTT  2203

Query  1937  GGTATCAGCGATCTTCATTGAATGCCGGGAGGCGTTTCCTCGCCA---TGCAC-ATGGT-  1991
          | |  | || ||  ||  |||| ||  |||| |  |  ||| | |||
Sbjct  2204  ATTTTT-GAGA-CTGTTTTCTATGCTGG-----TTTCTTTGGGGAACACTACACTAAGGTA  2255
Query  1992  GTTAATTACTCCAGCATAATCTTCTGCTTCCAT-TTCTTCTCTCCCTCTTTTAAAATTG  2050
          | | |  | |  |||  | |  |  | | || |||| |  |||| | | ||
Sbjct  2256  GCTTACAAGTGT-GCACCACCATGCCCCGCGATATTCTTAT-----TTTGGAGACTG  2306
Query  2051  TGTTTTCTATGTTGGCTTCTCTCGAGAGAACCAGTGTAAGCTACAACCTAACTTTTGTTG  2110
          |  ||||| ||| |||| ||  | |||| |  |||| ||  ||| |  |||||
Sbjct  2307  T--TTTCTATGCTGGTTTCTTTG--GGAACTACACTAAGGTAG--CTTCA---TTGTTG  2357
Query  2111  GAACAAATTTTCCAAACC--GCCCTTTGCCCTA-GTGGCAGAGA----CAATTCACAAA  2163
          | | |||||  ||  |  |||| | |  |||| | |||||  ||| || ||||
Sbjct  2358  GCATAAATTTCTCAGTTCAGGCCCATATCTCCTAAGTAGCAGAACTAAGCAAATCTCAAA  2417
Query  2164  CACAGCCCTTTAAAAAGGCTTAGGGATCACTAAGGGGATTTCTAGAAGAGCGACCTGTAA  2223
          || | ||||  ||||| || |  |||||  ||| |||| | |||  |||||
Sbjct  2418  CAAACCCCTC-AAAAAGACTGATGTC-CACTAAACGGACTTCTAAATAGCT-CCTGTAA  2474
Query  2224  TCCTAAGTATTTACAAGACGAGGCTAACCTCCAGCGAGCGTGACAGCCCAGGGAGGGTGC  2283
          |||| || ||||| || ||  |||||  || | |  |  || |  ||
Sbjct  2475  TCCTGAGCATTTACAAGGCG--GCAGACCTCCTATAAGGGAGTAAAT--ATGAAAC-GC  2529
Query  2284  GAGGCCTGTTCAAATGCTAGCTCCATAAATA-AAGCAATTTCTCCGGCAGTTTCTGAAA  2342
          |  ||||| ||||| || |  ||  ||||| ||||| |  ||  ||||
Sbjct  2530  G---CCTGTTCAAATGCTAGGTGCGTGGATAGAAGCAATTTCTCAGAAAG---CTGAAG  2583
Query  2343  GTAGGAAAGGTTACATTTAAGGTTGCGTTTGTAGCATTTCAGTGTGTTGCCGACCTCAGC  2402
          | |  ||||| ||||  ||||| ||||| ||||| | |||||
Sbjct  2584  GCACCAAAGGTTATATTT-----GTTAGCATTTCAGTGTGTTGCCAAACTCAGC  2631
Query  2403  TACAGCATCCCTGCAAGGCCTCGGGAGACC-CAGAAGTTTCTCGC---CCCTTAGATCCA  2458
          |||| |  |||| | ||||  || |  |||  |||| ||
Sbjct  2632  TACAGTA-----GAGATCACAGA---TTCCCTATTTCCCAGAGATTCA  2671
Query  2459  AACTTGAGCAACCCGGAGTCTGGATTCTGGGAAGTCTCAGCTGTCCTGCGGTTGTGCC  2518
          || || |||| |||  ||| |  |||  |||| ||| ||  ||  |
Sbjct  2672  AAATTTCAGCAGCCCC---TCTCTAACTATGG-----CTCAGA-GTCGTGTCATTA--CA  2719

Query  2519  GGGGCCCCAGGTCTGGAGGGGACCAGTGGCCGTGTGGCTTCTACTGCTGGGCTGGAAGTC  2578
          |||||  || |  ||  | ||  ||  ||  | |
Sbjct  2720  TATGCCCCA-----ACAACAACCC-----CCACCCCTATCCT---ACCC  2755

```

```

Query 2579 GGGCCTCCTAGCTCTGCA-GTCCGAGGCTTGGAGCCAGGTGCCTGGACCCCCAGGTTGCC 2637
          ||||| | | ||| || | | | |||| ||| | | ||| |||
Sbjct 2756 CCGCCTCACACGT--GCAAGTACTATCACAGTTGCCAA---CCTAG---CAGAGCT-GCC 2806
Query 2638 CTCCACCCTGTGCGGGCGGGATGTGACCAGATGTTGGCCTCATCTGC-CAGACAGAGTGC 2696
          ||| | | ||| || | || ||| || ||| ||| ||| |||
Sbjct 2807 ATCC-----TAAGGTCGAG--GTCGCC-GCT-TTGGCTG--TGTGCACAGGCA-AGCGC 2853

Query 2697 CGGGGCCCAGGGTCAAGGCCGTTGTGGC--TGGTGTGAGGCGCCCGGTGCGCGGCCAGCA 2754
          | |||| | |||| | ||| || | || ||| ||| | | ||
Sbjct 2854 CCTCACCCA-----ATGGCCCT--GGCCTTGCTATG-GGTGC---GTGAGTTG--AGAT 2899
Query 2755 GGAGCGCCTGGCTCCATTTCCACCCCTTTCTCGACGGGACCGCCCCGGTGG----GTGAT 2810
          | || | ||| || || || || ||| | ||| ||| |||
Sbjct 2900 GATGCTC-TGG-----ACTCT-----GAGGTGAAGGCCAC--TGGAACAGTGAA 2940
Query 2811 TAACAGATTTGGGGTGGTTTGCTCATGGTGGGGACCCCTCGCCGCCTGAGAACCTGCAAA 2870
          || || | | || || | || || |||| ||| |
Sbjct 2941 AAA-AGCTAACGCAGGGCTTTTACCTAGT-----CCCCTT----CCTTTGG----- 2981
Query 2871 GAGAAATGACGGGCCTGTGTCAAGGAGCCCAAGTCGCGGGGAAGTGT-TGCAGGGAGGCA 2929
          || ||| ||| | | ||| | | | |||| || ||| ||| |||
Sbjct 2982 -----TGGTGGG--TGTTT-ACGGAACATATTT---GGGATCTGAGTGTATGGTCGCA 3028
Query 2930 CTCCGGGAGGTCCCGCGTGCCCGTCCAGGGAGCAATGCGTCCTCGGGTTCGTCCCCAGCC 2989
          | | | | || || | || || || || | | ||| | | |
Sbjct 3029 CCACAATAAAGCCTTAA--CCTATATAGT-AGAATTTTCACT--GTAATCATTAAGAACT 3083
Query 2990 GCGTCTACGCGCTCCGTCTCCCTTCAC-GTCCGGCATTCGTGGTGCCCGGAGCCCGA 3048
          | | | ||| || || || |||| ||| | || ||| ||| |
Sbjct 3084 GAGATT----GCCACCACCACC---TCACTGTCTG-----TGTCAACCACAGC---A 3126
Query 3049 CGCCCCGCGTCCGGACCTGGAGGCAGCCCTGGGTCTCCGGATCAGGCCAGCGGCCAAAGG 3108
          || ||| | || |||| || ||| |||| | || |||
Sbjct 3127 GGCT-----GGAGC---AGTCAGC-----TCAGGAACAGGCAAAA--CCTTAGG 3165
Query 3109 GTCGCCGACGCACCTGTTCCAGGGCCTCCA---CATCATGGCCCTCCCTCGGGTTAC 3165
          || | | | |||| || || |||| || || |||
Sbjct 3166 -TCCCTCCGCCTACCTAA-----CCTTCAATACATCAAGGA-----TAGGCTT-- 3207
Query 3166 CCCACAGCCTAGGCCGATTTCGACCTCTCTCCGCTGGGGCCCTCGCTGGCG--TCCCTGCA 3223
          | || | | || | |||| | || | || | |||| | |||| ||
Sbjct 3208 --CTTTGCTT-GCCCAA---ACCTCGCCCCAGTCTAGACCAC-CTGGGGATTCCCAGCT 3259
Query 3224 CCCTGGGAGCGCGAGCGGCGCGGGCGGGGAAGCGCGGCCAGACCCCCGGGTCCGCCC 3283
          | || |||| | || | || |||| ||| ||| |||
Sbjct 3260 C-----AGGGCGAAAAGGAAGC---CCGAGAAGCATTCTGTAGA-----GGGAAATCCT 3305
Query 3284 GGAGCAGCTGCGCTGTCTGGGGCCAGGCCGGGCTCCCAGTGGATTGCGGGGCACAGACGCC 3343
          | | || |||| || || || || || || ||| ||| |
Sbjct 3306 GCATGAG-TGCGC-----CC-----CCTTTCGTTACTCCAACACAT---C 3341

```

```

Query  3344  CAGGACCGCGCTTCCCACGTGGCGGAGGGACTGG---GGACC-CGGGCACCCGTCCTGCC  3399
          ||| | | | ||   || |||| | || ||   || || | |||| |   ||
Sbjct  3342  CAGCAAC-CACTGA--ACTTGGCCGGGGAACACACCTGGTCCTCATGCACCAGCATTGTG  3398
Query  3400  -CCTTCACCTTCCAGCTCCGCCTCCTCCGCGCGGACCCCGCCCGTCC-CGACCCCTCCC  3457
          || ||| |   | | |   | || ||   ||||| ||| || | || | |
Sbjct  3399  ACCATCAACGGAAAAGTACTATTGCTGCG-----ACCCGCCCCTTCCGCTACAACGCTT  3453

Query  3458  GGGTCCCCGGC--CCAGCCCCCTCCGGGCCCTCCCAGCCCCTCCCCTTCCTTTC--CGCG  3513
          || | || |   || |||| |||   | ||||| || || || ||| || |
Sbjct  3454  GGTCCGCCTGAATCCCGCCCCTTCCTC-CGTTCCCAGCC--TCATCTT--TTTCGTCGTG  3508
Query  3514  GCCCCGCCCTCTCCTCGCGGC--GCGAGTTTC-AGGCAG-CGCT-GCGTCCTGCTGC--G  3566
          | | | | | ||| |   | ||   ||| | ||| | || || || || | | |
Sbjct  3509  GACTCTCAGTGGCCTGGGTCCTGGCTGTTTTCTAAGCACACCCTTGCATCTTGGTTCCCG  3568
Query  3567  CACGTGGGAAGCCCTGGCCCCGGCCACCCCGCG  3600
          ||||| ||| ||| |||||   | |
Sbjct  3569  CACGTGGGAGGCCCAT--CCCGGCCTTGAGCACA  3600

```

B. Dot Matrix Plot of human and mouse *TERT* promoter.

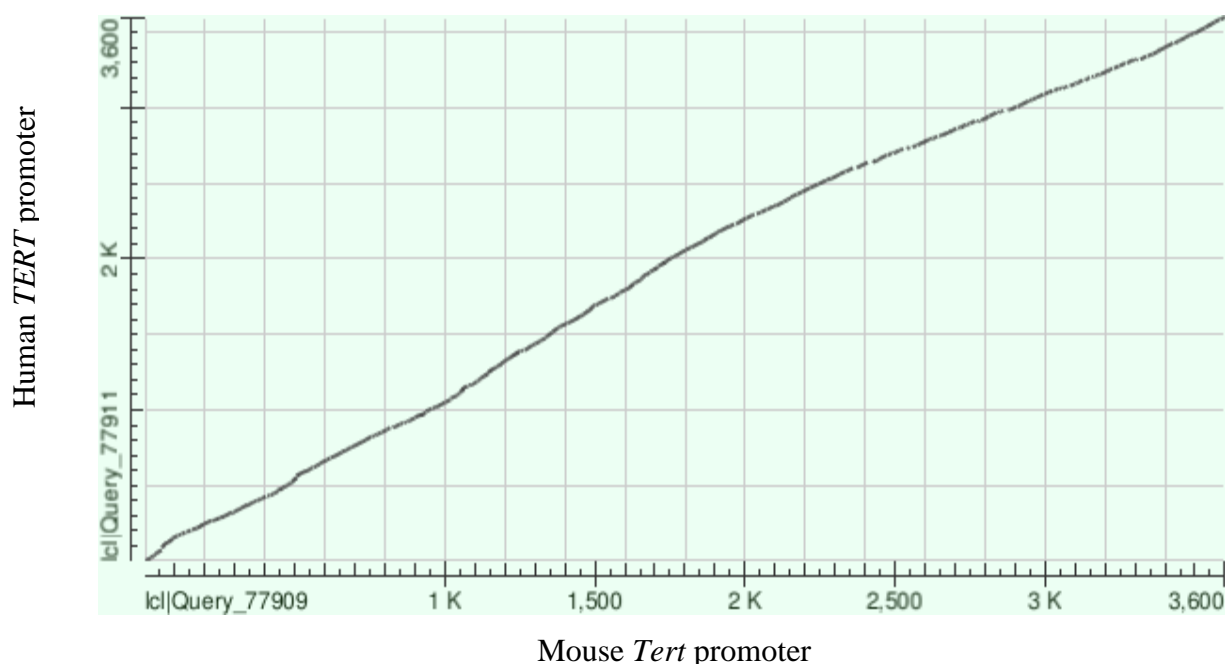


Figure 28. Dot Matrix of sequence similarity between the human and mouse *TERT* promoter DNA. This dot matrix view shows regions of similarity based upon the BLAST results. The query (mouse *Tert* promoter) sequence is represented on the X-axis and the numbers represent the bases/residues of the query. The subject (human *TERT* promoter) is represented on the Y-axis and again the numbers represent the bases/residues of the subject. Alignments are shown in the plot as lines. Plus strand and protein matches are slanted from the bottom left to the upper right corner, minus strand matches are slanted from the upper left to the lower right. The number of lines shown in the plot is the same as the number of alignments found by BLAST (Unaltered text provided from NCBI)

C. Copy of Approved Animal Protocol



September 22, 2017

Kishore Wary
Pharmacology
M/C 868

Office of Animal Care and
Institutional Biosafety Committees (MC 672)
Office of the Vice Chancellor for Research
206 Administrative Office Building
1737 West Polk Street
Chicago, Illinois 60612-7227

Dear Dr. Wary:

The protocol indicated below was reviewed at a convened ACC meeting in accordance with the Animal Care Policies of the University of Illinois at Chicago on **8/15/2017**. *The protocol was not initiated until final clarifications were reviewed and approved on 9/22/2017. The protocol is approved for a period of 3 years with annual continuation.*

Title of Application: Mechanisms of Cellular Dedifferentiation, Neovascularization and Tissue Repair

ACC Number: 17-129

Initial Approval Period: 9/22/2017 to 8/15/2018

Current Funding: *Portions of this protocol are supported by the funding sources indicated in the table below.*

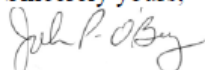
Number of funding sources: 2

Funding Agency	Funding Title			Portion of Proposal Matched
AHA- American Heart Association	Mechanisms of Ischemic Preconditioning Mediated de novo Neovascularization (Institutional # 00341669)			All matched
Funding Number	Current Status	UIC PAF NO.	Performance Site	Funding PI
17GRNT33700162	Funded		UIC	Kishore K Wary
Funding Agency	Funding Title			Portion of Proposal Matched
NIH	Mechanisms of Endothelial Regeneration after Ischemic Stress (Institutional # 00318059)			All matched
Funding Number	Current Status	UIC PAF NO.	Performance Site	Funding PI
R01HL138534 (years 1-5 original)	Pending		UIC	Kishore K Wary

This institution has Animal Welfare Assurance Number A3460.01 on file with the Office of Laboratory Animal Welfare (OLAW), NIH. **This letter may only be provided as proof of IACUC approval for those specific funding sources listed above in which all portions of the funding proposal are matched to this ACC protocol.**

In addition, all investigators are responsible for ensuring compliance with all federal and institutional policies and regulations related to use of animals under this protocol and the funding sources listed on this protocol. Please use OLAW's "*What Investigators Need to Know about the Use of Animals*" (<http://grants.nih.gov/grants/olaw/InvestigatorsNeed2Know.pdf>) as a reference guide. Thank you for complying with the Animal Care Policies and Procedures of UIC.

Sincerely yours,



John P. O'Bryan, PhD
Chair, Animal Care Committee
JPO /mbb

cc: BRL, ACC File, Jugajyoti Baruah, Suhrita Chaudhuri

VIII. CITED LITERATURE

Aird, W. C. 2012. "Endothelial Cell Heterogeneity." *Cold Spring Harbor Perspectives in Medicine* 2 (1): a006429.

———. 2008. "Endothelium in Health and Disease." *Pharmacological Reports : PR* 60 (1): 139-143.

———. 2007. "Phenotypic Heterogeneity of the Endothelium: I. Structure, Function, and Mechanisms." *Circulation Research* 100 (2): 158-173.

Aisagbonhi, O., M. Rai, S. Ryzhov, N. Atria, I. Feoktistov, and A. K. Hatzopoulos. 2011. "Experimental Myocardial Infarction Triggers Canonical Wnt Signaling and Endothelial-to-Mesenchymal Transition." *Disease Models & Mechanisms* 4 (4): 469-483.

Anderson, J. L. and D. A. Morrow. 2017. "Acute Myocardial Infarction." *The New England Journal of Medicine* 376 (21): 2053-2064.

Anversa, P., A. Leri, M. Rota, T. Hosoda, C. Bearzi, K. Urbanek, J. Kajstura, and R. Bolli. 2007. "Concise Review: Stem Cells, Myocardial Regeneration, and Methodological Artifacts." *Stem Cells (Dayton, Ohio)* 25 (3): 589-601.

Awgulewitsch, C. P., L. T. Trinh, and A. K. Hatzopoulos. 2017. "The Vascular Wall: A Plastic Hub of Activity in Cardiovascular Homeostasis and Disease." *Current Cardiology Reports* 19 (6): 51-017-0861-y.

Bar, C., B. Bernardes de Jesus, R. Serrano, A. Tejera, E. Ayuso, V. Jimenez, I. Formentini, et al. 2014. "Telomerase Expression Confers Cardioprotection in the Adult Mouse Heart After Acute Myocardial Infarction." *Nature Communications* 5: 5863.

Baruah, J., R. Hitzman, J. Zhang, S. Chaudhuri, V. Mastej, and K. K. Wary. 2017. "The Allosteric Glycogen Synthase Kinase-3 Inhibitor NP12 Limits Myocardial Remodeling and Promotes Angiogenesis in an Acute Myocardial Infarction Model." *The Journal of Biological Chemistry* 292 (50): 20785-20798.

Benjamin, E. J., S. S. Virani, C. W. Callaway, A. R. Chang, S. Cheng, S. E. Chiuve, M. Cushman, et al. 2018. "Heart Disease and Stroke Statistics-2018 Update: A Report from the American Heart Association." *Circulation*.

Bergmann, M. W. 2010. "WNT Signaling in Adult Cardiac Hypertrophy and Remodeling: Lessons Learned from Cardiac Development." *Circulation Research* 107 (10): 1198-1208.

Biteau, B., C. E. Hochmuth, and H. Jasper. 2011. "Maintaining Tissue Homeostasis: Dynamic Control of Somatic Stem Cell Activity." *Cell Stem Cell* 9 (5): 402-411.

Blackburn, E. H. 1991. "Structure and Function of Telomeres." *Nature* 350 (6319): 569-573.

Blackburn, E. H. and K. Collins. 2011. "Telomerase: An RNP Enzyme Synthesizes DNA." *Cold Spring Harbor Perspectives in Biology* 3 (5): 10.1101/cshperspect.a003558.

Blackburn, E. H., E. S. Epel, and J. Lin. 2015. "Human Telomere Biology: A Contributory and Interactive Factor in Aging, Disease Risks, and Protection." *Science (New York, N.Y.)* 350 (6265): 1193-1198.

Bohm, F. and J. Pernow. 2007. "The Importance of Endothelin-1 for Vascular Dysfunction in Cardiovascular Disease." *Cardiovascular Research* 76 (1): 8-18.

Boyer, L. A., T. I. Lee, M. F. Cole, S. E. Johnstone, S. S. Levine, J. P. Zucker, M. G. Guenther, et al. 2005. "Core Transcriptional Regulatory Circuitry in Human Embryonic Stem Cells." *Cell* 122 (6): 947-956.

Brade, T., J. Manner, and M. Kuhl. 2006. "The Role of Wnt Signalling in Cardiac Development and Tissue Remodelling in the Mature Heart." *Cardiovascular Research* 72 (2): 198-209.

Brown, S., C. M. Pineda, T. Xin, J. Boucher, K. C. Suozzi, S. Park, C. Matte-Martone, et al. 2017. "Correction of Aberrant Growth Preserves Tissue Homeostasis." *Nature* 548 (7667): 334-337.

Busch, C., M. Oppitz, M. Wehrmann, P. Schweizer, and U. Drews. 2008. "Immunohistochemical Localization of Nanog and Oct4 in Stem Cell Compartments of Human Sacrococcygeal Teratomas." *Histopathology* 52 (6): 717-730.

Cadigan, K. M. 2008. "Wnt-Beta-Catenin Signaling." *Current Biology : CB* 18 (20): R943-7.

Carabello, B. A. 2014. "Is Cardiac Hypertrophy Good Or Bad? the Answer, of Course, is Yes." *JACC.Cardiovascular Imaging* 7 (11): 1081-1083.

Carreno, J. E., F. Apablaza, M. P. Ocaranza, and J. E. Jalil. 2006. "Cardiac Hypertrophy: Molecular and Cellular Events." *Revista Espanola De Cardiologia* 59 (5): 473-486.

Chambers, I., D. Colby, M. Robertson, J. Nichols, S. Lee, S. Tweedie, and A. Smith. 2003. "Functional Expression Cloning of Nanog, a Pluripotency Sustaining Factor in Embryonic Stem Cells." *Cell* 113 (5): 643-655.

Chambers, I., J. Silva, D. Colby, J. Nichols, B. Nijmeijer, M. Robertson, J. Vrana, K. Jones, L. Grotewold, and A. Smith. 2007. "Nanog Safeguards Pluripotency and Mediates Germline Development." *Nature* 450 (7173): 1230-1234.

Chang, M. W., J. Grillari, C. Mayrhofer, K. Fortschegger, G. Allmaier, G. Marzban, H. Katinger, and R. Voglauer. 2005. "Comparison of Early Passage, Senescent and hTERT Immortalized Endothelial Cells." *Experimental Cell Research* 309 (1): 121-136.

Chavakis, E. and S. Dimmeler. 2002. "Regulation of Endothelial Cell Survival and Apoptosis during Angiogenesis." *Arteriosclerosis, Thrombosis, and Vascular Biology* 22 (6): 887-893.

Chen, T., J. Du, and G. Lu. 2012. "Cell Growth Arrest and Apoptosis Induced by Oct4 Or Nanog Knockdown in Mouse Embryonic Stem Cells: A Possible Role of Trp53." *Molecular Biology Reports* 39 (2): 1855-1861.

Clevers, H., K. M. Loh, and R. Nusse. 2014. "Stem Cell Signaling. an Integral Program for Tissue Renewal and Regeneration: Wnt Signaling and Stem Cell Control." *Science (New York, N.Y.)* 346 (6205): 1248012.

Cohen, E. D., Y. Tian, and E. E. Morrisey. 2008. "Wnt Signaling: An Essential Regulator of Cardiovascular Differentiation, Morphogenesis and Progenitor Self-Renewal." *Development (Cambridge, England)* 135 (5): 789-798.

Dauwe, D., B. Pelacho, A. Wibowo, A. S. Walravens, K. Verdonck, H. Gillijns, E. Caluwe, et al. 2016. "Neovascularization Potential of Blood Outgrowth Endothelial Cells from Patients with Stable Ischemic Heart Failure is Preserved." *Journal of the American Heart Association* 5 (4): e002288.

David, R., C. Brenner, J. Stieber, F. Schwarz, S. Brunner, M. Vollmer, E. Mentele, et al. 2008. "MesP1 Drives Vertebrate Cardiovascular Differentiation through Dkk-1-Mediated Blockade of Wnt-Signalling." *Nature Cell Biology* 10 (3): 338-345.

Davidson, S. M. and M. R. Duchon. 2007. "Endothelial Mitochondria: Contributing to Vascular Function and Disease." *Circulation Research* 100 (8): 1128-1141.

De Bock, K., M. Georgiadou, and P. Carmeliet. 2013. "Role of Endothelial Cell Metabolism in Vessel Sprouting." *Cell Metabolism* 18 (5): 634-647.

Deanfield, J. E., J. P. Halcox, and T. J. Rabelink. 2007. "Endothelial Function and Dysfunction: Testing and Clinical Relevance." *Circulation* 115 (10): 1285-1295.

Dejana, E., K. K. Hirschi, and M. Simons. 2017. "The Molecular Basis of Endothelial Cell Plasticity." *Nature Communications* 8: 14361.

Deng, Q., Y. Huo, and J. Luo. 2014. "Endothelial Mechanosensors: The Gatekeepers of Vascular Homeostasis and Adaptation Under Mechanical Stress." *Science China.Life Sciences* 57 (8): 755-762.

Dimmeler, S. and A. M. Zeiher. 2000. "Endothelial Cell Apoptosis in Angiogenesis and Vessel Regression." *Circulation Research* 87 (6): 434-439.

Edo, M. D. and V. Andres. 2005. "Aging, Telomeres, and Atherosclerosis." *Cardiovascular Research* 66 (2): 213-221.

Falchetti, M. L., M. P. Mongiardi, P. Fiorenzo, G. Petrucci, F. Pierconti, I. D'Agnano, G. D'Alessandris, et al. 2008. "Inhibition of Telomerase in the Endothelial Cells Disrupts Tumor Angiogenesis in Glioblastoma Xenografts." *International Journal of Cancer* 122 (6): 1236-1242.

- Farah, C., L. Y. M. Michel, and J. L. Balligand. 2018. "Nitric Oxide Signalling in Cardiovascular Health and Disease." *Nature Reviews.Cardiology*.
- Favero, G., C. Paganelli, B. Buffoli, L. F. Rodella, and R. Rezzani. 2014. "Endothelium and its Alterations in Cardiovascular Diseases: Life Style Intervention." *BioMed Research International* 2014: 801896.
- Franco, C. A., S. Liebner, and H. Gerhardt. 2009. "Vascular Morphogenesis: A Wnt for Every Vessel?" *Current Opinion in Genetics & Development* 19 (5): 476-483.
- Frati, C., M. Savi, G. Graiani, C. Lagrasta, S. Cavalli, L. Prezioso, P. Rossetti, et al. 2011. "Resident Cardiac Stem Cells." *Current Pharmaceutical Design* 17 (30): 3252-3257.
- Frey, N. and E. N. Olson. 2003. "Cardiac Hypertrophy: The Good, the Bad, and the Ugly." *Annual Review of Physiology* 65: 45-79.
- Gimbrone, M. A., Jr and G. Garcia-Cardena. 2016. "Endothelial Cell Dysfunction and the Pathobiology of Atherosclerosis." *Circulation Research* 118 (4): 620-636.
- Goodwin, A. M., K. M. Sullivan, and P. A. D'Amore. 2006. "Cultured Endothelial Cells Display Endogenous Activation of the Canonical Wnt Signaling Pathway and Express Multiple Ligands, Receptors, and Secreted Modulators of Wnt Signaling." *Developmental Dynamics : An Official Publication of the American Association of Anatomists* 235 (11): 3110-3120.
- Greber-Platzer, S., M. Marx, C. Fleischmann, C. Suppan, M. Dobner, and M. Wimmer. 2001. "Beta-Myosin Heavy Chain Gene Mutations and Hypertrophic Cardiomyopathy in Austrian Children." *Journal of Molecular and Cellular Cardiology* 33 (1): 141-148.
- Greider, C. W. and E. H. Blackburn. 1985. "Identification of a Specific Telomere Terminal Transferase Activity in Tetrahymena Extracts." *Cell* 43 (2 Pt 1): 405-413.
- Guo, Z. K., K. Guo, H. Luo, L. M. Mu, Q. Li, and Y. Q. Chang. 2015. "The Expression Analysis of Nanog in the Developing Rat Myocardial Tissues." *Cellular Physiology and Biochemistry : International Journal of Experimental Cellular Physiology, Biochemistry, and Pharmacology* 35 (3): 866-874.
- Hart, A. H., L. Hartley, M. Ibrahim, and L. Robb. 2004. "Identification, Cloning and Expression Analysis of the Pluripotency Promoting Nanog Genes in Mouse and Human." *Developmental Dynamics : An Official Publication of the American Association of Anatomists* 230 (1): 187-198.
- Higashi, Y., Y. Kihara, and K. Noma. 2012. "Endothelial Dysfunction and Hypertension in Aging." *Hypertension Research : Official Journal of the Japanese Society of Hypertension* 35 (11): 1039-1047.
- Hill, J. A. 2015. "Braking Bad Hypertrophy." *The New England Journal of Medicine* 372 (22): 2160-2162.

Hoffmeyer, K., A. Raggioli, S. Rudloff, R. Anton, A. Hierholzer, I. Del Valle, K. Hein, R. Vogt, and R. Kemler. 2012. "Wnt/Beta-Catenin Signaling Regulates Telomerase in Stem Cells and Cancer Cells." *Science (New York, N.Y.)* 336 (6088): 1549-1554.

Hogan, N. T., M. B. Whalen, L. K. Stolze, N. K. Hadeli, M. T. Lam, J. R. Springstead, C. K. Glass, and C. E. Romanoski. 2017. "Transcriptional Networks Specifying Homeostatic and Inflammatory Programs of Gene Expression in Human Aortic Endothelial Cells." *eLife* 6: 10.7554/eLife.22536.

Jeter, C. R., T. Yang, J. Wang, H. P. Chao, and D. G. Tang. 2015. "Concise Review: NANOG in Cancer Stem Cells and Tumor Development: An Update and Outstanding Questions." *Stem Cells (Dayton, Ohio)* 33 (8): 2381-2390.

Kajstura, J., N. Gurusamy, B. Ogorek, P. Goichberg, C. Clavo-Rondon, T. Hosoda, D. D'Amario, et al. 2010. "Myocyte Turnover in the Aging Human Heart." *Circulation Research* 107 (11): 1374-1386.

Kamo, T., H. Akazawa, and I. Komuro. 2015. "Cardiac Nonmyocytes in the Hub of Cardiac Hypertrophy." *Circulation Research* 117 (1): 89-98.

Kazmi, R. S., S. Boyce, and B. A. Lwaleed. 2015. "Homeostasis of Hemostasis: The Role of Endothelium." *Seminars in Thrombosis and Hemostasis* 41 (6): 549-555.

Kempf, T. and K. C. Wollert. 2004. "Nitric Oxide and the Enigma of Cardiac Hypertrophy." *BioEssays : News and Reviews in Molecular, Cellular and Developmental Biology* 26 (6): 608-615.

Kerkela, R., J. Ulvila, and J. Magga. 2015. "Natriuretic Peptides in the Regulation of Cardiovascular Physiology and Metabolic Events." *Journal of the American Heart Association* 4 (10): e002423.

Khazaei, M., F. Moien-Afshari, and I. Laher. 2008. "Vascular Endothelial Function in Health and Diseases." *Pathophysiology : The Official Journal of the International Society for Pathophysiology* 15 (1): 49-67.

Kluge, M. A., J. L. Fetterman, and J. A. Vita. 2013. "Mitochondria and Endothelial Function." *Circulation Research* 112 (8): 1171-1188.

Kockx, M. M. and M. W. Knaapen. 2000. "The Role of Apoptosis in Vascular Disease." *The Journal of Pathology* 190 (3): 267-280.

Kohler, E. E., J. Baruah, N. Urao, M. Ushio-Fukai, T. Fukai, I. Chatterjee, and K. K. Wary. 2014. "Low-Dose 6-Bromoindirubin-3'-Oxime Induces Partial Dedifferentiation of Endothelial Cells to Promote Increased Neovascularization." *Stem Cells (Dayton, Ohio)* 32 (6): 1538-1552.

- Kohler, E. E., C. E. Cowan, I. Chatterjee, A. B. Malik, and K. K. Wary. 2011. "NANOG Induction of Fetal Liver Kinase-1 (FLK1) Transcription Regulates Endothelial Cell Proliferation and Angiogenesis." *Blood* 117 (5): 1761-1769.
- Komatsu, K. and T. Fujimori. 2015. "Multiple Phases in Regulation of Nanog Expression during Pre-Implantation Development." *Development, Growth & Differentiation* 57 (9): 648-656.
- Komiya, Y. and R. Habas. 2008. "Wnt Signal Transduction Pathways." *Organogenesis* 4 (2): 68-75.
- Korn, C., B. Scholz, J. Hu, K. Srivastava, J. Wojtarowicz, T. Arnsperger, R. H. Adams, M. Boutros, H. G. Augustin, and I. Augustin. 2014. "Endothelial Cell-Derived Non-Canonical Wnt Ligands Control Vascular Pruning in Angiogenesis." *Development (Cambridge, England)* 141 (8): 1757-1766.
- Kraft, T., J. Montag, A. Radocaj, and B. Brenner. 2016. "Hypertrophic Cardiomyopathy: Cell-to-Cell Imbalance in Gene Expression and Contraction Force as Trigger for Disease Phenotype Development." *Circulation Research* 119 (9): 992-995.
- Krijnen, P. A., R. Nijmeijer, C. J. Meijer, C. A. Visser, C. E. Hack, and H. W. Niessen. 2002. "Apoptosis in Myocardial Ischaemia and Infarction." *Journal of Clinical Pathology* 55 (11): 801-811.
- Kwon, C., K. R. Cordes, and D. Srivastava. 2008. "Wnt/Beta-Catenin Signaling Acts at Multiple Developmental Stages to Promote Mammalian Cardiogenesis." *Cell Cycle (Georgetown, Tex.)* 7 (24): 3815-3818.
- Li, S., K. Guo, J. Wu, Z. Guo, and A. Li. 2017. "Altered Expression of C-Kit and Nanog in a Rat Model of Adriamycin-Induced Chronic Heart Failure." *American Journal of Cardiovascular Disease* 7 (2): 57-63.
- Lim, S. L., C. S. Lam, V. F. Segers, D. L. Brutsaert, and G. W. De Keulenaer. 2015. "Cardiac Endothelium-Myocyte Interaction: Clinical Opportunities for New Heart Failure Therapies Regardless of Ejection Fraction." *European Heart Journal* 36 (31): 2050-2060.
- Loh, K. M., R. van Amerongen, and R. Nusse. 2016. "Generating Cellular Diversity and Spatial Form: Wnt Signaling and the Evolution of Multicellular Animals." *Developmental Cell* 38 (6): 643-655.
- Luo, H., Q. Li, J. Pramanik, J. Luo, and Z. Guo. 2014. "Nanog Expression in Heart Tissues Induced by Acute Myocardial Infarction." *Histology and Histopathology* 29 (10): 1287-1293.
- MacDonald, B. T., K. Tamai, and X. He. 2009. "Wnt/Beta-Catenin Signaling: Components, Mechanisms, and Diseases." *Developmental Cell* 17 (1): 9-26.
- Marinou, K., C. Christodoulides, C. Antoniadis, and M. Koutsilieris. 2012. "Wnt Signaling in Cardiovascular Physiology." *Trends in Endocrinology and Metabolism: TEM* 23 (12): 628-636.

- Mazzotta, S., C. Neves, R. J. Bonner, A. S. Bernardo, K. Docherty, and S. Hoppler. 2016. "Distinctive Roles of Canonical and Noncanonical Wnt Signaling in Human Embryonic Cardiomyocyte Development." *Stem Cell Reports* 7 (4): 764-776.
- Michiels, C. 2003. "Endothelial Cell Functions." *Journal of Cellular Physiology* 196 (3): 430-443.
- Mitsui, K., Y. Tokuzawa, H. Itoh, K. Segawa, M. Murakami, K. Takahashi, M. Maruyama, M. Maeda, and S. Yamanaka. 2003. "The Homeoprotein Nanog is Required for Maintenance of Pluripotency in Mouse Epiblast and ES Cells." *Cell* 113 (5): 631-642.
- Molkentin, J. D. and G. W. Dorn 2nd. 2001. "Cytoplasmic Signaling Pathways that Regulate Cardiac Hypertrophy." *Annual Review of Physiology* 63: 391-426.
- Moretto-Zita, M., H. Jin, Z. Shen, T. Zhao, S. P. Briggs, and Y. Xu. 2010. "Phosphorylation Stabilizes Nanog by Promoting its Interaction with Pin1." *Proceedings of the National Academy of Sciences of the United States of America* 107 (30): 13312-13317.
- Mouton, J. M., L. van der Merwe, A. Goosen, M. Revera, P. A. Brink, J. C. Moolman-Smook, and C. Kinnear. 2016. "MYBPH Acts as Modifier of Cardiac Hypertrophy in Hypertrophic Cardiomyopathy (HCM) Patients." *Human Genetics* 135 (5): 477-483.
- Oka, S., R. Alcendor, P. Zhai, J. Y. Park, D. Shao, J. Cho, T. Yamamoto, B. Tian, and J. Sadoshima. 2011. "PPARalpha-Sirt1 Complex Mediates Cardiac Hypertrophy and Failure through Suppression of the ERR Transcriptional Pathway." *Cell Metabolism* 14 (5): 598-611.
- Oka, T., H. Akazawa, A. T. Naito, and I. Komuro. 2014. "Angiogenesis and Cardiac Hypertrophy: Maintenance of Cardiac Function and Causative Roles in Heart Failure." *Circulation Research* 114 (3): 565-571.
- Orlic, D., J. Kajstura, S. Chimenti, I. Jakoniuk, S. M. Anderson, B. Li, J. Pickel, et al. 2001. "Bone Marrow Cells Regenerate Infarcted Myocardium." *Nature* 410 (6829): 701-705.
- Pan, G. and J. A. Thomson. 2007. "Nanog and Transcriptional Networks in Embryonic Stem Cell Pluripotency." *Cell Research* 17 (1): 42-49.
- Perez-Rivero, G., M. P. Ruiz-Torres, J. V. Rivas-Elena, M. Jerkic, M. L. Diez-Marques, J. M. Lopez-Novoa, M. A. Blasco, and D. Rodriguez-Puyol. 2006. "Mice Deficient in Telomerase Activity Develop Hypertension because of an Excess of Endothelin Production." *Circulation* 114 (4): 309-317.
- Piazzolla, D., A. R. Palla, C. Pantoja, M. Canamero, I. P. de Castro, S. Ortega, G. Gomez-Lopez, et al. 2014. "Lineage-Restricted Function of the Pluripotency Factor NANOG in Stratified Epithelia." *Nature Communications* 5: 4226.
- Pinto, A. R., A. Ilinykh, M. J. Ivey, J. T. Kuwabara, M. L. D'Antoni, R. Debuque, A. Chandran, et al. 2016. "Revisiting Cardiac Cellular Composition." *Circulation Research* 118 (3): 400-409.

Pircher, A., L. Treps, N. Bodrug, and P. Carmeliet. 2016. "Endothelial Cell Metabolism: A Novel Player in Atherosclerosis? Basic Principles and Therapeutic Opportunities." *Atherosclerosis* 253: 247-257.

Ramakrishnan, A. B. and K. M. Cadigan. 2017. "Wnt Target Genes and Where to Find Them." *F1000Research* 6: 746.

Ramasamy, S. K., A. P. Kusumbe, and R. H. Adams. 2015. "Regulation of Tissue Morphogenesis by Endothelial Cell-Derived Signals." *Trends in Cell Biology* 25 (3): 148-157.

Ramlee, M. K., J. Wang, W. X. Toh, and S. Li. 2016. "Transcription Regulation of the Human Telomerase Reverse Transcriptase (hTERT) Gene." *Genes* 7 (8): 10.3390/genes7080050.

Red-Horse, K., Y. Crawford, F. Shojaei, and N. Ferrara. 2007. "Endothelium-Microenvironment Interactions in the Developing Embryo and in the Adult." *Developmental Cell* 12 (2): 181-194.

Reis, M. and S. Liebner. 2013. "Wnt Signaling in the Vasculature." *Experimental Cell Research* 319 (9): 1317-1323.

Richardson, G. D., D. Breault, G. Horrocks, S. Cormack, N. Hole, and W. A. Owens. 2012. "Telomerase Expression in the Mammalian Heart." *FASEB Journal : Official Publication of the Federation of American Societies for Experimental Biology* 26 (12): 4832-4840.

Rocha, S. F. and R. H. Adams. 2009. "Molecular Differentiation and Specialization of Vascular Beds." *Angiogenesis* 12 (2): 139-147.

Rock, K. L. and H. Kono. 2008. "The Inflammatory Response to Cell Death." *Annual Review of Pathology* 3: 99-126.

Rodda, D. J., J. L. Chew, L. H. Lim, Y. H. Loh, B. Wang, H. H. Ng, and P. Robson. 2005. "Transcriptional Regulation of Nanog by OCT4 and SOX2." *The Journal of Biological Chemistry* 280 (26): 24731-24737.

Rubanyi, G. M. 1993. "The Role of Endothelium in Cardiovascular Homeostasis and Diseases." *Journal of Cardiovascular Pharmacology* 22 Suppl 4: S1-14.

Sahin, E. and R. A. Depinho. 2010. "Linking Functional Decline of Telomeres, Mitochondria and Stem Cells during Ageing." *Nature* 464 (7288): 520-528.

Samarzija, I., P. Sini, T. Schlange, G. Macdonald, and N. E. Hynes. 2009. "Wnt3a Regulates Proliferation and Migration of HUVEC Via Canonical and Non-Canonical Wnt Signaling Pathways." *Biochemical and Biophysical Research Communications* 386 (3): 449-454.

Sandoo, A., J. J. van Zanten, G. S. Metsios, D. Carroll, and G. D. Kitas. 2010. "The Endothelium and its Role in Regulating Vascular Tone." *The Open Cardiovascular Medicine Journal* 4: 302-312.

Segura, A. M., O. H. Frazier, and L. M. Buja. 2014. "Fibrosis and Heart Failure." *Heart Failure Reviews* 19 (2): 173-185.

Selvetella, G., E. Hirsch, A. Notte, G. Tarone, and G. Lembo. 2004. "Adaptive and Maladaptive Hypertrophic Pathways: Points of Convergence and Divergence." *Cardiovascular Research* 63 (3): 373-380.

Shimizu, I. and T. Minamino. 2016. "Physiological and Pathological Cardiac Hypertrophy." *Journal of Molecular and Cellular Cardiology* 97: 245-262.

Silva, J., J. Nichols, T. W. Theunissen, G. Guo, A. L. van Oosten, O. Barrandon, J. Wray, S. Yamanaka, I. Chambers, and A. Smith. 2009. "Nanog is the Gateway to the Pluripotent Ground State." *Cell* 138 (4): 722-737.

Sprague, A. H. and R. A. Khalil. 2009. "Inflammatory Cytokines in Vascular Dysfunction and Vascular Disease." *Biochemical Pharmacology* 78 (6): 539-552.

Stylianidis, V., K. C. M. Hermans, and W. M. Blankesteyn. 2017. "Wnt Signaling in Cardiac Remodeling and Heart Failure." *Handbook of Experimental Pharmacology* 243: 371-393.

Takahashi, K. and S. Yamanaka. 2006. "Induction of Pluripotent Stem Cells from Mouse Embryonic and Adult Fibroblast Cultures by Defined Factors." *Cell* 126 (4): 663-676.

Tang, D. G. and C. J. Conti. 2004. "Endothelial Cell Development, Vasculogenesis, Angiogenesis, and Tumor Neovascularization: An Update." *Seminars in Thrombosis and Hemostasis* 30 (1): 109-117.

Tardiff, J. C. 2006. "Cardiac Hypertrophy: Stressing Out the Heart." *The Journal of Clinical Investigation* 116 (6): 1467-1470.

Theodoris, C. V., F. Mourkioti, Y. Huang, S. S. Ranade, L. Liu, H. M. Blau, and D. Srivastava. 2017. "Long Telomeres Protect Against Age-Dependent Cardiac Disease Caused by NOTCH1 Haploinsufficiency." *The Journal of Clinical Investigation* 127 (5): 1683-1688.

Torres-Padilla, M. E. and I. Chambers. 2014. "Transcription Factor Heterogeneity in Pluripotent Stem Cells: A Stochastic Advantage." *Development (Cambridge, England)* 141 (11): 2173-2181.

Treibel, T. A., R. Kozor, K. Menacho, S. Castelletti, H. Bulluck, S. Rosmini, S. Nordin, V. Maestrini, M. Fontana, and J. C. Moon. 2017. "Left Ventricular Hypertrophy Revisited: Cell and Matrix Expansion have Disease-Specific Relationships." *Circulation* 136 (25): 2519-2521.

van de Schans, V. A., J. F. Smits, and W. M. Blankesteyn. 2008. "The Wnt/Frizzled Pathway in Cardiovascular Development and Disease: Friend Or Foe?" *European Journal of Pharmacology* 585 (2-3): 338-345.

van Empel, V. P., A. T. Bertrand, L. Hofstra, H. J. Crijns, P. A. Doevendans, and L. J. De Windt. 2005. "Myocyte Apoptosis in Heart Failure." *Cardiovascular Research* 67 (1): 21-29.

van Empel, V. P. and L. J. De Windt. 2004. "Myocyte Hypertrophy and Apoptosis: A Balancing Act." *Cardiovascular Research* 63 (3): 487-499.

Walsh, K. and I. Shiojima. 2007. "Cardiac Growth and Angiogenesis Coordinated by Intertissue Interactions." *The Journal of Clinical Investigation* 117 (11): 3176-3179.

Wang, X. Y., Y. Lan, W. Y. He, L. Zhang, H. Y. Yao, C. M. Hou, Y. Tong, et al. 2008. "Identification of Mesenchymal Stem Cells in Aorta-Gonad-Mesonephros and Yolk Sac of Human Embryos." *Blood* 111 (4): 2436-2443.

Winn, R. K. and J. M. Harlan. 2005. "The Role of Endothelial Cell Apoptosis in Inflammatory and Immune Diseases." *Journal of Thrombosis and Haemostasis : JTH* 3 (8): 1815-1824.

Wong, L. S., H. Oeseburg, R. A. de Boer, W. H. van Gilst, D. J. van Veldhuisen, and P. van der Harst. 2009. "Telomere Biology in Cardiovascular Disease: The TERC-/- Mouse as a Model for Heart Failure and Ageing." *Cardiovascular Research* 81 (2): 244-252.

Xie, X., L. Piao, G. S. Cavey, M. Old, T. N. Teknos, A. K. Mapp, and Q. Pan. 2014. "Phosphorylation of Nanog is Essential to Regulate Bmi1 and Promote Tumorigenesis." *Oncogene* 33 (16): 2040-2052.

Yamaguchi, S., K. Kurimoto, Y. Yabuta, H. Sasaki, N. Nakatsuji, M. Saitou, and T. Tada. 2009. "Conditional Knockdown of Nanog Induces Apoptotic Cell Death in Mouse Migrating Primordial Germ Cells." *Development (Cambridge, England)* 136 (23): 4011-4020.

Yang, J., E. Chang, A. M. Cherry, C. D. Bangs, Y. Oei, A. Bodnar, A. Bronstein, C. P. Chiu, and G. S. Herron. 1999. "Human Endothelial Cell Life Extension by Telomerase Expression." *The Journal of Biological Chemistry* 274 (37): 26141-26148.

Yates, A. and I. Chambers. 2005. "The Homeodomain Protein Nanog and Pluripotency in Mouse Embryonic Stem Cells." *Biochemical Society Transactions* 33 (Pt 6): 1518-1521.

Yuldasheva, N. Y., S. T. Rashid, N. J. Haywood, P. Cordell, R. Mughal, H. Viswambharan, H. Imrie, et al. 2014. "Haploinsufficiency of the Insulin-Like Growth Factor-1 Receptor Enhances Endothelial Repair and Favorably Modifies Angiogenic Progenitor Cell Phenotype." *Arteriosclerosis, Thrombosis, and Vascular Biology* 34 (9): 2051-2058.

Zhang, X., I. Neganova, S. Przyborski, C. Yang, M. Cooke, S. P. Atkinson, G. Anyfantis, et al. 2009. "A Role for NANOG in G1 to S Transition in Human Embryonic Stem Cells through Direct Binding of CDK6 and CDC25A." *The Journal of Cell Biology* 184 (1): 67-82.

Zhang, Y., L. Toh, P. Lau, and X. Wang. 2012. "Human Telomerase Reverse Transcriptase (hTERT) is a Novel Target of the Wnt/Beta-Catenin Pathway in Human Cancer." *The Journal of Biological Chemistry* 287 (39): 32494-32511.

Zhou, P. and W. T. Pu. 2016. "Recounting Cardiac Cellular Composition." *Circulation Research* 118 (3): 368-370.

Zurek, M., J. Altschmied, S. Kohlgruber, N. Ale-Agha, and J. Haendeler. 2016. "Role of Telomerase in the Cardiovascular System." *Genes* 7 (6): 10.3390/genes7060029.

IX. VITA

Jugajyoti Baruah

Education

Ph.D. Cellular and Molecular Pharmacology University of Illinois at Chicago, Chicago, IL	2018
M.Sc. Biomedical Genetics Vellore Institute of Technology University (VITU), Vellore, India	2011
B.Sc. Biotechnology Minor(s): Genetics and Biochemistry Garden City College, Bangalore University, Bangalore, India	2009

Experience

University of Illinois at Chicago, Chicago, IL Department of Pharmacology Graduate Research Assistant (Kishore Wary lab)	2013-
North Eastern Hill University (NEHU), Shillong, India Department of Zoology Junior Research Fellow (Veena Tandon lab)	2011-2012
University of Illinois at Chicago, Chicago, IL Department of Pharmacology Visiting Research Intern (Kishore Wary lab)	2011

Grants/Funding

Center for Clinical and Translational Sciences (CCTS)- PECTS Fellowship	2016
American Heart Association (AHA) Midwest Affiliate Predoctoral Fellowship	2015-2016

Honors

UIC College of Medicine Forum (Gold Medal, First Place)	2018
ATVB Travel Grant for Young Investigator	2017
Basic Cardiovascular Sciences (BCVS) Travel Grant	2017
ASPET Mentoring Network: Coaching for Career Development	2017
Graduate Student Council Travel award	2017

Graduate College Student Presenter award	2017
Basic Cardiovascular Sciences (BCVS) Travel Grant	2016
ATVB Travel Grant for Young Investigator	2016
ASPET Experimental Biology, Molecular Pharmacology Graduate Student Best abstract Presentation, Finalist	2016
Chancellor's Student Service Award	2016
University Rank in M.S Program, 3 rd place	2011
University Scholarship Semester Abroad Program, Master's Thesis work at the University of Illinois at Chicago, USA	2011

Memberships

American Heart Association and American Stroke Association.
 North American Vascular Biology Organization.
 American Society for Pharmacology and Experimental Therapeutics.
 International Society for Stem Cell Research.

Academic Service/Teaching Experience

TA for GCLS 503 Cell Biology, Fall 2017
 Treasurer, Graduate Education in Medical Sciences Student Association (GEMSSA).2015
 Department Representative, Dep. Of Pharmacology, Graduate Student Council. 2014-2015

Peer-Reviewed Publications (* Indicates First authorship)

Kohler EE, **Baruah J**, Urao N, Ushio-Fukai M, Fukai T, Chatterjee I, Wary KK. Low-dose 6-bromindirubin-3'-oxime induces partial dedifferentiation of endothelial cells to promote increased neovascularization. *Stem Cells*. 2014; 32(6):1538-1552.

Oh M, Zhang C, LeMaster E, Adamos C, Berdyshev E, Bogachkov Y, Kohler EE, **Baruah J**, Chraufnagel DE, Wary KK, and Levitan I. Oxidized-LDL Signals through Rho-GTPase to Induce Endothelial Cell Stiffening and Promote Capillary Formation. *J Lipid Res*. 2016; 57(5):791-808.

Chatterjee I, **Baruah J**, Kohler EE and Wary KK. Endothelial Lipid Phosphate Phosphatase-3 Deficiency that Causes Disruption of Barrier Integrity, is a Modifier of Cardiovascular Development. *Cardiovascular Res*. 2016; 111(1):105-118.

Wary A, Wary N, **Baruah J**, Mastej V, Wary KK. Chromatin-modifying agents convert fibroblasts to OCT4+ and VEGFR-2+ capillary tube-forming cells. *PLoS One*. 2017 3;12(5).

Zhang C, Adamos C, Oh M, **Baruah J**, Ayee M, Mehta D, Wary KK and Levitan I. OxLDL-induced endothelial proliferation via Rho/ROCK/Akt/p27kip1 signaling: prevention by cholesterol loading. *AJP-Cell Physiology*. 2017 313(3):C340-C351

Baruah J*, Hitzman R, Zhang J, Chaudhuri S and Wary KK. The allosteric glycogen synthase kinase-3 inhibitor NP12 limits myocardial remodeling and promotes angiogenesis in an acute myocardial infarction model. *Journal of Biological Chemistry*. 292(50):20785-20798.

Baruah J*, Hitzman R, Chaudhuri S, Mastej V and Wary KK. Nanog haploinsufficiency disrupts coronary endothelial cell homeostasis and mediates cardiac hypertrophy. 2018 (*in submission*)

Baruah J* and Wary KK. Role of Transcription factor Nanog beyond Pluripotency (Review) (*in preparation*)

Presentations

1. **Baruah J**, Kohler EE, Wary KK. Characterization of Asymmetric Cell Division during Angiogenesis. UIC/UIUC Third Stem Cell and Regenerative Medicine Symposium, Chicago, IL. May 20, 2011 (Poster).
2. **Baruah J** and Wary KK. Nanog Regulation of Endothelial Asymmetric Cell Division. Experimental Biology, San Diego, CA 2014 (Poster).
3. **Baruah J** and Kishore Wary. Allosteric Inhibition of Glycogen Synthase Kinase-3 β Mimics Canonical Wnt Signaling to Induce Neovascularization. North American Vascular Biology Conference, Asilomar, CA Oct 20th, 2014 (Poster).
4. **Baruah J** and Kishore Wary. Tideglusib, a novel allosteric inhibitor of Glycogen Synthase Kinase-3- β mimics canonical Wnt signaling. American Heart Association (AHA) Scientific Sessions, Chicago, IL Nov 17th, 2014 (Poster).
5. **Baruah J** and Wary KK. Tideglusib, an allosteric inhibitor of Glycogen Synthase Kinase (GSK)-3 β increases Angiogenic activities of Endothelial Cells. Experimental Biology, Boston, MA, April 2015 (Poster).
6. **Baruah J** and KK Wary. Wnt Induced hTERT expression Protect Endothelial Cells from Apoptosis. VASCULATA-2015, Charlottesville, VA. Aug 3rd, 2015 (Poster).
7. **Baruah J**, Ribeiro I, KK Wary. Reactivation of hTERT and Telomerase Activity in Vascular Endothelial Cells. AHA Research Network Symposium, Chicago, IL Sept 18th, 2015 (Poster).
8. **Baruah J**, Hitzman R, Zhang J and Wary KK Small molecule approach to activate canonical Wnt signaling in Endothelial Cells. College of Medicine Research Forum, Chicago, IL Dec 2015 (Poster).

9. **Baruah J**, Hitzman R, Zhang J and Wary KK. A Novel Activator of Canonical Wnt Signaling. Experimental Biology, San Diego, CA April 4th, 2016 (Platform and poster).
10. **Baruah J**, Hitzman R, Zhang J and Wary KK. Allosteric Inhibition of Glycogen Synthase Kinase-3 β Reduces Fibrosis, Secondary to Increased Neovascularization in a Mouse Model of Myocardial Ischemia-Reperfusion Injury. GEMS Research Symposium, Chicago, IL Sept 2016 (Platform).
11. **Baruah J**, Hitzman R, Zhang J and Wary KK. An Allosteric Inhibitor of Glycogen Synthase Kinase-3 β Protects the Heart from Ischemia-Reperfusion Injury. 19th International Vascular Biology Meeting (IVBM), Oct 2016, Boston, MA (Poster).
12. **Baruah J**, Hitzman R, Ribeiro I, Zhang J and Wary KK. A non-canonical role of Nanog in adult vascular endothelial cell homeostasis. AHA Scientific Sessions, New Orleans, LA. Nov 14th, 2016 (Poster).
13. **Baruah J**, Hitzman R, Ribeiro I, Zhang J and Wary KK. A non-canonical role of Nanog in adult vascular endothelial cell homeostasis. ATVB Early Career Reception, AHA Scientific Sessions, New Orleans, LA. Nov 15th, 2016 (Poster).
14. **Baruah J**, Hitzman R, Zhang J and Wary KK. Endothelial cell-specific deletion of a single Nanog allele demonstrates its crucial role in the microenvironment of adult tissues. Experimental Biology, Chicago, IL April 2017 (Poster).
15. **Baruah J**, Chaudhuri S, Mastej V and Wary KK. Repurposing an orphan drug, NP12, to mitigate Myocardial Fibrosis and Restore Coronary Blood Supply. VASCULATA, Chicago, IL July 2017 (Poster).
16. **Baruah J**, Chaudhuri S, Mastej V and Wary KK. Low-Level Nanog Expression Maintains Endothelial Cell Homeostasis in Adult Vascular Bed. VASCULATA, Chicago, IL July 2017 (Poster).
17. **Baruah J**, Hitzman R, Zhang J, Chaudhuri S, Mastej V and Wary KK. Small molecule NP12 mitigates myocardial fibrosis and restores coronary blood supply. UIC College of Medicine Forum. Chicago, Dec. 2017 (Poster)